行政院國家科學委員會專題研究計畫　成果報告

固固固固固固固固固固固固固固固固固固固固固研究(2/2)

計畫類別：個別型計畫
計畫編號：NSC93-2113-M-002-016-
執行期間：93年08月01日至94年09月30日
執行單位：國立臺灣大學化學系暨研究所

計畫主持人：陳固中

報告類型：完整報告
報告附件：出席國際會議研究心得報告及發表論文
處理方式：本計畫可公開查詢

中　華　民　國 95年1月2日

行政院國家科學委員會補助專題研究計畫 ☑成果報告
□期中進度報告

固態核磁共振對多肽與生物活性玻璃相互作用之研究

計畫類別：☑ 個別型計畫　　□ 整合型計畫
計畫編號：NSC 93-2113-M-002-016
執行期間：　93 年 08 月 01 日至 94 年 9 月 30 日

計畫主持人：陳振中
共同主持人：
計畫參與人員：

成果報告類型(依經費核定清單規定繳交)：□精簡報告　☑完整報告

本成果報告包括以下應繳交之附件：
□赴國外出差或研習心得報告一份
□赴大陸地區出差或研習心得報告一份
☑出席國際學術會議心得報告及發表之論文各一份
□國際合作研究計畫國外研究報告書一份

處理方式：除產學合作研究計畫、提升產業技術及人才培育研究計畫、
列管計畫及下列情形者外，得立即公開查詢
□涉及專利或其他智慧財產權，□一年□二年後可公開查詢

執行單位：國立台灣大學化學系

中　華　民　國　94　年　12　月　30　日

摘要

此計畫之重點是研究附於生物活性玻璃上的多肽之結構。計畫的動因乃是要明白人體內骨胳形成的機理，以利發展新一代的生物材料。我們的研究有三個具體目標：（一）分析 hydroxyapatite 在矽玻璃表面的結晶過程；（二）發展新的固態核磁共振技術，用以測量多肽的脊柱扭轉角度 ψ；（三）測量附於矽玻璃表面的多肽之二級結構。

首先，我們以溶膠—凝膠技術合成均勻球狀的矽玻璃系統，以固態核磁共振光譜觀察其於人工體液中如何生成羥基磷灰石。此研究亦衍生另一副題：我們與台大化學系牟中原教授合作，以固態核磁共振光譜觀察 octacalcium phosphate 如何轉化成 hydroxyapatite。此相轉變過程在生物礦化領域中受高度重視，因它有可能是 hydroxyapatite 在生物中的礦化機理。這部份的工作成果豐碩，內容已發表於三篇 SCI 期刊，並有一篇在審議中:

1. YH Tseng, J Zhan, KSK Lin, CY Mou and JCC Chan, **2004 SEPT**, “High Resolution ^{31}P NMR Study of Octacalcium Phosphate,” *Solid State Nucl. Magn. Reson.*, *26*, 99-104.
2. YH Tseng, Y Mou, CY Mou and JCC Chan, **2005 JUN**, “Double-Quantum NMR spectroscopy based on finite pulse RFDR,” *Solid State Nucl. Magn. Reson.*, *27*, 266-270.
3. KSK Lin, YH Tseng, Y Mou, YC Hsu, CM Yang and JCC Chan, **2005 AUG** “Mechanistic Study of Apatite Formation on Bioactive Glass Surface Using ^{31}P Solid-State NMR Spectroscopy,” *Chem. Mater.*, *17*, 4493-4501.
4. YH Tseng, CY Mou and JCC Chan, “Transformation of Octacalcium Phosphate to Hydroxyapatite: A Study of the Molecular Mechanism by SEM, TEM, XRD and Solid-State NMR Spectroscopy,” submitted.

對於第二個目標，我們成功地發展出一新穎的高分辨固態核磁共振技術，利用 J 耦合作爲極化傳遞之機理，此技術當可應用於測量含 ^{13}C 和 ^{15}N 均勻標籤的多肽的二級結構。部份結果已發表於以下 SCI 期刊:

1. Y Mou, JCH Chao, JCC Chan, **2006**, “Efficient Spin-Spin Scalar Coupling Mediated C-13 Homonuclear Polarization Transfer in Solid-State NMR Spectroscopy,” *Solid State Nucl. Magn. Reson.*, in press.
2. Y Mou and JCC Chan, **2006**, “Frequency Selective Polarization Transfer Based on Multiple Chemical Shift Precession,” *Chem. Phys. Lett.*, in press.

本計劃的第三個目標，乃是把選定的多肽 DpSpSEEKFLRRIGRFG，附於矽玻璃的表面，然後以多種固態核磁共振技術來測量其結構，探討多肽的二級構形與礦物的表面結構有何特定關係。目前我們已部份地完成此目標。計劃中的多肽已純化成功，經 FT-IR，TGA，固態 UV 光譜與 ninhydrin 試劑等測量，我們初步肯定多肽已成功附上矽玻璃表面的 hydroxyapatite，唯數量上仍不足以進行固態核磁共振之測量，需要更多時間於樣品製備上。整體而言，我們已初步建立一體系，成功證明固態核磁共振於生物礦化上有極佳之應用前景。

Abstract

The main objective of this proposal is to study the conformation of a polypeptide when it is adsorbed to bioactive glasses. The motivation is to understand in detail the bone mineralization process in human body for long-term implants development. This proposal comprises three specific aims: (i) characterization of the crystallization process of hydroxyapatite (HAp) on gel-silica glass surface; (ii) development of new solid-state nuclear magnetic resonance (SSNMR) technique for the determination of backbone torsion angle ψ of polypeptide; (iii) determination of the secondary structure of polypeptide adsorbed on gel-silica glass surface.

To accomplish the first aim, we have prepared a sol-gel glass system with novel morphology, which can greatly facilitate the study of the molecular mechanism of HAp formation on glass surface when soaked in simulated body fluid. Furthermore we also prepare an inorganic model system to study the mechanism of octacalcium phosphate (OCP) to HAp conversion, which has been postulated as the biomineralization mechanism of bones and teeth. This part of the work has resulted in three articles (published in SCI journals) and one manuscript (submitted) thesis:

1. YH Tseng, J Zhan, KSK Lin, CY Mou and JCC Chan, **2004 SEPT**, “High Resolution ^{31}P NMR Study of Octacalcium Phosphate,” *Solid State Nucl. Magn. Reson., 26*, 99-104.
2. YH Tseng, Y Mou, CY Mou and JCC Chan, **2005 JUN**, “Double-Quantum NMR spectroscopy based on finite pulse RFDR,” *Solid State Nucl. Magn. Reson.*, *27*, 266-270.
3. KSK Lin, YH Tseng, Y Mou, YC Hsu, CM Yang and JCC Chan, **2005 AUG** “Mechanistic Study of Apatite Formation on Bioactive Glass Surface Using ^{31}P Solid-State NMR Spectroscopy,” *Chem. Mater.*, *17*, 4493-4501.
4. YH Tseng, CY Mou and JCC Chan, “Transformation of Octacalcium Phosphate to Hydroxyapatite: A Study of the Molecular Mechanism by SEM, TEM, XRD and Solid-State NMR Spectroscopy,” submitted.

For the second aim, we have developed a novel technique to accomplish the polarization transfer via the scalar coupling. This technique is expected to find a very useful application in backbone torsion angle determination. Parts of the results have been documented in two manuscripts accepted for publication in SCI journals:

3. Y Mou, JCH Chao, JCC Chan, **2006**, “Efficient Spin-Spin Scalar Coupling Mediated C-13 Homonuclear Polarization Transfer in Solid-State NMR Spectroscopy,” *Solid State Nucl. Magn. Reson.*, in press.
4. Y Mou and JCC Chan, **2006**, “Frequency Selective Polarization Transfer Based on Multiple Chemical Shift Precession,” *Chem. Phys. Lett.*, in press.

We have partially accomplished the third aim by preparing a 15-residue polypeptide DpSpSEEKFLRRIGRFG and attach it on synthetic HAp crystals. The system has been well characterized by FT-IR, solid-state UV spectroscopy and ninhydrin test. While more works have to be done to characterize the conformation of the attached peptide, we have established a very solid foundation for further study.

Content

I. Introduction

In the post-genomic era, proteomics has become the new frontier in biological science. While most biotech and drug companies focus on identifying proteins associated with diseases, there are academic consortia working on different topics such as cell signaling. These large-scale research efforts, which heavily rely on cutting-edge robotics and x-ray crystallography, are expected to generate several hundred protein crystal structures a year. Nevertheless, in view of the vast complexity of proteomics, the structure-function relationships of many proteins would remain unknown in the near future. Biomineralization, which is a process describing the formation of composite materials in organisms, is a particularly challenging research area in proteomics because it is extremely difficult to study the interaction between two dissimilar organic (e.g. collagen fibrils) and inorganic nanophases (e.g. hydroxyapatite, calcium carbonate) by diffraction techniques. Thus, it has long been a mystery how living organisms control the mineral deposition with hierarchical structures. To date, the molecular mechanism of the interaction between the biopolymers and the mineral surfaces remains largely unknown. Yet our knowledge of the molecular mechanism of biomineralization is crucial for the development of implant biomaterials, e.g. bioactive glasses. Therefore in this project we manage to study the mechanism of surface reaction occurring on bioactive glass surface when soaked in simulated body fluid. Glasses that are bioactive must exhibit certain solubility to allow the necessary reactions to take place between the living tissues and the glass surface. In this proposal, we suggest to investigate the interaction between polypeptides and bioactive glasses using solid-state NMR (SSNMR) spectroscopy. In the past ten years SSNMR spectroscopy has been established as an element-selective, inherently quantitative method suited to the study of amorphous and compositionally complex systems. Many advanced SSNMR methods have been developed for the determination of internuclear distance and backbone torsion angles in isotopically labeled polypeptides. In this pilot study of SSNMR investigation of biomineralization, we manage to apply many different advanced SSNMR techniques to study different aspects of biomineralization. To the best of our knowledge, this proposal represents the first systematic investigation of the interaction between a polypeptide and bioactive glasses at the molecular level.

This project focuses on the interaction between bioactive glasses and polypeptides. There are three specific aims, *viz.* (i) characterization of the crystallization process of hydroxyapatite (HAP) on gel-silica glass surface; (ii) development of new SSNMR technique for the determination of backbone torsion angle ψ of polypeptides; (iii) determination of the secondary structure of polypeptide adsorbed on gel-silica glass surface. In the following sections, we will first discuss the results obtained for the characterization of the HAp crystallization process on bioactive glass surface, followed by a series of three articles on the study of the octacalcium phosphate to HAp transformation mechanism. Then, we will discuss the new pulse sequence with the acronym (MCSP) developed for homonuclear polarization transfer under magic-angle spinning. Finally, we will summarize some preliminary data obtained for the study of the glass-peptide interaction.

II. Results

II-A. Formation mechanism of Hydroxyapatite

Chem. Mater. **2005,** *17,* 4493−4501 4493

Mechanistic Study of Apatite Formation on Bioactive Glass Surface Using ^{31}P Solid-State NMR Spectroscopy

Kyle S. K. Lin,[†] Yao-Hung Tseng,[†] Yun Mou,[†] Yu-Chuan Hsu,[‡] Chia-Min Yang,[‡] and
Jerry C. C. Chan*,[†]

Department of Chemistry, National Taiwan University, No. 1, Section 4, Roosevelt Road,
Taipei, Taiwan, and Department of Chemistry, National Tsing Hua University, 101,
Section 2 Kuang Fu Road, Hsinchu, Taiwan

Received March 25, 2005. Revised Manuscript Received June 11, 2005

The molecular mechanism of apatite formation on bioactive glass surface is studied using the techniques of XRD, EDX, SEM, FT-IR, and solid-state ^{31}P NMR. Using the sol−gel method a bioactive glass system containing glass beads of 2 to 3 microns in size is prepared with the composition containing 30% CaO − 70% SiO$_2$. Our experimental data support the apatite formation mechanism proposed by Hench concerning the precipitation and crystallization of calcium phosphate. The phosphate ions initially deposited on the glass surface are largely in amorphous phase and have substantial amount of water molecules in the surrounding. As the soaking time in simulated body fluid increases, some of the water molecules diffuse out of the phosphate lattice, leading to the formation of a crystalline phase. Our data show that the structure of the crystalline phase is different from type B carbonate apatite but similar to hydroxyapatite.

Introduction

Glasses that are bioactive must exhibit a certain solubility to allow the necessary reactions to take place between the living tissues and the glass surface. Nowadays, it is generally accepted that the bonding of silica-glass to living tissue is primarily due to the formation of a mineral layer similar in composition to hydroxyapatite (HAp, $Ca_{10}(PO_4)_6(OH)_2$) on the glass surface.[1,2] A general mechanism of apatite formation on bioactive surfaces had been proposed by Hench and co-workers.[1,2] Accordingly, the process is divided into five stages: (i) Surface dealkalization by cation exchange with H^+, leading to a high pH local environment; (ii) Loss of soluble silica in the form of $Si(OH)_4$; (iii) Repolymerization of $Si(OH)_4$ to form a SiO_2-rich layer; (iv) Precipitation of Ca^{2+} and PO_4^{3-} ions in the silica-rich layer to form an amorphous $CaO-P_2O_5$ film; (v) Crystallization of the amorphous film by incorporation of OH^- or CO_3^{2-} anions. Numerous in-vitro studies had been carried out to understand the apatite formation process on the bioactive glasses soaked in simulated body fluid (SBF). In particular, the studies of binary $CaO-SiO_2$ glasses by Vallet-Regí and co-workers have shown that the Ca/P ratio varies from 1.6 in the apatite core to 1.2 on the apatite surface where a high population of HPO_4^{2-} ions is found.[3−5] It has also been suggested based on infrared spectroscopic data that the apatite formed on bioactive glass surface is hydroxycarbonate apatite.[3,6−8] Very recently, X-ray spectroscopy was used to demonstrate the formation of amorphous calcium phosphate at the early stage of SBF soaking.[9]

To shed more light on the stages (iv) and (v) of apatite formation, one can investigate the phosphorus environment during the course of apatite formation. In the past 15 years, solid-state NMR spectroscopy has been established as an element-selective, inherently quantitative method suited to the study of glass systems.[10] Recently, high-resolution solid-state ^{31}P NMR studies of the apatite formation on $CaO-SiO_2$ and Na_2O-SiO_2 glass systems had been reported.[11,12] The authors prepared the glass samples using the conventional melt-quench method and use the magic-angle spinning (MAS) technique to observe the ^{31}P NMR signals of the glasses with different soaking periods in SBF. However, the obtained ^{31}P NMR data do not have any significant implication because only a single ^{31}P peak was observed for each sample, where the chemical shift and line width data had very limited variation. Since many advanced solid-state NMR methods have been developed for the determination of internuclear distance,[13−15] it is possible to extract useful

---

[†] Department of Chemistry, National Taiwan University, No. 1, Section 4, Roosevelt Road, Taipei, Taiwan.

[‡] Department of Chemistry, National Tsing Hua University, 101, Section 2 Kuang Fu Road, Hsinchu, Taiwan.

(1) Hench, L. L.; West, J. K. *Life Chem. Reports* **1996**, *13*, 187.
(2) Hench, L. L. *J. Am. Ceram. Soc.* **1991**, *74*, 1487.
(3) Izquierdo-Barba, I.; Salinas, A. J.; Vallet-Regí, M. *J. Biomed. Mater. Res.* **1999**, *47*, 243.
(4) Martinez, A.; Izquierdo-Barba, I.; Vallet-Regí, M. *Chem. Mater.* **2000**, *12*, 3080.
(5) Vallet-Regí, M.; Perez-Pariente, J.; Izquierdo-Barba, I.; Salinas, A. J. *Chem. Mater.* **2000**, *12*, 3770.
(6) Vallet-Regí, M.; Arcos, D.; Perez-Pariente, J. *J. Biomed. Mater. Res.* **2000**, *51*, 23.
(7) Sepulveda, P.; Jones, J. R.; Hench, L. L. *J. Biomed. Mater. Res.* **2002**, *61*, 301.
(8) Yan, H. W.; Zhang, K.; Blanford, C. F.; Francis, L. F.; Stein, A. *Chem. Mater.* **2001**, *13*, 1374.
(9) Skipper, L. J.; Sowrey, F. E.; Pickup, D. M.; Fitzgerald, V.; Rashid, R.; Drake, K. O.; Lin, Z.; Saravanapavan, P.; Hench, L. L.; Smith, M. E.; Newport, R. J. *J. Biomed. Mater. Res.* **2004**, *70A*, 354.
(10) Eckert, H. *Prog. Nucl. Magn. Reson. Spectrosc.* **1992**, *24*, 159.
(11) Hayakawa, S.; Tsuru, S.; Iida, H.; Ohtsuki, C.; Osaka, A. *Phys. Chem. Glasses* **1996**, *37*, 188.
(12) Hayakawa, S.; Tsuru, K.; Ohtsuki, C.; Osaka, A. *J. Am. Ceram. Soc.* **1999**, *82*, 2155.
(13) Baldus, M. *Prog. Nucl. Magn. Reson. Spectrosc.* **2002**, *41*, 1.

10.1021/cm050654c CCC: $30.25

structural information concerning the apatite formation using more sophisticated NMR techniques than MAS. In view of the fact that a variety of advanced NMR techniques such as ^{31}P{^{1}H} cross-polarization (CP) at variable contact delays,[16] dipolar dephasing technique,[17] heteronuclear correlation spectroscopy (HETCOR),[18−20] differential cross polarization,[21,22] and multinuclear double-resonance techniques[23] had been used to characterize the structures of synthetic hydroxyapatite, calcified tissues and apatite formation in glass matrix with tremendous success, it is somewhat surprising that ^{31}P solid-state NMR spectroscopy has not been actively employed in the study of apatite formation on bioactive glasses. Furthermore, it has been found that the rate of apatite formation on bioactive glasses depends on the texture and the dimension of the glass particles.[24,25] Therefore, one of the difficulties to study apatite formation on a sol−gel glass surface is that the sizes and morphologies of the glass debris at the micrometer scale may be very irregular. Given such irregularity in particle size, the phosphate units in different parts of the glass sample may be at different stages of apatite formation, rendering the interpretation of experimental data very difficult.

In this work, we chose to use a series of solid-state ^{31}P NMR techniques including ^{31}P{^{1}H} Lee-Goldburg spectroscopy[26,27] and ^{31}P homonuclear double-quantum (DQ) NMR[28] to monitor the formation of apatite on a CaO (30%)-SiO$_2$ (70%) sol−gel glass system soaked in SBF. To enhance the ^{31}P signal arising from the glass surface, poly(acrylic acid) of high molecular weight was used as a polymer template to obtain microspherical gel-silica glasses.[29] These small glass beads with uniform size and morphology are used as a high-surface area medium for NMR investigations of bioactivity. The glass preparation and the SBF soaking procedure were based on the work of Hench and co-workers.[25]

Experimental Section

Crystalline HAp was obtained from Sigma−Aldrich. All other chemicals including the monetite (CaHPO$_4$) crystalline standard were obtained from Acros Organics and used as received. The hydroxyl content of the HAp sample had been verified to be stoichiometric based on NMR spin-counting technique using the monetite sample as the reference.[20]

Table 1. Temperature Schedule for the Glass Preparation

Stage		Ramp (°C/min)	Destination temp (°C)	Duration (hr)
Aging	1	0.1	60	5.8
	2	0	60	50
	3	−0.083	35	5
Drying	1	0.1	60	5.8
	2	0.075	150	20
	3	0.025	180	20
	4	0	180	12
	5	−2.4	35	1
stabilization	1	0.875	105	1.5
	2	0.25	160	3.7
	3	0.5	500	11.3
	4	0.046	700	72.5
	5	0	700	1
	6	−1.8	40	6

Gel-Silica Glasses. The gel-silica glasses containing 30 mol % CaO and 70 mol % SiO$_2$ were prepared by mixing the following reagents in a 50 mL FALCON tube: 7 mL of Si(OC$_2$H$_5$)$_4$ (98%), 3.157 g of Ca(NO$_3$)$_2$•4H$_2$O, 7.19 g of poly(acrylic acid) (MW 240000, 25 wt % in H$_2$O, partial sodium salt), 4.372 mL of deionized water and 0.136 mL of 14 *N* nitric acid. The tube was hermetically sealed and placed in an oven for aging. The aged sample was then dried under humid condition, where the gels were transferred from the tube to a beaker and then placed in a 6 L humidifier filled with 1.5 L of deionized water. The dried gels were then stabilized at high temperature to form glasses. The temperature schedules for aging, drying and stabilization are summarized in Table 1.

***In Vitro* Bioactivity.** Segments of 200 mg of the gel glasses were immersed in 500 mL of SBF, which was prepared by dissolving reagent-grade NaCl (136.9 mM), NaHCO$_3$ (4.18 mM), KCl (3.00 mM), K$_2$HPO$_4$•3H$_2$O (1.00 mM), MgCl$_2$•6H$_2$O (1.50 mM), CaCl$_2$ (3.76 mM), and Na$_2$SO$_4$ (0.50 mM) in deionized water.[30] The SBF solution was buffered at pH 7.4 using tris(hydroxymethyl)aminomethane (53.82 mM) and HCl (43.97 mM). The freshly prepared SBF solution was filtered through a 1 μm filter before use. The glass samples in SBF were incubated in an orbital shaker under 175 rpm at 37 °C for various periods: 20 min, 1 h, 3 h, 6 h, 12 h and 21.5 h. To terminate the reactions after the different soaking periods, the glass powder was collected by filtration through a 1 μm filter and then rinsed by deionized water, ethanol and acetone. The samples were dried at room temperature under reduced pressure for one to 2 days and then taken for NMR measurements.

Characterization. X-ray diffraction analysis was performed on a Mac Science 18MPX diffractometer, using Cu−Kα radiation (λ = 1.5418 Å). The field emission scanning electron microscopy (FE-SEM) and the energy-dispersive X-ray (EDX) analysis were done on a JEOL-JSM-6700F field emission scanning electron microscope (operating at 10 kV) equipped with an Oxford INCA energy-

---

(14) Luca, S.; Heise, H.; Baldus, M. *Accounts Chem. Res.* **2003**, *36*, 858.
(15) Schnell, I. *Prog. Nucl. Magn. Reson. Spectrosc.* **2004**, *45*, 145.
(16) Rothwell, W. P.; Waugh, J. S.; Yesinowski, J. P. *J. Am. Chem. Soc.* **1980**, *102*, 2637.
(17) Aue, W. P.; Roufosse, A. H.; Glimcher, M. J.; Griffin, R. G. *Biochemistry* **1984**, *23*, 6110.
(18) Santos, R. A.; Wind, R. A.; Bronnimann, C. E. *J. Magn. Reson. Ser. B* **1994**, *105*, 183.
(19) Kaflak-Hachulska, A.; Samoson, A.; Kolodziejski, W. *Calcif. Tissue Int.* **2003**, *73*, 476.
(20) Cho, G. Y.; Wu, Y. T.; Ackerman, J. L. *Science* **2003**, *300*, 1123.
(21) Wu, Y.; Ackerman, J. L.; Strawich, E. S.; Rey, C.; Kim, H. M.; Glimcher, M. J. *Calcif. Tissue Int.* **2003**, *72*, 610.
(22) Isobe, T.; Nakamura, S.; Nemoto, R.; Senna, M.; Sfihi, H. *J. Phys. Chem. B* **2002**, *106*, 5169.
(23) Chan, J. C. C.; Ohnsorge, R.; Meise-Gresch, K.; Eckert, H.; Holand, W.; Rheinberger, V. *Chem. Mater.* **2001**, *13*, 4198.
(24) Pereira, M. M.; Clark, A. E.; Hench, L. L. *J. Am. Ceram. Soc.* **1995**, *78*, 2463.
(25) Saravanapavan, P.; Jones, J. R.; Pryce, R. S.; Hench, L. L. *J. Biomed. Mater. Res.* **2003**, *64A*, 110.
(26) van Rossum, B. J.; de Groot, C. P.; Ladizhansky, V.; Vega, S.; de Groot, H. J. M. *J. Am. Chem. Soc.* **2000**, *122*, 3465.
(27) Ladizhansky, V.; Vega, S. *J. Chem. Phys.* **2000**, *112*, 7158.
(28) Ernst, R. R.; Bodenhausen, G.; Wokaun, A. *Principles of Nuclear Magnetic Resonance in One and Two Dimensions*. Clarendon Press: Oxford, 1987.
(29) Gallardo, J.; Galliano, P. G.; Lopez, J. M. P. *Biomaterials* **2002**, *23*, 4277.
(30) Kokubo, T.; Kushitani, H.; Sakka, S.; Kitsugi, T.; Yamamuro, T. *J. Am. Ceram. Soc.* **1990**, *78*, 2463.

dispersive X-ray spectrometer. Absorbance FT-IR spectra were collected using a Magna-IR 550 spectrometer (series II), in the range of 400−4000 cm^{-1}. The BET surface areas of the glass samples were obtained from the N_2 adsorption−desorption isotherm measured using a Micrometry Tristar system, where the samples were degassed at 200 °C under reduced pressure (10^{-3} Torr) for 16−20 h before each measurement.

Solid-State NMR. All NMR experiments were carried out at ^{31}P and ^{1}H frequencies of 121.5 and 300.1 MHz, respectively, on a Bruker DSX300 NMR spectrometer equipped with a commercial 4-mm probe. All spectra were measured at room temperature. The sample was confined to the middle 1/3 of the rotor volume using Teflon spacers. MAS frequency variation was limited to ± 3 Hz using a commercial pneumatic control unit. Chemical shifts were externally referenced to 85% phosphoric acid and TMS for ^{31}P and ^{1}H, respectively. The ^{31}P spin-relaxation times (T_1) were determined by the saturation-recovery technique. The ^{31}P MAS spectra were measured at a spinrate of 10 kHz and with 60 kHz proton decoupling. An exponential window function of 80 Hz line broadening was applied to each FID before the Fourier transformation. Recycle delay was set to 43 s. The ^{31}P spin counting experiments were performed using $Ag_7P_3S_{11}$ as the intensity standard (recycle delay 300 s). The ^{31}P{^{1}H} CPMAS experiments with variable contact times were done at a spinrate of 10 kHz. Recycle delay was set to 4 s. During the contact time the ^{1}H nutation frequency was set equal to 50 kHz and that of ^{31}P was ramped through the Hartmann−Hahn matching sideband.[31]

The ^{31}P{^{1}H} Lee-Goldburg CP heteronuclear correlation (LG-CP HETCOR) spectra were measured at a spinrate of 10 kHz. The flip angle of the pulse after the t_1 evolution is adjusted so that the spin-temperature inversion can be realized by phase alternating the first $\pi/2$ pulse. During the contact time (2 ms) the ^{1}H nutation frequency and the resonance offset were set equal to 50 and 35.35 kHz, respectively, to fulfill the Lee-Goldburg irradiation condition. Proton decoupling during the acquisition time was set to 60 kHz. Quadrature detection in the F_1 dimension was achieved by the hypercomplex approach. Typically, for each t_1 increment 32 transients were accumulated, and a total of 256 increments were done at steps of 10 μs.

The ^{31}P DQ experiments were carried out under MAS spinning frequency of 10 kHz based on the so-called HSMAS-DQ technique.[32,33] To prepare the initial spin system identically for each transient, a saturation comb was applied prior to the recovery delay (12 s). During the DQ excitation and reconversion periods, the ^{31}P $\pi/2$ and π pulses were set to 3 and 12 μs long, respectively. The π pulse trains were phase cycled according to the XY-8 scheme.[34] The DQ reconversion period was set equal to the excitation period. Proton decoupling was set to 100 and 60 kHz during the DQ excitation/reconversion periods and the acquisition time, respectively. A more detailed description of the experiment was given elsewhere.[33] The pulse sequences used for the ^{31}P-^{31}P DQ measurements and ^{31}P{^{1}H} Lee-Goldburg CP heteronuclear correlation (LG-CP HETCOR) are shown in Figure 1.

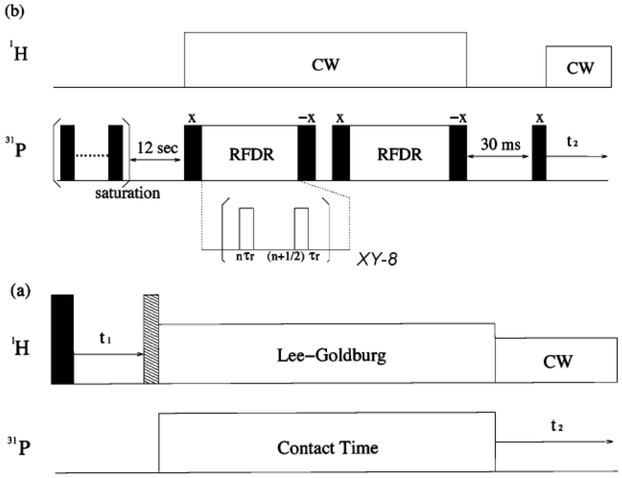

Figure 1. Pulse sequences used for the (a) ^{31}P{^{1}H} LG-CP heteronuclear correlation. The filled and open rectangles denote 90° and 180° pulses, respectively. The shaded rectangle represents a pulse with a flip angle equal to 144.7° for our spectrometer (b) ^{31}P double-quantum measurements.

Results and Analyses

Glass Preparation. The SEM image of the glass samples before SBF soaking is shown in Figure 2a, in which beads of diameter ca. 3 μm were observed. The glass beads were shown to be amorphous by XRD measurements. For comparison, another batch of glass sample was prepared using the same protocol except that no template molecules were added. The gel glasses hence obtained have very irregular sizes and morphologies (see Figure 2b), and they are not considered any further in the subsequent discussion.

SEM, EDX and BET surface areas. A series of samples were obtained by soaking the glass beads in SBF for different periods, viz. 20 min, 1 h, 3 h, 6 h, 12 h and 21.5 h. All the soaked glass samples will henceforth be labeled based on their soaking times. Referring to the SEM image of the 3-hr sample shown in Figure 3a, there are trace amounts of minerals deposited on the glass surface. As expected, the SEM images of samples with longer soaking time show that more minerals are deposited (data not shown). Figure 3b shows the SEM image of the 21.5-hr sample. The minerals deposited on the glass surface have a morphology similar to the crystal habit of apatite formed on bioactive glasses.[35,36] In principle we can use EDX to determine the Ca/P ratio of the minerals. However, the high calcium content of our base glass rendered this analysis not trivial. Since our instrument has only limited resolution, we carefully selected the mineral debris which were remote from any glass beads for our EDX analysis. The average Ca/P ratios for the 6-hr, 12-hr and 21.5-hr samples were found to be 1.47, 1.47 and 1.63, respectively. The Ca/P ratio is calculated as 1.67 based on the ideal

---

(31) Metz, G.; Wu, X. L.; Smith, S. O. *J. Magn. Reson. A* **1994**, *110*, 219.
(32) Oyler, N. A.; Tycko, R. *J. Phys. Chem. B* **2002**, *106*, 8382.
(33) Tseng, Y. H.; Mou, Y.; Mou, C. Y.; Chan, J. C. C. *Solid State Nucl. Magn. Reson.* **2005**, *27*, 266.
(34) Gullion, T.; Baker, D. B.; Conradi, M. S. *J. Magn. Reson.* **1990**, *89*, 479.
(35) Li, P. J.; Ohtsuki, C.; Kokubo, T.; Nakanishi, K.; Soga, N.; Nakamura, T.; Yamamuro, T. *J. Am. Ceram. Soc.* **1992**, *75*, 2094.
(36) Li, P.; Nakanishi, K.; Kokubo, T.; de Groot, K. *Biomaterials* **1993**, *14*, 963.

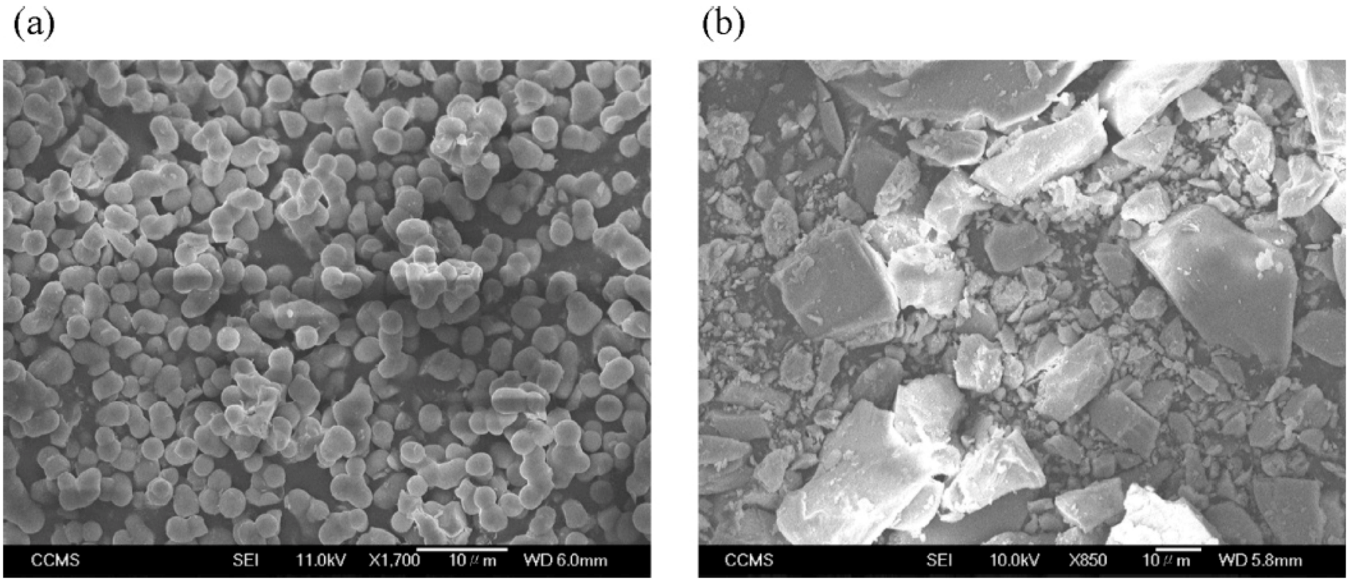

Figure 2. SEM images of the glasses prepared (a) with poly(acrylic acid)s used as the templates and (b) without template molecules.

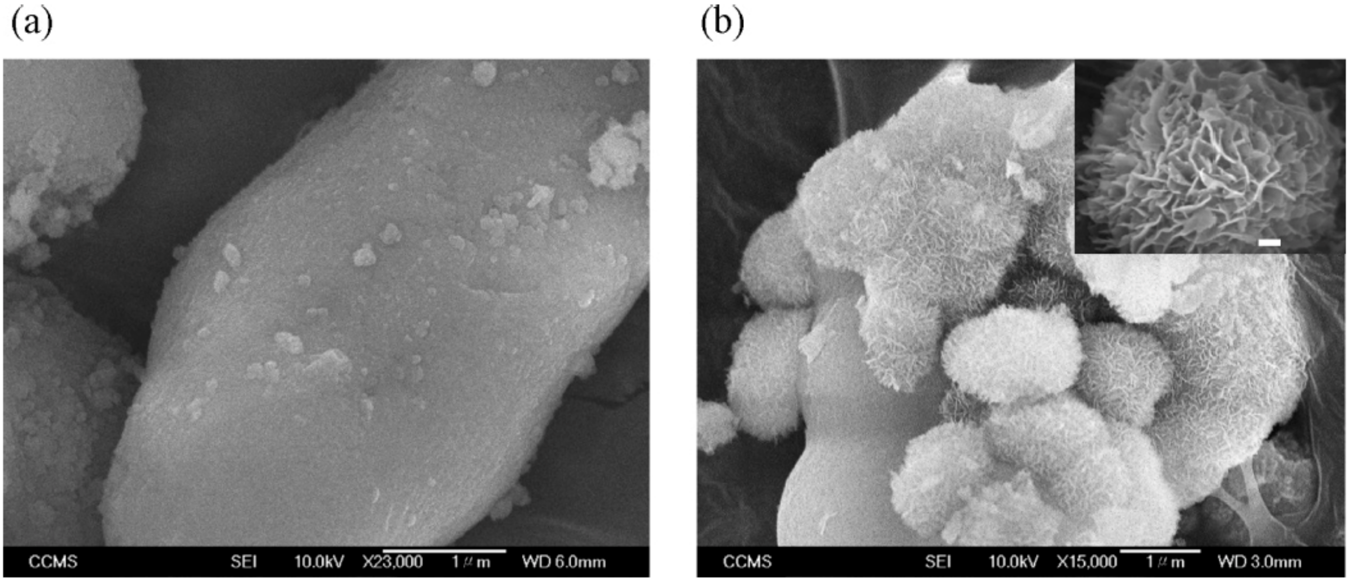

Figure 3. SEM images of the glass beads soaked in SBF for (a) 3 h and (b) 21.5 h. The scale bar of the inset is of 100 nm.

stoichiometry of pure HAp. We are not able to find any debris in the 3-hr sample even after sonification. Before soaking in SBF solution, the glass sample has a BET surface area of 140 m^2/g. As the soaking time increases, the BET surface areas of the samples eventually increase to nearly 300 m^2/g.

XRD and FT-IR. To identify the minerals formed on the glass surface, the XRD patterns of our sample series were measured. Referring to Figure 4, there are several sharp diffraction peaks (marked by dots and asterisks) clearly observed for the 1-hr, 3-hr and 6-hr samples. The peaks marked by asterisks originate from calcite but we are not able to identify the peak marked by dots (Fig. S1 of the Supporting Information). Calcite formation was also identified in a recent XRD study of binary $CaO-SiO_2$ study.[4] For the 6-hr sample, an additional broad peak at 2θ equal to 32° becomes apparent (marked by an arrow), suggesting the incipient formation of a low crystallinity apatite-like phase on the glass surface.[37] As the soaking time increases further to 21.5 h, the overall diffraction pattern becomes quite similar to that of crystalline HAp.[35,37] However, the resolution of the diffraction pattern remains poor for the 21.5-hr sample. This could be attributed to the size/imperfection/strain of the crystallites.[37,38] Together with the large BET surface area determined for our 21.5-hr sample, the apatite crystallites are likely nanosized. Figure 5 shows the FT-IR data measured for the sample series. The samples were dried at 80 °C for 18 h before the measurements. The absorption peaks corresponding to the P−O bending mode are observed in the 12-hr sample and become more intense in the 21.5-hr sample, revealing the presence of PO_4^{3-} or HPO_4^{2-} ions.[8,25,39] The peak at 875 cm^{-1} is assigned to the CO stretching of CO_3^{2-} ions.[3,7] This CO stretching peak was also clearly observed in other studies of $CaO-SiO_2$ glasses.[7,8] The OH stretch at

---

(37) Vallet-Regi, M.; Romero, A. M.; Ragel, C. V.; LeGeros, R. Z. *J. Biomed. Mater. Res.* **1999**, *44*, 416.

(38) Klug, H. P.; Alexander, L. E. *X-ray diffraction procedures of polycrystalline and amorphous materials*. John Wiley & Sons: New York, 1974.

(39) Takadama, H.; Kim, H. M.; Kokubo, T.; Nakamura, T. *Chem. Mater.* **2001**, *13*, 1108.

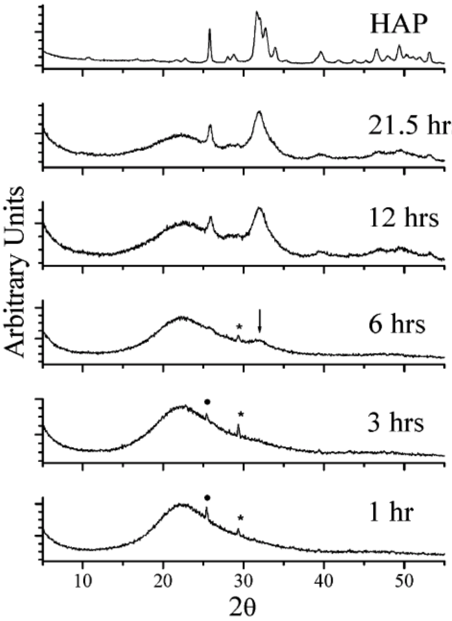

Figure 4. XRD patterns of the HAp crystalline standard and the glass samples with selected soaking periods in SBF. The peaks marked with asterisks are due to calcite. The peaks marked with filled circles are not identified. The arrow marks the onset of the diffraction peak of the apatite crystalline phase.

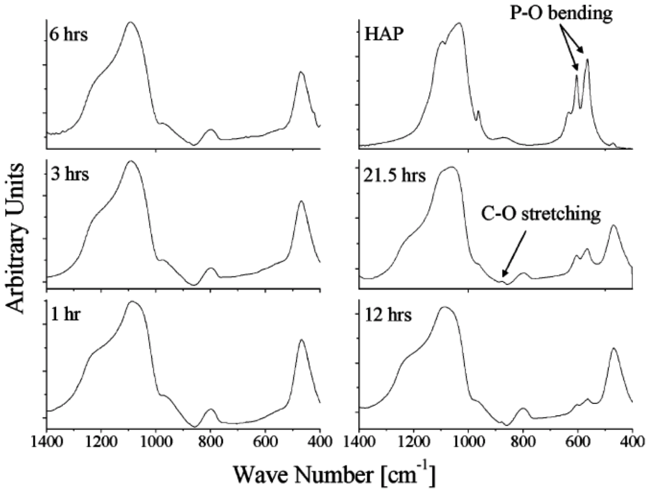

Figure 5. FT-IR spectra of the HAp crystalline standard and the glass samples with selected soaking periods in SBF.

3572 cm^{-1} is not observed for our soaked samples because of the poor crystallinity of the apatite crystallites.

^{31}P MAS NMR. The ^{31}P spin−lattice relaxation times of our sample series were ca. 35 s. All the ^{31}P MAS spectra of the sample series invariably have a major peak positioned at around 3.3 ± 0.2 ppm, which is tentatively assigned to be the PO_4^{3-} signal because the signals of HPO_4^{2-} ions in octacalcium phosphate and monetite are more shielded ($\leq$ 1.4 ppm).[40,41] To verify that the ^{31}P signal is not arising from incomplete washing, a control sample was prepared with soaking time in SBF of 20 s only. The very weak ^{31}P signal of the control sample proves that the amounts of the PO_4^{3-} ions due to residual SBF are very minor in all the soaked samples (data not shown). The amounts of the PO_4^{3-} ions deposited on the glass surface were determined by NMR spin-counting technique. Figure 6 plots the full line widths at half-maximum ($\Delta\nu_{(1/2)}$) and the percentage by mass of PO_4^{3-} versus the soaking times. While the ^{31}P chemical shift data do not show any significant variation, there is an interesting trend in the line width data. The $\Delta\nu_{(1/2)}$ data of the 20-min, 30-min, 1-hr and 3-hr samples are ca. 5.8 ppm and decrease down to ca. 4.3 ppm for other samples with longer soaking times. The line widths were estimated by fitting the peak by a 50% Gaussian- 50% Lorentzian line shape. The error bars were estimated by comparing the fitted line widths and those measured directly at half-maximum. The line width data indicate that initially (soaking time $\leq$ 3 h) the phosphate ions deposited on the glass surface were largely amorphous. This interpretation is consistent with an earlier study,[42] in which the ^{31}P line width of synthetic amorphous calcium phosphate was reported to be ca. 5 ppm larger than that of crystalline HAp. As expected, the amount of PO_4^{3-} ions increases monotonically as the soaking time increases. The amount of deposited PO_4^{3-} ions reached a plateau after 12-hr soaking due to the consumption of the phosphate ions in the SBF solution.

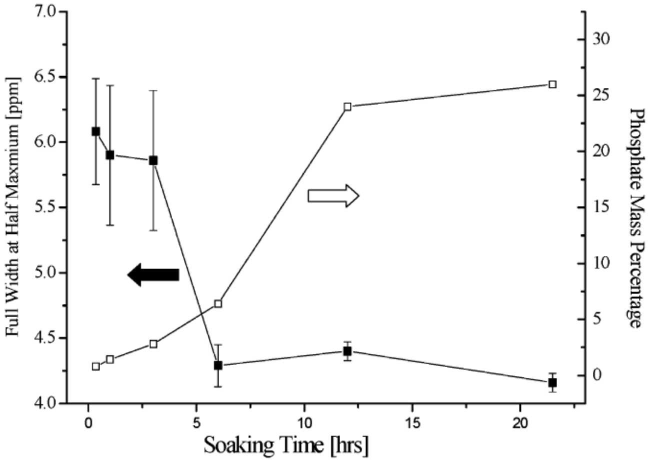

Figure 6. Plot of fullwidths at half-maximum of the ^{31}P MAS signals and the mass percentage of the phosphate ions.

^{31}P{^{1}H} LG-CP HETCOR. The proximities of the phosphate and hydrogen sites were studied by ^{31}P{^{1}H} LG-CP HETCOR. Figure 7 shows the HETCOR spectrum of the 21.5-hr sample. Since the spin diffusion among the ^{1}H spins during the CP contact time is suppressed, our data clearly show that there are at least two different phosphorus species formed on the glass surface. While the ^{31}P peak correlated with the ^{1}H signal at 0.2 ppm is readily assigned to HAp (henceforth referred to as the apatite component),[43] it is not trivial to assign the ^{31}P signal correlated with the ^{1}H signal at 5.0 ppm. Figure 8 shows the projection of Figure 7 along the ^{1}H dimension which has two salient features. First, the sideband pattern has a large span (ca. 45 kHz) but the overall sideband intensities is significantly less than the center band at 5.0 ppm. It implies that there exists another signal at 5.0 ppm which does not have any significant

---

(40) Tseng, Y. H.; Zhan, J. H.; Lin, K. S. K.; Mou, C. Y.; Chan, J. C. C. *Solid State Nucl. Magn. Reson.* **2004**, *26*, 99.

(41) Wu, Y. T.; Glimcher, M. J.; Rey, C.; Ackerman, J. L. *J. Mol. Biol.* **1994**, *244*, 423.

(42) Tropp, J.; Blumenthal, N. C.; Waugh, J. S. *J. Am. Chem. Soc.* **1983**, *105*, 22.

(43) Yesinowski, J. P.; Eckert, H. *J. Am. Chem. Soc.* **1987**, *109*, 6274.

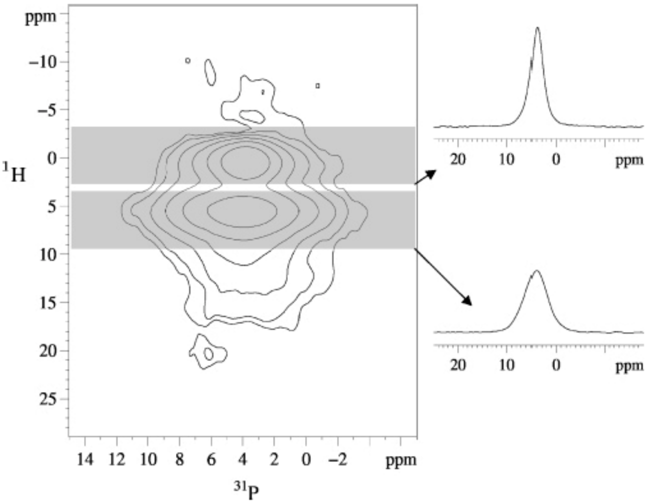

Figure 7. Two-dimensional $^{31}P\{^1H\}$ LG-CP HETCOR spectrum measured for the 21.5-hr sample. The projections of the shaded area along the ^{31}P dimension were shown to highlight the different $\Delta\nu_{(1/2)}$ for the two major spectral components.

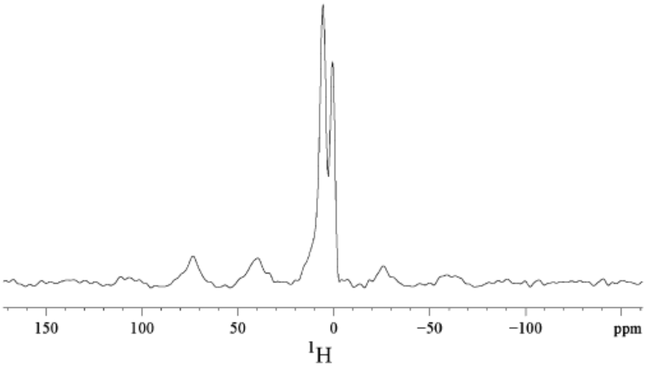

Figure 8. ^1H projection of the $^{31}P\{^1H\}$ LG-CP HETCOR spectrum of Figure 7.

spinning sideband manifold. Second, the sideband pattern is rather asymmetric compared with those arising from isolated structural water.[43] In comparison, the CP−HETCOR spectra reported for bovine cortical bone is quite similar to ours except that the H_2O signal does not have any significant spinning sidebands.[20] Therefore, we suggest that the ^1H signal at 5.0 ppm is due to two spectral components. The component with weaker sideband manifold is presumably due to the surface-absorbed water with weak dipolar couplings to the PO_4^{3-} ions.[20] The one with significant sideband intensities is due to the structural water hydrogen-bonded to the PO_4^{3-} ions, which may undergo the following hydrolysis reaction:

$$PO_4^{3-} + H_2O = HPO_4^{2-} + OH^-$$

The ^{31}P chemical shift value (3.2 ppm) suggests that the hydrogen bonding is modulated by molecular motions and/or chemical exchange because ^{31}P NMR measurements on octacalcium phosphate show that the isolated PO_4^{3-} ions, hydrogen bonded PO_4^{3-} ions and the HPO_4^{2-} ions have chemical shifts equal to 3.7, 2.0 and −0.2 ppm, respectively.[40] Also, it had been pointed out in a ^{31}P NMR study of nonstoichiometric HAp that HPO_4^{2-} ions undergoing molecular motions would have the same isotropic chemical shift as the PO_4^{3-} ions in HAp, and that discrete and rigid HPO_4^{2-} ions are not found in nonstoichiometric HAp samples with Ca/P ratios equal to 1.46 and 1.33.[16]

The apatite component of the LG-CP HETCOR spectrum (Figure 7) has ^{31}P $\Delta\nu_{(1/2)}$ equal to 2.8 ppm. Since the $\Delta\nu_{(1/2)}$ value of crystalline HAp was found to be 1.7 ppm, the apatite nanocrystals formed on the glass surface appears to be structurally close to crystalline HAp. The ^{31}P signal correlated to both surface and structural water signals has $\Delta\nu_{(1/2)}$ equal to 5.3 ppm (the water component), showing that the spatial arrangements of these phosphate ions are more disordered. Additional LG-CP HETCOR spectra were obtained for other glass samples with shorter soaking times. The LG-CP HETCOR spectrum of the 3-hr sample does not have any apatite component and the spectra of the 6-hr and 21.5-hr samples have very similar spectral features except that the relative intensity of the apatite component is larger for the 21.5-hr sample (Figs. S2 and S3 of the Supporting Information). Hence, the step like decrease in the line width data of the 6-hr sample (Figure 6) is due to the incipient formation of apatite crystallites. For the 21.5-hr sample, the $\Delta\nu_{(1/2)}$ value of the ^{31}P MAS signal (4.2 ppm) indicates that a significant portion of the phosphorus species still has considerable structural disorder, which is due to both the surface phosphorus and the phosphorus species in an amorphous state. Unfortunately, it is difficult to unambiguously determine the relative populations of these two components by deconvoluting the MAS spectra. In principle, one may measure a series of LG-CP HETCOR spectra with different contact times for each sample in order to monitor the changes in the CP dynamics of the different phosphate species. In view of the difficulties of controlling the water content of our samples over a long period, we do not plan to perform these extremely time-consuming experiments.

$^{31}P\{^1H\}$ CPMAS with Variable Contact Times. To investigate the protonation state of the phosphorus species, $^{31}P\{^1H\}$ variable contact time CPMAS experiments were measured for our sample series and two model crystalline compounds, viz. HAp and monetite. The ^{31}P signals as a function of contact time were fitted by the following equation:

$$I(t) = I_0\{1 - \exp(-t/\tau_{CP})\}\exp(-t/T_{1\rho}^H)$$

The τ_{CP} values of HAp and monetite were found to be 795 ± 32 and 314 ± 14 μs, respectively. The $T_{1\rho}^H$ value of monetite was measured to be 9.8 ± 0.4 ms but our contact time scale ($\leq$ 8 ms) is too short to characterize the $T_{1\rho}^H$ of HAp. As expected, in monetite the stronger ^{31}P-^1H and ^1H-^1H dipolar interactions result in the shorter τ_{CP} and $T_{1\rho}^H$ values, respectively. Figure 9 summarizes the τ_{CP} and $T_{1\rho}^H$ values of selected glass samples, where the raw data can be found in Fig. S4 of the Supporting Information. The τ_{CP} values of the samples with soaking times $\leq$ 3 h are quite similar to that measured for HAp. There is a step increase in τ_{CP} for the 6-hr sample. While the τ_{CP} values are similar for the 6-hr and the 12-hr samples, there is another increase in τ_{CP} for the 21.5-hr sample. Invariably all the τ_{CP} values are much larger than that determined for monetite. On the other hand, the $T_{1\rho}^H$ values of the soaked samples increase

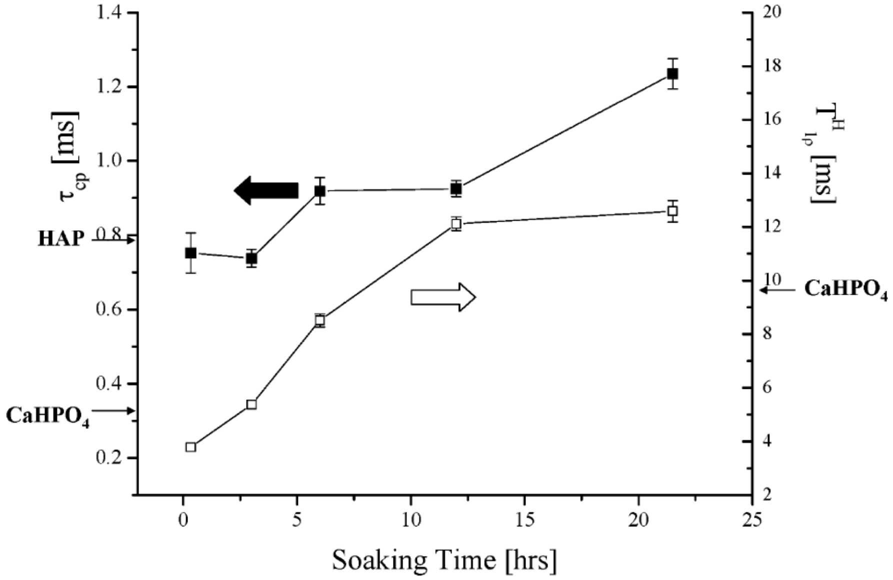

Figure 9. Plot of the τ_{CP} and $T^H_{1\rho}$ values of selected glass samples. The arrows mark the values corresponding to crystalline HAp and monetite.

gradually and reach a plateau after 12 h of SBF soaking. In an XPS study it has been concluded that a high population of HPO_4^{2-} ions is present on the surface of CaO(20%)-SiO$_2$-(80%) glasses after soaking in SBF.[5] Although our τ_{CP} data can completely rule out the presence of any rigid and discrete HPO_4^{2-} ions, these data remain compatible with the presence of HPO_4^{2-} ions undergoing restricted motion and/or chemical exchange. Consistent with the LG-CP HETCOR data, the relatively short $T^H_{1\rho}$ values indicate that the ^{31}P CP signals of our samples with short soaking times are mainly arising from the phosphate ions interacting with both the surface water and structural water, whereby dipolar coupling among the protons of the water molecules is significant. As the phosphate structure becomes more HAp-like, the decrease in the amount of structural water relative to the phosphate ions results in an increase in $T^H_{1\rho}$. The gradual increase in τ_{CP} reveals that the ^{31}P-^1H CP dynamics between the OH$^-$ and the PO_4^{3-} species of the apatite component are weaker than that in crystalline HAp. Presumably the OH$^-$ ions are in chemical exchange with other water molecules.

^{31}P Double-Quantum NMR. When two or more nuclear spins are close in proximity, they become coupled through the homonuclear dipole–dipole interaction. The magnitude of such interaction is inversely proportional to the third power of the internuclear distance. The so-called DQ coherence is a concerted evolution of coupled spins, which can be excited and detected under the irradiation of carefully designed rf pulse sequence. Referring to the HSMAS-DQ pulse sequence shown in Figure 1, a systematic variation in the DQ excitation and reconversion periods can be used to probe the van Vleck's second moment of the coupled spins,[44] whose magnitude depends on both the number of interacting spins and the internuclear distances:

$$M_2 = \frac{3}{5}\gamma^4\hbar^2 I(I+1)\sum_j \frac{1}{r_j^6}$$

Qualitatively, the larger the second moment, the faster the growth of the DQ signal. As a crude approximation, the build up of the DQ signals is described by a parabolic function.[45,46] By numerical simulations of multiple-spin systems, we have recently shown that the DQ signals will be attenuated by dephasing effects due to other passive spins.[33] Therefore, we chose to approximate the decay of the DQ signals by a Gaussian function for our multiple-spin systems.[47] Overall, the following empirical equation is used to fit the DQ signals as a function of excitation time:

$$I(\tau_{exe}) = A\tau_{exe}^{\ 2} \exp\{-\tau_{exe}^{\ 2}/B\}$$

where the rate of the initial DQ signal buildup is described by the parameter A, which is proportional to the M_2 of the interacting nuclear spins; the constant B describes the decay of the DQ signal. The excitation profile of the DQ signals, which had been normalized with respect to the MAS signals measured under identical conditions (spinning frequency, saturation comb and relaxation delay), was fitted by the above empirical equation (Fig. S5 of the Supporting Information). The variation of the parameter A reflects the same variation in M_2. We also measured the A value for HAp so that we can calibrate the proportionality constant between A and M_2 (Table 2). Figure 10 shows the M_2 values of the soaked samples as a function of soaking time. The results indicate that initially the M_2 value of the phosphate units is about 53% of that of the crystalline HAp (M_2^{HAp}). Then, the M_2 increases to 83% of M_2^{HAp} for the 1-hr sample. As the soaking time increases further, the M_2 values increase only moderately and become eventually equal to that of crystalline HAp within experimental error. For comparison, the M_2 value determined by Ackerman and co-workers for the highly crystalline and poorly crystalline type B carbonate apatite are both equal to 75% of M_2^{HAp}.[48] Therefore, the apatite structure formed on the glass surface appears to be different

---

(44) Abragam, A. *Principles of Nuclear Magnetism*. Clarendon Press: Oxford, 1961.
(45) Bertmer, M.; Eckert, H. *Solid State Nucl. Magn. Reson.* **1999**, *15*, 139.
(46) Gunne, J.; Eckert, H. *Chem.-Eur. J.* **1998**, *4*, 1762.
(47) Engelsberg, M.; Norberg, R. E. *Phys. Rev. B* **1972**, *5*, 3395.

Table 2. Fitting Parameters *A* and *B* of the ^{31}P Homonuclear DQ Excitation Profiles. The Proportionality Constant between *A* and M_2 Is Calibrated by Comparing the *A* Value and the Calculated M_2 of Crystalline HAp

Sample	A (ms^{-2})	B (ms^2)	M_2 ($\times 10^6$ rad^2/s^2)
20-min	4.9 ± 0.7	5.4 ± 0.5	4.0 ± 0.6
1-hr	7.7 ± 0.7	6.5 ± 0.4	6.3 ± 0.5
3-hr	7.8 ± 0.3	7.5 ± 0.2	6.4 ± 0.3
6-hr	7.9 ± 0.7	7.8 ± 0.4	6.5 ± 0.6
12-hr	9.0 ± 0.4	7.2 ± 0.3	7.4 ± 0.4
21.5-hr	9.1 ± 0.5	6.8 ± 0.3	7.4 ± 0.4
HAp	9.4 ± 0.4	6.1 ± 0.2	7.7[a]
Octacalcium phosphate	- -	- -	6.9[a,b]

[a] Calculated values based on the X-ray structures of crystalline HAp (ref 54) and octacalcium phosphate (ref 59). [b] The average of the six phosphorus sites.

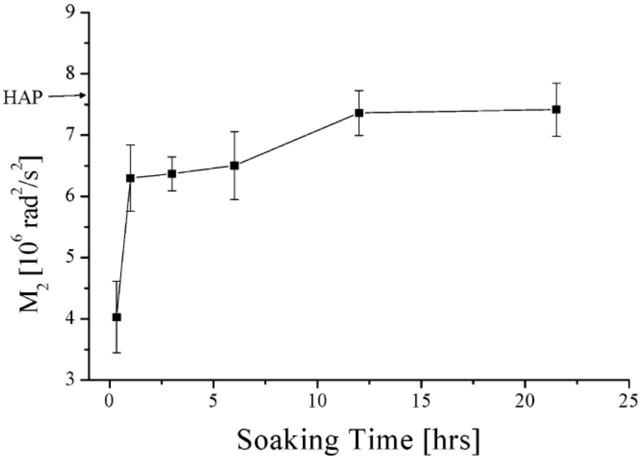

Figure 10. Plot of the ^{31}P-^{31}P second moment for selected samples. The arrow marks the value corresponding to crystalline HAp.

from that of synthetic type B carbonate apatite, in which some of the phosphate ions are substituted by carbonate ions (ca. 9% by mass).[49] We believe that the carbonate content of the apatite formed on our glass surface, if any, must be substantially less than 9% by mass. We note in passing that octacalcium phosphate has been postulated as a precursor phase of apatite formation in biomineralization. For comparison, the calculated M_2 value of octacalcium phosphate is also included in Table 2. On the other hand, since the values of the parameter B are affected by both the ^{31}P spin–spin relaxation times and the spatial arrangement of the interacting phosphorus species, it is difficult to interpret the data trend unequivocally.

Discussion and Conclusion

Bioactive Glass Beads. Our sol–gel glass system has the salient feature that it is rather uniform in size and morphology (Figure 2a). Furthermore, the use of high-humidity drying is expected to produce a homogeneous distribution of the calcium ions in our base glass.[50] Consequently, our experimental data should faithfully reflect the chemical environments of the phosphate ions at different stages of apatite formation, although it has been shown that the chemical composition of the apatite layer formed on bioactive glasses is very heterogeneous.[5] While glass beads of similar size (2–3 microns) have been reported earlier,[29] to our knowledge this work represents the first attempt in the literature to investigate their bioactivity.

^{31}P{^{1}H} LG-CP HETCOR Spectroscopy. ^{31}P{^{1}H} CP–HETCOR spectra have been reported for crystalline HAp and bovine cortical bone.[18–20] In particular, the ^{1}H homonuclear decoupled CP–HETCOR approach has been demonstrated for a long time.[18] This sophisticated multiple-pulse based approach, which can suppress ^{1}H-^{1}H spin diffusion during the contact time period, has not been widely applied in the study of calcified tissues because of the rather involved setup procedure. In this work, we have demonstrated that the LG-CP method, which was originally developed for the study of ^{1}H-^{13}C multiple-spin systems,[26,27] can be easily and successfully applied for the study of apatite minerals. Because the LG irradiation can effectively suppress the homonuclear dipolar coupling, our spectrum shown in Figure 7 has a much better resolution than the one measured based on the regular CP approach (data not shown). In a recent study of bone and dental materials, it has been shown that CP with very short contact time will selectively enhance the signals of the phosphorus species near the apatite surface.[48] For the sake of spectral sensitivity, however, we deliberately used a longer contact time (2 ms) for our LG-CP HETCOR measurement because LG irradiation will attenuate the polarization transfer rate considerably.[26,27] Furthermore, our glass samples after the SBF soaking were merely dried at room temperature under reduced pressure, therefore the apatites of colloidal dimensions contained a significant amount of surface-adsorbed water which might have condensed to form a "liquidlike" layer.[43] As a result, the rapid chemical exchange and molecular motions of the surface waters may also have attenuated the polarization transfer rate of the phosphorus species near the apatite surface.

^{31}P-^{31}P Second Moment. For the SBF soaking condition used in our study, heterogeneous nucleation (phosphate cluster adsorption on substrate surface) has been shown to be the predominant mechanism of HAp formation.[51] In a subsequent study, micropatterns of HAp have been obtained by modifying the electrostatic potential of the substrate surface.[52] Similarly, the growth and coalescence of crystallites adsorbed on a surface has been suggested as the mechanism for HAp formation on self-assembled monolayers.[53] Our ^{31}P-^{31}P M_2 values determined for the apatite formed on the glass surface reflects the variation in the "phosphorus density" as a function of soaking time. The M_2 values for spherical cluster sizes of 5 Å, 8 Å, 10, 15, and 20 Å were calculated to be 5.8, 7.0, 7.4, 7.6 and 7.7 × 10^6 rad^2/s^2, based on the geometry of crystalline HAP.[54] These figures show that the increase in M_2 value (× 10^6 rad^2/s^2) from the 20-min sample (4.0 ± 0.6) to the 1-hr sample (6.3 ± 0.5) is most likely due to a significant increase in the local

---

(48) Wu, Y. T.; Ackerman, J. L.; Kim, H. M.; Rey, C.; Barroug, A.; Glimcher, M. J. *J. Bone Miner. Res.* **2002**, *17*, 472.
(49) Fleet, M. E.; Liu, X. *J. Solid State Chem.* **2004**, *177*, 3174.
(50) Zhong, J.; Greenspan, D. C. *J. Biomed. Mater. Res.* **2000**, *53*, 694.
(51) Zhu, P. X.; Masuda, Y.; Yonezawa, T.; Koumoto, K. *J. Am. Ceram. Soc.* **2003**, *86*, 782.
(52) Zhu, P. X.; Masuda, Y.; Koumoto, K. *Biomaterials* **2004**, *25*, 3915.
(53) Tarasevich, B. J.; Chusuei, C. C.; Allara, D. L. *J. Phys. Chem. B* **2003**, *107*, 10367.
(54) Wilson, R. M.; Elliott, J. C.; Dowker, S. E. P. *Am. Miner.* **1999**, *84*, 1406.

phosphorus density instead of crystallite coalescence. The further increase in the M_2 value from the 3-hr sample (6.4 ± 0.3) to the 21.5-hr sample (7.4 ± 0.4) can be ascribed to the formation of the crystalline phase, where the phosphate units are packed closer than those in amorphous state. In principle, the ^{31}P-^{31}P second moment of the minerals deposited on the glass surface can also be obtained by measuring the attenuation of spin−echo intensities as a function of inter-pulse delay under static condition.[48] Although our method is more involved in the experimental setup, it offers a lot better spectral resolution than the spin−echo approach, which has to be carried out under static conditions.

Formation of Apatite. Initially, the phosphorus density of the mineral layer deposited on the glass surface was substantially smaller than that in crystalline HAp. After 1 h of SBF soaking, there was a significant increase in the phosphorus density of the phosphorus species. Presumably an amorphous layer with constituents similar to HAp had formed on the glass surface (Figure 10). The water molecules in the amorphous layer had restricted motion only and some of them were hydrogen-bonded to the neighboring PO_4^{3-} ions, possibly in equilibrium with HPO_4^{2-} (Figure 8). The amorphous layer grew continuously as the soaking time increased. The only noticeable change in the period between 1-hr and 3-hr is that the amount of structural water relative to the phosphate content decreased considerably. This interpretation is consistent with the corresponding increase in the $T_{1\rho}^{H}$ values (Figure 9). After 6 h of SBF soaking, a considerable amount of apatite nanocrystals had been formed (Figures 6). The deposition rate of PO_4^{3-} ions on the glass surface hence increased considerably between 6 and 12 h, presumably due to the epitaxial crystal growth. The PO_4^{3-} deposition was basically completed after 12 h of SBF soaking as evidenced by the moderate increase in phosphate mass percentage after 21.5 h. Overall, our data favor the Hench mechanism concerning the precipitation and crystallization of the phosphate ions and are consistent with the recent results of X-ray spectroscopic study.[9] In view of the fact that calcite is present at the early stage of apatite formation (Figure 4), one should be cautious in interpreting the C−O stretching mode observed in the FT-IR spectra because calcite also has an IR absorption at 875 cm^{-1}. Nevertheless, another characteristic absorption of calcite (a weaker absorption at 714 cm^{-1}) is not found in our FT-IR spectra.[55]

As an alternative to the Hench mechanism, it has been argued that the gel-silica may provide epitaxial sites for the growth of HAp.[56] However, if it were the case for our glass system, the line widths of the ^{31}P signals would not have such a big variation as illustrated in Figure 6. On the other hand, Hayakawa et al. reported that the ^{31}P signals indeed have very similar line widths for Na_2O (20%)-SiO_2 (80%) glasses with different soaking periods in SBF. In addition, recent X-ray photoelectron spectroscopy and TEM-EDX studies on a similar glass system shows that the formation of calcium silicate precede the precipitation of calcium phosphate on the glass surface.[39,57] Therefore, it is not clear if a universal mechanism exists for the apatite formation on all kinds of bioactive glasses. Also, since the nature of the calcium phosphate phases precipitated from the SBF solution depends strongly on the solution composition, it is helpful to maintain a more constant SBF composition for studies relevant to in-vivo applications.[58]

Acknowledgment. This work was supported by a grant from the National Science Council under the contract number NSC 93-2113-M-002-016. The insightful and detailed comments of the anonymous reviewers are gratefully acknowledged.

Supporting Information Available: Detailed assignment of the XRD pattern of the 1-hr and 3-hr samples, LG-CP HETCOR spectra of the 3-hr and 6-hr samples, fittings of the CPMAS raw data, fittings of the DQ raw data. This material is available free charge via the Internet at http://pubs.acs.org.

CM050654C

---

(55) Aizenberg, J.; Muller, D. A.; Grazul, J. L.; Hamann, D. R. *Science* **2003**, *299*, 1205.
(56) Karlsson, K. H.; Froberg, K.; Riingbom, T. *J. Non-Cryst. Solids* **1989**, *112*, 69.
(57) Takadama, H.; Kim, H. M.; Kokubo, T.; Nakamura, T. *J. Am. Ceram. Soc.* **2002**, *85*, 1933.
(58) Vallet-Regi, M.; Ragel, C. V.; Salinas, A. J. *Eur. J. Inorg. Chem.* **2003**, 1029.
(59) Mathew, M.; Brown, W. E.; Schroeder, L. W.; Dickens, B. *J. Cryst. Spec. Res.* **1988**, *18*, 235.

II-B. Characterization of Octacalcium Phosphate

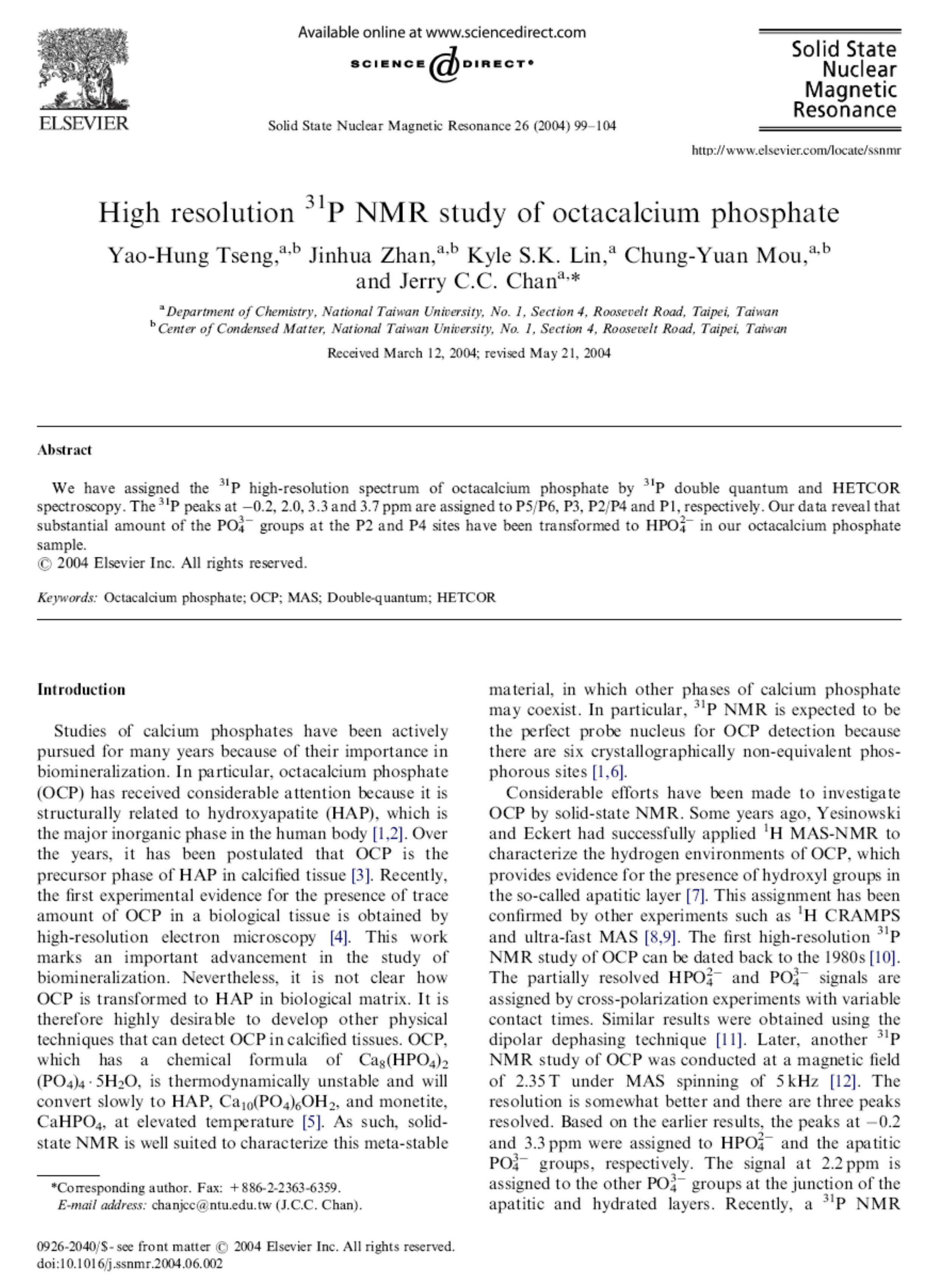

Available online at www.sciencedirect.com
SCIENCE DIRECT•

Solid State Nuclear Magnetic Resonance 26 (2004) 99–104

Solid State Nuclear Magnetic Resonance

http://www.elsevier.com/locate/ssnmr

High resolution ^{31}P NMR study of octacalcium phosphate

Yao-Hung Tseng,[a,b] Jinhua Zhan,[a,b] Kyle S.K. Lin,[a] Chung-Yuan Mou,[a,b] and Jerry C.C. Chan[a,]*

[a] *Department of Chemistry, National Taiwan University, No. 1, Section 4, Roosevelt Road, Taipei, Taiwan*
[b] *Center of Condensed Matter, National Taiwan University, No. 1, Section 4, Roosevelt Road, Taipei, Taiwan*

Received March 12, 2004; revised May 21, 2004

Abstract

We have assigned the ^{31}P high-resolution spectrum of octacalcium phosphate by ^{31}P double quantum and HETCOR spectroscopy. The ^{31}P peaks at −0.2, 2.0, 3.3 and 3.7 ppm are assigned to P5/P6, P3, P2/P4 and P1, respectively. Our data reveal that substantial amount of the PO_4^{3-} groups at the P2 and P4 sites have been transformed to HPO_4^{2-} in our octacalcium phosphate sample.

Keywords: Octacalcium phosphate; OCP; MAS; Double-quantum; HETCOR

Introduction

Studies of calcium phosphates have been actively pursued for many years because of their importance in biomineralization. In particular, octacalcium phosphate (OCP) has received considerable attention because it is structurally related to hydroxyapatite (HAP), which is the major inorganic phase in the human body [1,2]. Over the years, it has been postulated that OCP is the precursor phase of HAP in calcified tissue [3]. Recently, the first experimental evidence for the presence of trace amount of OCP in a biological tissue is obtained by high-resolution electron microscopy [4]. This work marks an important advancement in the study of biomineralization. Nevertheless, it is not clear how OCP is transformed to HAP in biological matrix. It is therefore highly desirable to develop other physical techniques that can detect OCP in calcified tissues. OCP, which has a chemical formula of $Ca_8(HPO_4)_2(PO_4)_4 \cdot 5H_2O$, is thermodynamically unstable and will convert slowly to HAP, $Ca_{10}(PO_4)_6OH_2$, and monetite, $CaHPO_4$, at elevated temperature [5]. As such, solid-state NMR is well suited to characterize this meta-stable material, in which other phases of calcium phosphate may coexist. In particular, ^{31}P NMR is expected to be the perfect probe nucleus for OCP detection because there are six crystallographically non-equivalent phosphorous sites [1,6].

Considerable efforts have been made to investigate OCP by solid-state NMR. Some years ago, Yesinowski and Eckert had successfully applied ^{1}H MAS-NMR to characterize the hydrogen environments of OCP, which provides evidence for the presence of hydroxyl groups in the so-called apatitic layer [7]. This assignment has been confirmed by other experiments such as ^{1}H CRAMPS and ultra-fast MAS [8,9]. The first high-resolution ^{31}P NMR study of OCP can be dated back to the 1980s [10]. The partially resolved HPO_4^{2-} and PO_4^{3-} signals are assigned by cross-polarization experiments with variable contact times. Similar results were obtained using the dipolar dephasing technique [11]. Later, another ^{31}P NMR study of OCP was conducted at a magnetic field of 2.35 T under MAS spinning of 5 kHz [12]. The resolution is somewhat better and there are three peaks resolved. Based on the earlier results, the peaks at −0.2 and 3.3 ppm were assigned to HPO_4^{2-} and the apatitic PO_4^{3-} groups, respectively. The signal at 2.2 ppm is assigned to the other PO_4^{3-} groups at the junction of the apatitic and hydrated layers. Recently, a ^{31}P NMR

---

*Corresponding author. Fax: +886-2-2363-6359.
E-mail address: chanjcc@ntu.edu.tw (J.C.C. Chan).

0926-2040/$ - see front matter © 2004 Elsevier Inc. All rights reserved.
doi:10.1016/j.ssnmr.2004.06.002

spectrum of OCP has been reported at 7.05 T and 9 kHz [13], which shows four well-resolved ^{31}P resonances. Unfortunately, the authors did not make any assignment at all because it is not trivial to assign the ^{31}P resonances based on the chemical shift data alone. Without a complete assignment of the ^{31}P spectrum of OCP, it is premature to apply ^{31}P NMR for the detection of OCP in biological tissues.

In this work, we demonstrate that ^{31}P double-quantum spectroscopy and $^{31}P\{^1H\}$ heteronuclear correlation (HETCOR) can be used to assign all the four resolved peaks of the ^{31}P MAS spectrum measured at 7.05 T and 10 kHz. Our assignment will not only establish ^{31}P NMR as a sensitive method for OCP detection, but also help facilitate the study of OCP to HAP transformation, which has been postulated as the mechanism for the formation of biological apatites [3].

2. Materials and methods

2.1. Sample preparation and characterization

Urea (99.5%), sodium phosphate monobasic dehydrate ($H_2NaPO_4 \cdot 2H_2O$) (99%) and calcium nitrate tetrahydrate ($Ca(NO_3)_2 \cdot 4H_2O$) (99%) were used as received (Acros). 10 mmol $Ca(NO_3)_2$ $4H_2O$, 10 mmol H_2NaPO_4 $2H_2O$ and 20 mmol urea were dissolved in 400 ml doubly distilled water and then sealed in a polypropylene container. The aqueous solution was kept at 100°C for 3 h. The precipitates thus obtained were filtered, washed and then dried at 60°C for 1 day.

X-ray diffraction analysis was performed on a Philips X'Pert diffractometer, using Cu Kα radiation ($\lambda = 1.5418$ Å). The field emission scanning electron micrograph (FE-SEM) was taken on a JEOL-JSM-6700F field emission scanning electron microscope operating at 10 kV.

2.2. Solid-state NMR

All NMR experiments were carried out at ^{31}P and ^1H frequencies of 121.5 and 300.1 MHz, respectively, on a Bruker DSX300 NMR spectrometer equipped with a commercial 4 mm MAS-NMR probe. All spectra were measured at room temperature. The sample was confined to the middle $\frac{1}{3}$ of the rotor volume using Teflon spacers. MAS frequency variation was limited to ± 3 Hz using a commercial pneumatic control unit. Chemical shifts were externally referenced to 85% phosphoric acid and TMS for ^{31}P and ^1H, respectively. The ^{31}P spin relaxation times (T_1) were determined by the saturation-recovery technique. The pulse sequences used for the ^{31}P double-quantum (DQ) experiment and $^{31}P\{^1H\}$ HETCOR measurements are shown in Fig. 1.

^{31}P DQ experiment was carried out under MAS spinning frequency of 6 kHz. Quadrature detection in the F_1 dimension was achieved by the hypercomplex approach. For each t_1 increment 64 transients were accumulated, and a total of 50 increments were done at steps of one rotor period. Recycle delay of 18 s was applied. To prepare the initial spin system identically for each transient, a saturation comb was applied prior the recycle delay. During the DQ excitation and reconversion periods, the ^{31}P rf nutation frequency was set to 42 kHz. The standard four-step phase cycling of the excitation block was used to select the DQ coherence. Probe ringdown and dc offset artifacts are suppressed by inverting the phase of the reading pulse and alternating addition and subtraction of FID signals. Together with CYCLOPS our phase cycling has a total of 32 steps.

The heteronuclear correlation (HETCOR) spectrum of OCP is measured by $^{31}P\{^1H\}$ cross polarization at a spinrate of 10 kHz. Recycle delay was set to 10 s. Contact time was set to 2.5 ms. During the contact time the ^1H nutation frequency was set equal to 50 kHz and that of ^{31}P was ramped through the Hartmann Hahn matching sideband [14]. Other conditions were similar to

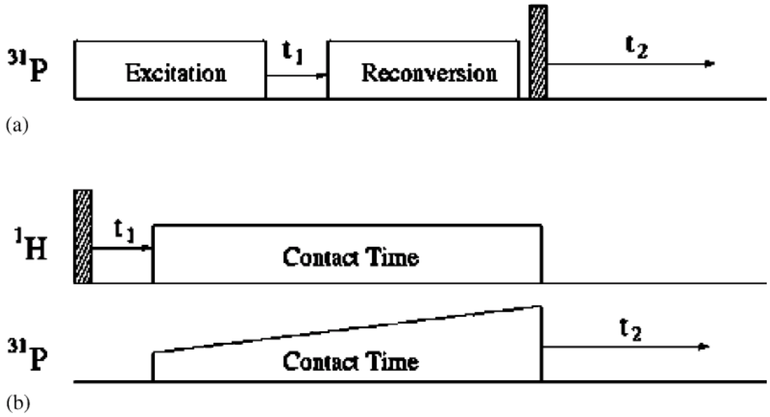

Fig. 1. Pulse sequences used for the (a) ^{31}P double-quantum and (b) $^{31}P\{^1H\}$ HETCOR measurements. The shaded rectangle denotes $\pi/2$ pulse.

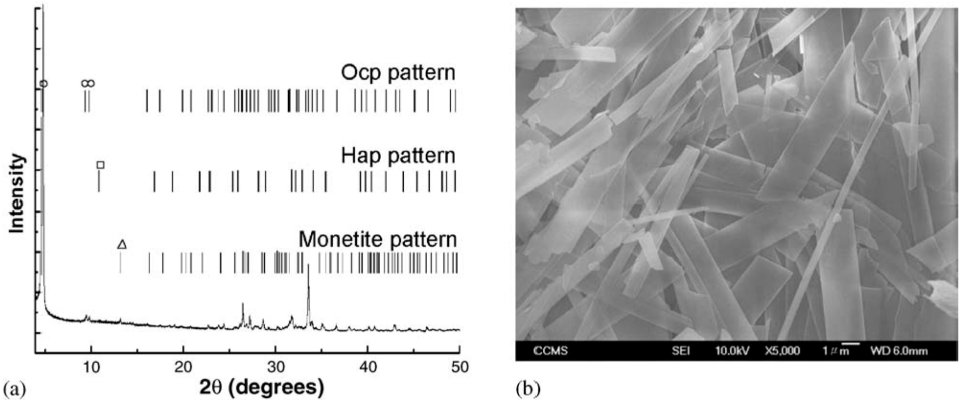

Fig. 2. (a) XRD pattern measured for the OCP sample; (b) SEM image of the OCP sample.

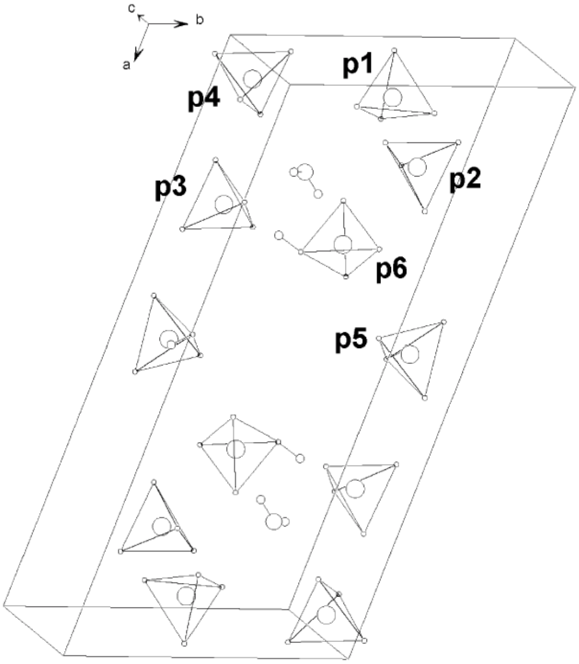

Fig. 3. Illustration of the unit cell of OCP. Among the 12 phosphorous sites only six of them are non-equivalent. The four PO_4^{3-} groups are labeled as P1–P4 and the two HPO_4^{2-} groups as P5 and P6. For simplicity all the water molecules are hidden except those corresponding to the OH sites of HAP.

those described in the DQ experiment. Spin-temperature inversion was incorporated with CYCLOPS, resulting in an eight-step phase cycling.

3. Results

3.1. XRD and SEM

The XRD data measured for our OCP sample is shown in Fig. 2a. The calculated patterns for OCP, HAP and monetite are aligned with the experimental pattern for comparison. The absence of the reflection at $2\theta = 10.8^\circ$ (the characteristic reflection of HAP) in the experimental pattern indicates that our sample does not contain any identifiable HAP. On the other hand, a minor amount of monetite is present in our OCP sample. The SEM image of our OCP sample is shown in Fig. 2b. The morphology of the sample is uniform and the crystals typically have rectangular shapes.

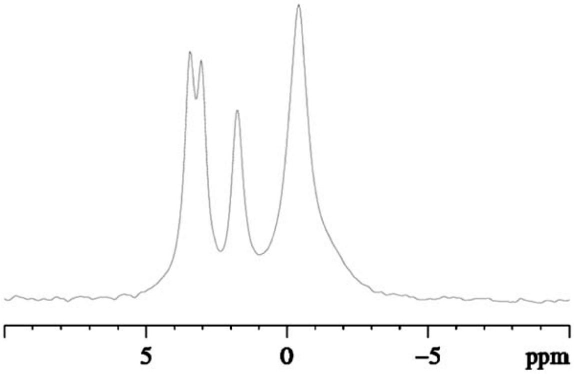

Fig. 4. ^{31}P MAS spectrum of OCP measured at 10 kHz MAS spinning. ^{1}H decoupling at 80 kHz was applied during acquisition. Recycle delay was set to 610 s.

For convenience, we have reproduced part of the crystallographic data of OCP in Fig. 3 [1]. Accordingly, there are six non-equivalent sites for phosphorus, in which P1 P4 are PO_4^{3-} groups while P5 and P6 are HPO_4^{2-} groups.

3.2. Solid-state NMR

The ^{31}P MAS spectrum of OCP is shown in Fig. 4. There are four resolved peaks positioned at −0.2, 2.0, 3.3 and 3.7 ppm with intensity ratio equal to 3:1:1:1 approximately. The spin lattice relaxation parameters of these peaks range from 89 to 123 s.

Our ^{31}P double quantum (DQ) spectrum is obtained by the POST-C7 sequence [15 17]. The DQ spectrum shown in Fig. 5. has four sets of auto- and cross-correlation peaks. Referring to the structural information shown in Table 1, we can preliminarily assign the

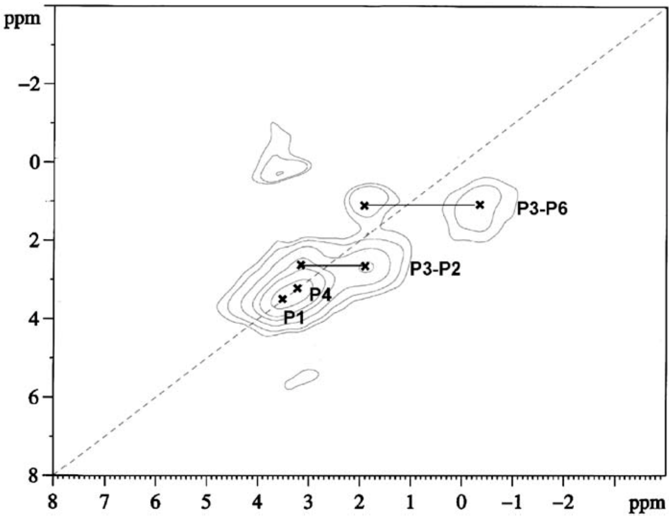

Fig. 5. ^{31}P double quantum spectrum of OCP. P3–P6 and P3–P2 connectivities are identified by the cross-correlation peaks. P1–P1 and P4–P4 connectivities are indicated by the auto-correlation peaks labeled as P1 and P4, respectively.

Table 1
Summary of the OCP internuclear distances which are relevant to the analyses of ^{31}P double quantum and ^{31}P{^{1}H} HETCOR experiments. All the distances are reported in angstrom

^{31}P DQ spectrum auto-correlation		^{31}P DQ spectrum cross-correlation		^{31}P{^{1}H} HETCOR[a]			
P1–P1	4.043	P2–P3	4.017	P6–O4	3.507	P2–H9	3.448
P4–P4	4.041	P3–P6	4.206	P4–O4	3.635	P4–H10	3.850
P5–P5	4.042	P5–P6	4.350	P2–O4	3.743	P2–H10	3.946
P2–P2	6.835	P1–P4	4.697	P6–O4	3.990	P4–H9	4.418
P3–P3	6.835	P1–P2	4.707	P1–O4	5.009	P3–H10	4.424
P6–P6	6.835	P2–P4	4.722			P1–H10	4.679
		P2–P6	4.951			P1–H9	5.164
		P1–P6	4.969				

[a] O(4), H(9) and H(10) correspond to the water molecule occupied at the OH site of HAP [1].

auto-correlation peaks at 3.3 ppm to P1 or P4. The same is true for the signal at 3.7 ppm. Unambiguous assignment can be made only when we incorporate the HETCOR data in our analysis (vide infra). Based on the positions of the cross-correlation peaks we can assign with certainty the resonances at 2.0 and 3.3 ppm to P3 and P2, respectively. The auto-correlation peak arising from P5 is not found in our DQ spectrum. Repeat measurement with proton decoupling at 80 kHz, our highest possible decoupling field, throughout the experiment gave the same result. Presumably the strong ^{1}H ^{31}P coupling for the HPO$_4^{3-}$ species renders the DQ signal undetectable. The same argument also explains the missing of the P5 P6 cross-peak. On the other hand, the observation of the cross-correlation peak between P3 (PO$_4^{3-}$) and P6 (HPO$_4^{2-}$) shows that P6 may undergo rapid molecular motion in the NMR time scale, which substantially attenuates the ^{1}H ^{31}P coupling. This explanation is consistent with the earlier observation that the chemical shift anisotropy measured for HPO$_4^{2-}$ in OCP increased when the temperature was lowered to −165°C [10]. Furthermore, the single-crystal X-ray diffraction study of OCP shows that there are six calcium ions surrounding P5 but only four Ca^{2+} for P6 [1]. Hence it is not unexpected that these two HPO$_4^{2-}$ groups have different molecular motions. We note that the closest distance between P1 and P6 is 4.969 Å, which seems too large to give a detectable DQ signal in our experiment.

For comparison we append the ^{1}H MAS spectrum next to the ^{1}H projection of our ^{31}P{^{1}H} HETCOR spectrum shown in Fig. 6. It has been established that the ^{1}H signal at 0.18 ppm arises from the OH group [7,9], which is correlated to the ^{31}P resonance at 3.3 ppm but not at 3.7 ppm. Referring to the structural data summarized in Table 1, P1 cannot account for the ^{31}P signal correlated to the hydroxyl ^{1}H signal. Together with the ^{31}P DQ data, we can therefore assign the ^{31}P signal at 3.7 ppm to P1, and the signal at 3.3 ppm to both P2 and P4. The relatively sharp ^{1}H peak at 1.44 ppm has been previously assigned to the O(5) water molecule, which is rather isolated from all the PO$_4^{3-}$ groups (closest distance 5.827 Å) [7]. The fact that this peak is not correlated to any PO$_4^{3-}$ groups in our

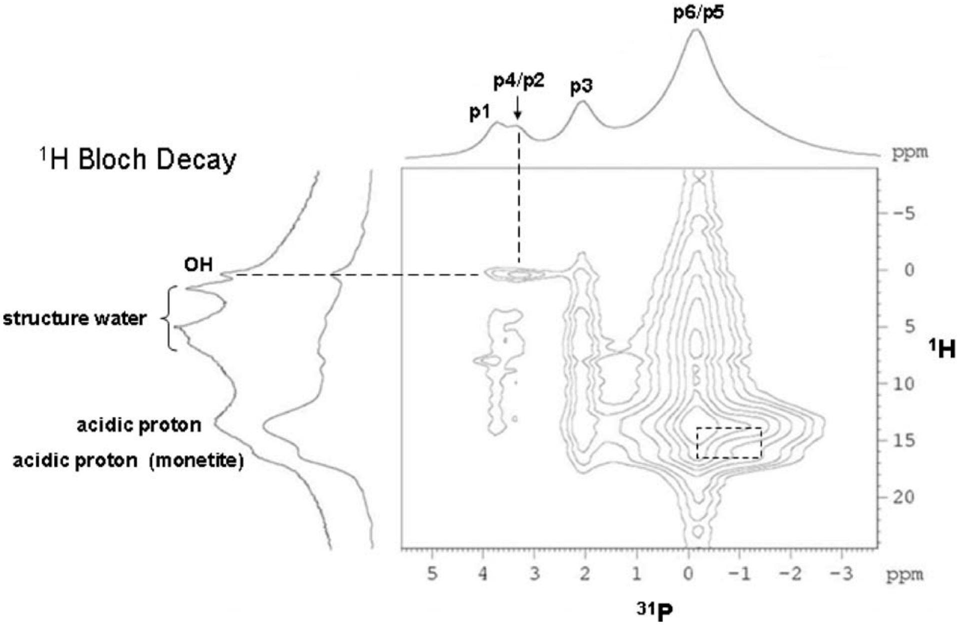

Fig. 6. ^{31}P{^{1}H} HETCOR spectrum of OCP. Projections of the ^{31}P and ^{1}H dimensions are shown. For comparison the ^{1}H MAS spectrum is appended next to the ^{1}H projection spectrum. The vertices of the rectangular box correspond to the cross peaks of monetite. Note that the OCP signal also contributes to the cross peak at −0.2 ppm (^{31}P) and 13.6 ppm (^{1}H).

HETCOR spectrum is consistent with this earlier assignment. As expected, the ^{31}P peak at −0.2 ppm (P5 and P6) is correlated to the ^{1}H signals at 5.5 and 13.34 ppm, which have been assigned to the structural water and the acidic proton of HPO_4^{2-} [7]. Our XRD data shows that there is small amount of monetite present in our OCP sample. The ^{31}P MAS spectrum of monetite measured by Rothwell et al. show two partially resolved peaks at 0.0 and −1.5 ppm [10]. The corresponding ^{1}H MAS spectrum reported by Yesinowski and Eckert shows two resonances at 13.6 and 16.2 ppm. Accordingly, we observe a set of cross peaks, marked with a rectangle in Fig. 6, between these ^{1}H and ^{31}P signals in our HETCOR spectrum. In comparison, the HETCOR spectrum of OCP reported by Santos and coworkers has rather poor resolution in the ^{31}P dimension [8], which is presumably due to the low field and slow MAS conditions employed in their experiment.

4. Discussion

OCP is a metastable compound and it will transform to HAP or monetite under hydrolysis or dehydration [3]. Conventionally, OCP can be prepared by a number of methods such as the hydrolysis of brushite or by mixing suitable calcium and phosphate salts at adjusted pH condition [18]. It has been recently shown that hydrolysis of urea will produce a uniform pH change in the bulk solution so that the precipitation of calcium phosphates will become more homogeneous [19,20]. The SEM image (Fig. 2b) shows that the morphology of the OCP crystal prepared in this fashion is indeed more uniform than those prepared by other methods (data not shown).

Our ^{31}P double quantum and ^{31}P{^{1}H} HETCOR results provide unequivocal assignments of the ^{31}P MAS spectrum, and yet it is surprising that the intensity ratio of the ^{31}P peaks is not consistent with what we expected from the crystallographic data (Fig. 3). According to our assignment, the peaks positioned at −0.2 (P5, P6), 2.0 (P3), 3.3 (P2, P4) and 3.7 (P1) ppm should have an intensity ratio of 2:1:2:1 but what has been measured for our OCP sample is 3:1:1:1. While one may argue that the presence of monetite in our sample makes the peak at −0.2 ppm more intense than expected, it is not conceivable that the amount of monetite could account for the exceedingly large population of HPO_4^{2-} [3]. In addition, the intensity of the resonance at 3.3 ppm indicates that the populations of P2 and P4 are significantly underrepresented in our OCP sample. To investigate the possibility of PO_4^{3-} substitution by CO_3^{2-} or HCO_3^- ions, we have conducted a ^{13}C Bloch decay measurement (10 kHz MAS spinning; recycle delay 300 s; number of scans 226). However, we did not observe any CO_3^{2-} or HCO_3^- signals (ca. 160 ppm) [21,22] except those arising from the Teflon spacer (111 ppm). Therefore, it is unlikely that substantial portion of the PO_4^{3-} sites is substituted by these ions. To rationalize the ^{31}P NMR peak intensity ratio we postulate that some of the PO_4^{3-} groups at the P2 and P4 sites are involved in the following transformation:

$PO_4^{3-} + H_2O \rightarrow HPO_4^{2-} + OH^-$(Scheme1).

This postulation is supported by our HETCOR result that the PO_4^{3-} groups at P2 and P4 are in close vicinity of the water molecule whose oxygen atom corresponds closely to the OH site in HAP (Table 1). Previously it has been postulated that the formation of OH group is occurred by the chemical exchange process between the P6 (HPO_4^{2-}) and the water molecule at the OH site [1]:

$HPO_4^{2-} + H_2O \rightarrow H_2PO_4^- + OH^-$(Scheme2).

In view of the fact that the phosphorous groups at P2, P4, P6 are at about the same distance to the OH site (see Table 1), the formation of OH group in our OCP sample may occur via both schemes. On the other hand, P1 is rather isolated from the water molecules and P3 is hydrogen bonded to one of the HPO_4^{2-} groups [1]. Therefore, both P1 and P3 are not involved in any chemical exchange processes.

In the literature, a recent ^{31}P MAS spectrum measured under similar conditions is very similar to ours except that the peak intensity of the P2/P4 site is significantly higher than that of ours [13]. Clearly, the extent of PO_4^{3-} hydrolysis (scheme 1) is largely dependent on the preparative conditions. Although it is very difficult to prepare OCP in pure form, ^{31}P NMR remains an effective analytical technique to study the structure of this mixed phase system. A systematic study of OCP structures prepared under different conditions will be the subject of a forthcoming article.

5. Conclusion

The high-resolution ^{31}P spectrum of OCP has been assigned based on ^{31}P double-quantum and ^{31}P{^{1}H} HETCOR experiments. The ^{31}P peaks at -0.2, 2.0, 3.3 and 3.7 ppm are assigned to P5/P6, P3, P2/P4 and P1, respectively. This assignment is consistent with all the earlier works in the literature. Our data reveal that substantial amount of the PO_4^{3-} groups at the P2 and P4 sites have been transformed to HPO_4^{2-} in our OCP sample. Overall, our results have provided a useful basis for the identification of OCP as well as the study of OCP to HAP transformation.

Acknowledgments

This work was supported by a grant from the National Science Council under the contract number NSC 92-2119-M-002-025.

References

[1] M. Mathew, W.E. Brown, L.W. Schroeder, B. Dickens, J. Cryst. Spec. Res. 18 (1988) 235–250.
[2] S.V. Dorozhkin, M. Epple, Angew. Chem. Int. Ed. 41 (2002) 3130–3146.
[3] W.E. Brown, J.P. Smith, J.R. Lehr, A.W. Frazier, Nature 196 (1962) 1050–1055.
[4] P. Bodier-Houlle, P. Steuer, J.-C. Voegel, F.J.G. Cuisinier, Acta Cryst. D 54 (1998) 1377–1381.
[5] W.E. Brown, L.W. Schroeder, J.S. Ferris, J. Phys. Chem. 83 (1979) 1385–1388.
[6] W.E. Brown, Nature 196 (1962) 1048–1050.
[7] J.P. Yesinowski, H. Eckert, J. Am. Chem. Soc. 109 (1987) 6274–6282.
[8] R.A. Santos, R.A. Wind, C.E. Bronnimann, J. Magn. Reson. Ser. B 105 (1994) 183–187.
[9] A. Kaflak-Hachulska, A. Samoson, W. Kolodziejski, Calcif. Tissue Int. 73 (2003) 476–486.
[10] W.P. Rothwell, J.S. Waugh, J.P. Yesinowski, J. Am. Chem. Soc. 102 (1980) 2637–2643.
[11] W.P. Aue, A.H. Roufosse, M.J. Glimcher, R.G. Griffin, Biochemistry 23 (1984) 6110–6114.
[12] J.L. Miquel, L. Facchini, A.P. Legrand, C. Rey, J. Lemaitre, Colloid Surface 45 (1990) 427–433.
[13] M. Iijima, D.G.A. Nelson, Y. Pan, A.T. Kreinbrink, M. Adachi, T. Goto, Y. Moriwaki, Calcif. Tissue Int. 59 (1996) 377–384.
[14] G. Metz, X.L. Wu, S.O. Smith, J. Magn. Reson. A 110 (1994) 219–227.
[15] M. Eden, M.H. Levitt, J. Chem. Phys. 111 (1999) 1511–1519.
[16] M. Hohwy, H.J. Jakobsen, M. Eden, M.H. Levitt, N.C. Nielsen, J. Chem. Phys. 108 (1998) 2686–2694.
[17] Y.K. Lee, N.D. Kurur, M. Helmle, O.G. Johannessen, N.C. Nielsen, M.H. Levitt, Chem. Phys. Lett. 242 (1995) 304–309.
[18] R.Z. LeGeros, Calcif. Tissue. Int. 37 (1985) 194–197.
[19] K. Matsuda, Y. Kaneko, H.J. Fei, K. Fujita, S. Mitsuzawa, Proc. Fac. Sci. Tokai Univ. 27 (1992).
[20] K.M. Udert, T.A. Larsen, M. Biebow, W. Gujer, Water Res. 37 (2003) 2571–2582.
[21] D. Stueber, A.M. Orendt, J.C. Facelli, R.W. Parry, D.M. Grant, Solid State Nucl. Magn. Reson. 22 (2002) 29–49.
[22] K. Beshah, C. Rey, M.J. Glimcher, M. Schimizu, R.G. Griffin, J. Solid State Chem. 84 (1990).

II-C. Solid-State NMR Characterization of Octacalcium Phosphate by Double Quantum Spectroscopy

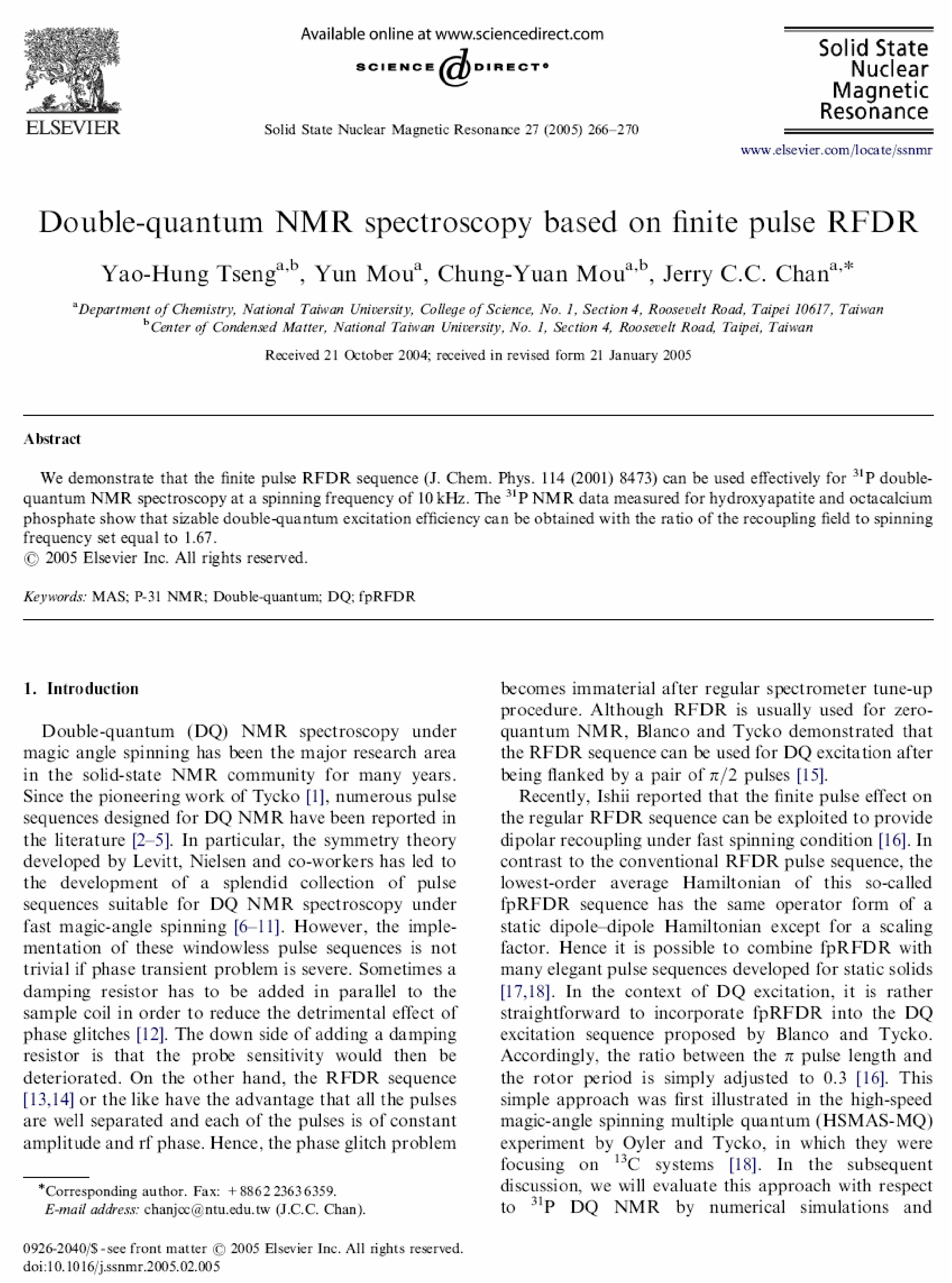

Available online at www.sciencedirect.com

SCIENCE DIRECT®

ELSEVIER

Solid State Nuclear Magnetic Resonance 27 (2005) 266–270

Solid State Nuclear Magnetic Resonance

www.elsevier.com/locate/ssnmr

Double-quantum NMR spectroscopy based on finite pulse RFDR

Yao-Hung Tseng[a,b], Yun Mou[a], Chung-Yuan Mou[a,b], Jerry C.C. Chan[a,*]

[a] *Department of Chemistry, National Taiwan University, College of Science, No. 1, Section 4, Roosevelt Road, Taipei 10617, Taiwan*
[b] *Center of Condensed Matter, National Taiwan University, No. 1, Section 4, Roosevelt Road, Taipei, Taiwan*

Received 21 October 2004; received in revised form 21 January 2005

Abstract

We demonstrate that the finite pulse RFDR sequence (J. Chem. Phys. 114 (2001) 8473) can be used effectively for ^{31}P double-quantum NMR spectroscopy at a spinning frequency of 10 kHz. The ^{31}P NMR data measured for hydroxyapatite and octacalcium phosphate show that sizable double-quantum excitation efficiency can be obtained with the ratio of the recoupling field to spinning frequency set equal to 1.67.

Keywords: MAS; P-31 NMR; Double-quantum; DQ; fpRFDR

---

1. Introduction

Double-quantum (DQ) NMR spectroscopy under magic angle spinning has been the major research area in the solid-state NMR community for many years. Since the pioneering work of Tycko [1], numerous pulse sequences designed for DQ NMR have been reported in the literature [2–5]. In particular, the symmetry theory developed by Levitt, Nielsen and co-workers has led to the development of a splendid collection of pulse sequences suitable for DQ NMR spectroscopy under fast magic-angle spinning [6–11]. However, the implementation of these windowless pulse sequences is not trivial if phase transient problem is severe. Sometimes a damping resistor has to be added in parallel to the sample coil in order to reduce the detrimental effect of phase glitches [12]. The down side of adding a damping resistor is that the probe sensitivity would then be deteriorated. On the other hand, the RFDR sequence [13,14] or the like have the advantage that all the pulses are well separated and each of the pulses is of constant amplitude and rf phase. Hence, the phase glitch problem becomes immaterial after regular spectrometer tune-up procedure. Although RFDR is usually used for zero-quantum NMR, Blanco and Tycko demonstrated that the RFDR sequence can be used for DQ excitation after being flanked by a pair of $\pi/2$ pulses [15].

Recently, Ishii reported that the finite pulse effect on the regular RFDR sequence can be exploited to provide dipolar recoupling under fast spinning condition [16]. In contrast to the conventional RFDR pulse sequence, the lowest-order average Hamiltonian of this so-called fpRFDR sequence has the same operator form of a static dipole–dipole Hamiltonian except for a scaling factor. Hence it is possible to combine fpRFDR with many elegant pulse sequences developed for static solids [17,18]. In the context of DQ excitation, it is rather straightforward to incorporate fpRFDR into the DQ excitation sequence proposed by Blanco and Tycko. Accordingly, the ratio between the π pulse length and the rotor period is simply adjusted to 0.3 [16]. This simple approach was first illustrated in the high-speed magic-angle spinning multiple quantum (HSMAS-MQ) experiment by Oyler and Tycko, in which they were focusing on ^{13}C systems [18]. In the subsequent discussion, we will evaluate this approach with respect to ^{31}P DQ NMR by numerical simulations and

---

[*] Corresponding author. Fax: +886 2 2363 6359.
E-mail address: chanjcc@ntu.edu.tw (J.C.C. Chan).

0926-2040/$ - see front matter © 2005 Elsevier Inc. All rights reserved.
doi:10.1016/j.ssnmr.2005.02.005

experimental measurements on octacalcium phosphate and hydroxyapatite. For convenience, we refer this approach to as HSMAS-DQ in the subsequent discussion.

2. Experimental

2.1. Sample preparation

Octacalcium phosphate was prepared and characterized as described previously [19]. Hydroxyapatite was used as received (Sigma-Aldrich).

2.2. Numerical simulations

All numerical studies in this work were carried out using SIMPSON (version 1.1.0) [20]. For our simulations, the maximum time step over which the Hamiltonian is approximated to be time-independent was set to 3.0 μs. Typically, a powder averaging scheme containing 100 REPULSION angles (α and β) [21] and 18 γ angles was chosen. Relaxation effects were ignored. Two series of spin clusters used for our simulations were constructed based on the structural parameters of octacalcium phosphate [22] and hydroxyapatite [23]. For octacalcium phosphate there are six non-equivalent sites for phosphorus, where P1 P4 are PO_4^{3-} groups while P5 and P6 are HPO_4^{2-} groups. For hydroxyapatite there is only one phosphorous site (PO_4^{3-}). In the octacalcium phosphate series, we have constructed seven spin clusters, viz. 2-P, 4-P, 5-P, 7-P, 2P H, 4P H and 5P 2H. As shown in Fig. 1(a), the two-spin system (2-P) involves P3 and P6. The 4-P, 5-P and 7-P spin clusters are constructed by adding two, three and five of the nearest phosphorous neighbors, respectively, to the basic 2-P system. When the acidic protons of the P5 and P6 species (HPO_4^{2-}) were added to the 2-P, 4-P and 5-P clusters, we obtained the 2P H, 4P H and 5P 2H clusters, respectively. In the hydroxyapatite series, similarly we have constructed three different spin clusters, viz. 2-P, 3-P and 5-P (Fig. 1b). For both series the chemical shift spans of PO_4^{3-} (40 ppm) and HPO_4^{2-} (121 ppm) were taken from the experimental data measured for hydroxyapatite and brushite, respectively [24]. For simplicity the orientations of the CSA tensors with respect to the dipolar framework were set arbitrarily.

2.3. Solid-state NMR

All NMR experiments were carried out at ^{31}P and ^{1}H frequencies of 121.5 and 300.1 MHz, respectively, on a Bruker DSX300 NMR spectrometer equipped with a commercial 4 mm MAS-NMR probe. All spectra were measured at a spinning frequency of 10 kHz. MAS frequency variation was limited to ±3 Hz using a commercial pneumatic control unit. The sample was confined to the middle 1/3 of the rotor volume using Teflon spacers. Chemical shifts were externally referenced to 85% phosphoric acid. The pulse sequence used for the ^{31}P DQ measurements is shown in Fig. 2. To prepare the initial spin system identically for each transient, a saturation comb was applied prior to the recycle delay. Recycle delay was set to 8 s. During the DQ excitation and reconversion periods, the ^{31}P $\pi/2$ and π pulses were set to 5 and 30 μs long, respectively. The π pulse trains were phase cycled according to the XY-16 scheme [25]. The DQ excitation and reconversion times were both set to 3.2 ms unless stated otherwise. The tachometer signals for pulse sequence synchronization were filtered with a home-built phase-locked loop circuit. Proton decoupling was set to 85 kHz. A z-filter of 30 ms without proton decoupling was applied after the reconversion period. The standard four-step phase cycling of the excitation block (0, $\pi/2$, π, $3\pi/2$) and

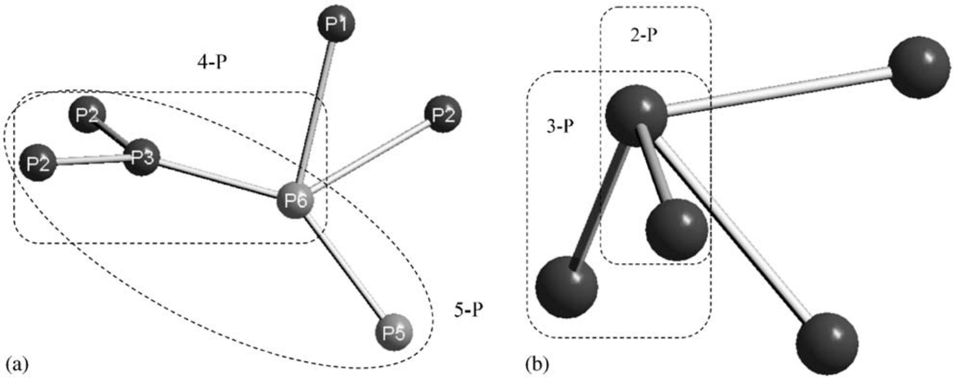

Fig. 1. The spin clusters constructed for numerical simulations. (a) Octacalcium phosphate series: 2-P, P3 and P6; 4-P, spins enclosed by the rectangle; 5-P, spins enclosed by the ellipse; 7-P, all spins. The dark and gray spheres represent PO_4^{3-} and HPO_4^{3-}, respectively. (b) Hydroxyapatite series: 2-P, 3-P, 5-P.

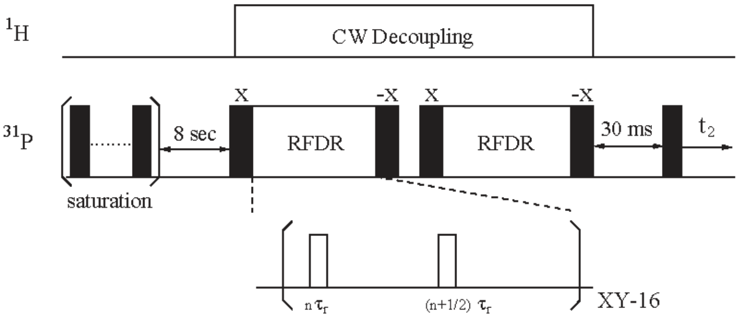

Fig. 2. Pulse sequences used for the ^{31}P DQ experiment. The filled and open rectangles denotes $\pi/2$ and π pulses, respectively.

receiver phase (0, π, 0, π) was used to select the DQ coherence [26]. Probe ringdown and dc offset artifacts were suppressed by inverting the phase of the first $\pi/2$ pulse and alternating addition and subtraction of FID signals. Together with CYCLOPS, our phase cycling has a total of 32 steps. For the two-dimensional DQ spectrum measurement, quadrature detection in the F_1 dimension was achieved by the hypercomplex approach. For each t_1 increment 32 transients were accumulated, and a total of 48 increments were done at steps of two rotor periods.

3. Results

3.1. Octacalcium phosphate

3.1.1. Numerical simulations

To evaluate the utility of HSMAS-DQ, we have carried out a series of simulations on the spin clusters 2-P, 4-P, 5-P and 7-P (octacalcium phosphate series). The closest internuclear distances of selected phosphorus spin pairs are listed in Table 1. Other simulation parameters were set equal to the experimental settings. To evaluate the effect of proton decoupling on the DQ excitation efficiency, we focus on a ^{31}P ^{31}P spin pair formed by PO_4^{3-} and HPO_4^{2-} in close proximity, i.e. P3 P6. Fig. 3(a) shows the numerical results of the excitation efficiency of the P3 P6 DQ coherence in different spin clusters. There is a dramatic decrease in the excitation efficiency when the cluster size increases from two spins to four spins. This observation can be understood by the fact that the passive spins in close proximity provide a strong dipolar dephasing of the excited DQ coherence. As expected, such dephasing effects are comparable for the 4-P, 5-P and 7-P systems. Note that P4 is not included in our spin clusters because it is rather remote from P3 or P6 (Table 1). To investigate the effect of proton decoupling, we repeat the above calculations on the 2P H, 4P H and 5P 2H spin clusters using a proton decoupling field of 85 kHz (Fig. 3b). Because the proton decoupling field is much larger than the ^{31}P recoupling field, the excitation profiles shown in Figs. 3a and b are quite similar.

Table 1
Closest internuclear distances (in Å) of selected phosphorus spin pairs in octacalcium phosphate

Auto-correlation		Cross-correlation	
P1–P1	4.043	P2–P3	4.017
P4–P4	4.041	P3–P6	4.206
P5–P5	4.042	P5–P6	4.350
P2–P2	6.835	P1–P4	4.697
P3–P3	6.835	P1–P2	4.707
P6–P6	6.835	P2–P4	4.722
		P2–P6	4.951
		P1–P6	4.969
		P4–P3	5.052
		P1–P3	5.494
		P4–P6	5.986

The data are grouped to facilitate the analysis of the two-dimensional ^{31}P DQ spectrum (Fig. 4).

3.1.2. Two-dimensional DQ spectrum

The two-dimensional ^{31}P DQ spectrum of octacalcium phosphate is shown in Fig. 4(a), in which there are eight sets of auto- and cross-correlation peaks. For convenience, in Fig. 4(b) we also reproduce the corresponding one-dimensional ^{31}P MAS spectrum and the spectral assignments reported earlier [19]. The correlation peaks of P2 P6, P1 P6, P1 P3 and P5 P5/P5 P6 were not observed in our previous work, where we employed windowless pulse sequence at a spinning frequency of 6 kHz [19]. Although the ^{31}P chemical shift span of HPO_4^{2-} is about 121 ppm [24], the relatively high intensity of the P5 P5/P5 P6 correlation peak demonstrates that the DQ excitation efficiency is not significantly attenuated by large CSA effect. Altogether these results illustrate the advantages of the HSMAS-DQ approach that the experiment can be carried out at fast spinning frequency and that the ratio of the recoupling to decoupling fields are small. In view of the fact that the closest distance between P1 and P3 is 5.494 Å, it is

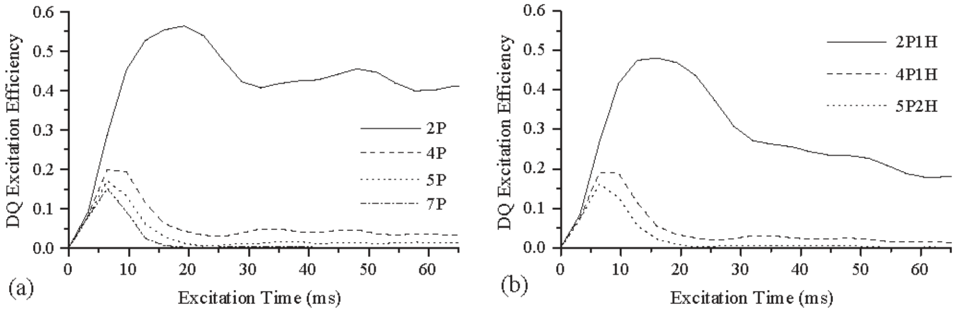

Fig. 3. Numerical simulations of the excitation efficiency of the P3–P6 DQ coherence in different spin clusters (octacalcium phosphate series). (a) 2-P, 4-P, 5-P and 7-P. (b) 2P–1H, 4P–1H and 5P–2H.

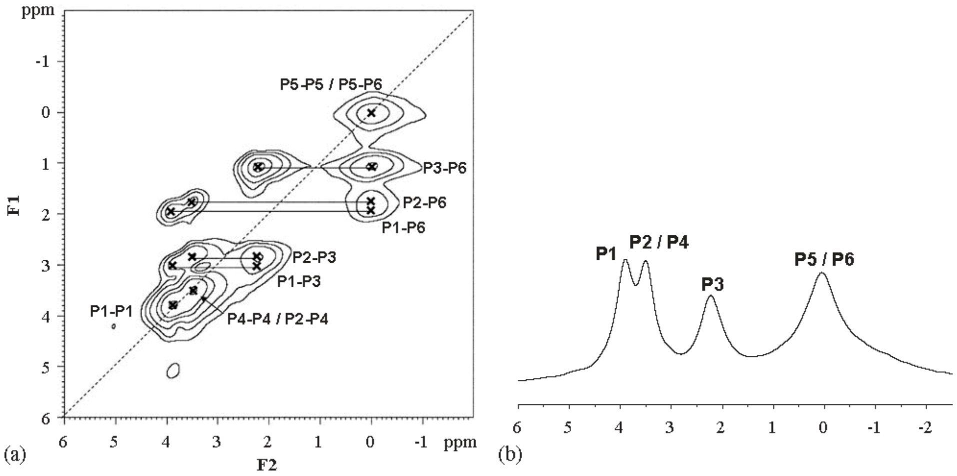

Fig. 4. NMR spectra of octacalcium phosphate measured under 10 kHz spinning frequency: (a) Two-dimensional ^{31}P DQ based on the HSMAS-DQ sequence; (b) MAS.

surprising that the intensity of the P1 P3 cross-correlation peak is comparable to that of P2 P3 (4.017 Å). This observation cannot be explained by different spectral assignments. We speculate that the P1 P3 cross-correlation arises from a relayed coherence transfer P1↔P6↔P3 because both P1 P6 and P6 P3 are in close proximity. To minimize the duty cycle in the proton channel, the *z*-filter was applied without proton decoupling. Therefore, higher order spin diffusion may also occur during the *z*-filtering period [27].

The ^{31}P Bloch decay signal after the saturation comb and relaxation delay (same as the DQ experiment) was taken as a reference signal. After normalizing the P3 P6 cross-peak intensities by the geometric mean of P3 and P6 reference signal intensities, the excitation efficiency for the P3 P6 DQ coherence is estimated to be ca. 20%.

3.2. Hydroxyapatite

Because hydroxyapatite has one phosphorous site only, it is a good model compound for the study of DQ coherence excitation profile. The closest ^{31}P ^{31}P distance in hydroxyapatite is 4.115 Å. The numerical simulations and the experimental data were shown in Fig. 5(a). Similar to what has been observed in octacalcium phosphate, the maximum DQ coherence excitation efficiency decreases as the spin cluster size increases. Nevertheless, the extent of the diminishment is not as dramatic as what we observed for octacalcium phosphate. The reason is simply due to the fact that all the spins in the cluster will contribute (different combinations of two spins) to the DQ coherence. As expected the simulation results converge towards the experimental data as the cluster size increases. Since we do not include any relaxation parameters in our simulations, the agreement between the simulation and the experimental data becomes worse at longer excitation times.

To compare the RFDR-based DQ excitation strategy [15] and the HSMAS-DQ approach, we repeat our simulations and experimental measurements by shortening all the π pulses from 30 to 7 μs. The results shown in Fig. 5(b) indicate that all the excitation profile maxima invariably appear at longer excitation times than those in Fig. 5(a). This observation is consistent with the simulation results of Oyler and Tycko [18].

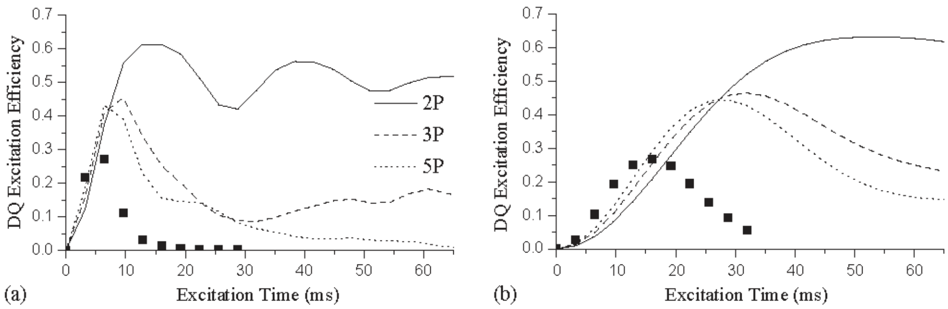

Fig. 5. Numerical simulations and experimental measurements of the excitation profile of the ^{31}P DQ coherence in hydroxyapatite at a spinning frequency of 10 kHz. The symbols, representing the experimental data, are larger than the error bars. (a) fpRFDR, π pulse = 30 μs (b) RFDR, π pulse = 7 μs.

Overall, both numerical and experimental data illustrate that the HSMAS-DQ method is a favorable option for ^{31}P DQ NMR under a spinning frequency of 10 kHz.

4. Discussion

Our simulation results illustrate that the excitation of DQ coherence is inherently difficult in multiple-spin system due to the dephasing effect of other passive spins. The strong dependence of the excitation profile on the spin cluster size is in line with the conclusion that distance measurement by DQ NMR spectroscopy in homonuclear spin system is practical only if the two-spin approximation holds [28].

In this work, we have demonstrated that HSMAS-DQ can be used effectively for ^{31}P DQ NMR spectroscopy. In spite of the favorable experimental results shown here, we make no claim that the HSMAS-DQ approach is in general superior to the C/R or any other windowless pulse sequences [8]. In fact, the theoretical maximum DQ excitation efficiency of HSMAS-DQ is less than those γ-encoded pulse sequences [6]. Nevertheless, we do recommend the HSMAS-DQ approach originally developed in Tycko group when the phase transient problem is a serious one.

Acknowledgment

This work was supported by grants from the National Science Council and the Ministry of Education. We thank Professor John Balbach (Physics Department, George Washington University) and Professor Carl Michal (Physics Department, University of British Columbia) for sharing with us their circuit designs for tachometer signal clean up. We thank Dr. Hans Foerster (Bruker, Karlsruhe) for technical advice. We thank one of the anonymous reviewers for bringing Ref. [27] to our attention.

References

[1] R. Tycko, G. Dabbagh, Chem. Phys. Lett. 173 (1990) 461–465.
[2] R. Tycko, Annu. Rev. Phys. Chem. 52 (2001) 575–606.
[3] M. Baldus, Prog. Nucl. Magn. Reson. Spectrosc. 41 (2002) 1–47.
[4] S. Luca, H. Heise, M. Baldus, Acc. Chem. Res. 36 (2003) 858–865.
[5] I. Schnell, Prog. Nucl. Magn. Reson. Spectrosc. 45 (2004) 145–207.
[6] Y.K. Lee, N.D. Kurur, M. Helmle, O.G. Johannessen, N.C. Nielsen, M.H. Levitt, Chem. Phys. Lett. 242 (1995) 304–309.
[7] M. Carravetta, M. Eden, X. Zhao, A. Brinkmann, M.H. Levitt, Chem. Phys. Lett. 321 (2000) 205–215.
[8] M.H. Levitt, Symmetry-Based Pulse Sequence in Magic-Angle Spinning Solid-State NMR, Wiley, Chichester, 2002.
[9] M. Hohwy, H.J. Jakobsen, M. Eden, M.H. Levitt, N.C. Nielsen, J. Chem. Phys. 108 (1998) 2686–2694.
[10] M. Hohwy, C.M. Rienstra, C.P. Jaroniec, R.G. Griffin, J. Chem. Phys. 110 (1999) 7983–7992.
[11] A. Brinkmann, M. Eden, M.H. Levitt, J. Chem. Phys. 112 (2000) 8539–8554.
[12] J. Gunne, H. Eckert, Chem.-Eur. J. 4 (1998) 1762–1767.
[13] T. Gullion, S. Vega, Chem. Phys. Lett. 194 (1992) 423–428.
[14] A.E. Bennett, C.M. Rienstra, J.M. Griffiths, W.G. Zhen, P.T. Lansbury, R.G. Griffin, J. Chem. Phys. 108 (1998) 9463–9479.
[15] F.J. Blanco, R. Tycko, J. Magn. Reson. 149 (2001) 131–138.
[16] Y. Ishii, J. Chem. Phys. 114 (2001) 8473–8483.
[17] Y. Ishii, J.J. Balbach, R. Tycko, Chem. Phys. 266 (2001) 231–236.
[18] N.A. Oyler, R. Tycko, J. Phys. Chem. B 106 (2002) 8382–8389.
[19] Y.H. Tseng, J.H. Zhan, K.S.K. Lin, C.Y. Mou, J.C.C. Chan, Solid State Nucl. Magn. Reson. 26 (2004) 99–104.
[20] M. Bak, J.T. Rasmussen, N.C. Nielsen, J. Magn. Reson. 147 (2000) 296–330.
[21] M. Bak, N.C. Nielsen, J. Magn. Reson. 125 (1997) 132–139.
[22] M. Mathew, W.E. Brown, L.W. Schroeder, B. Dickens, J. Crystallogr. Spectrosc. Res. 18 (1988) 235–250.
[23] M.I. Kay, R.A. Young, A.S. Posner, Nature 204 (1964) 1050–1052.
[24] Y. Wu, J.L. Ackerman, E.S. Strawich, C. Rey, H.M. Kim, M.J. Glimcher, Calcif. Tissue Int. 72 (2003) 610–626.
[25] T. Gullion, D.B. Baker, M.S. Conradi, J. Magn. Reson. 89 (1990) 479–484.
[26] R.R. Ernst, G. Bodenhausen, A. Wokaun, Principles of Nuclear Magnetic Resonance in One and Two Dimensions, Clarendon Press, Oxford, 1987.
[27] L.-S. Du, M.H. Levitt, C.P. Grey, J. Magn. Reson. 140 (1999) 242–249.
[28] J. Gunne, J. Magn. Reson. 165 (2003) 18–32.

II-D. Transformation of Octacalcium Phosphate to Hydroxyapatite: A Study of the Molecular Mechanism by SEM, TEM, XRD and Solid-State NMR Spectroscopy (submitted)

Biomineralization is a biological process describing the formation of minerals in living organisms.[1] Calcium phosphates are the major inorganic constituents of biological hard tissues in vertebrates, existing in the form with close resemblance to hydroxyapatite (HAp, $Ca_{10}(PO_4)_6(OH)_2$).[2] The so-called biological apatite or dahllite refers to poorly crystallized nonstoichiometric carbonate-containing HAp. Whether biological apatite is formed by direct precipitation or through an intermediate phase remains an unsettled issue in the field of biomineralization.[2,3] Because of the structural similarity between HAp and octacalcium phosphate (OCP, $Ca_8H_2(PO_4)_6{\cdot}5H_2O$), OCP has been hypothesized as the precursor phase of biological apatite.[4] The most compelling evidence for this hypothesis is the observation of an OCP "central dark line" in many biological apatites and in some synthetically prepared HAp.[5-7] OCP is thermodynamically less stable than hydroxyapatite and it is often found as an intermediate phase during the precipitation of HAp.[8,9] Many in-vitro studies of calcium phosphate precipitation have been carried out to elucidate the dependence of the thermodynamic events and the crystal morphology on the degree of supersaturation,[10] temperature,[11,12] pH conditions[13,14] and the rate of precipitation.[15-22] The most informative results hitherto reported were obtained from X-ray powder diffraction (XRD), scanning electron microscopy (SEM) and transmission electron microscopy (TEM).[3]

OCP can be described as an alternating layer structure of apatite layer and hydrated layer,[23] where the apatite layer is structurally very similar to HAp.[24,25] According to the OCP precursor model proposed by Brown,[4] the first calcium phosphate crystals formed in a supersaturated solution under physiological condition are OCP like. The subsequent hydrolysis step leads to the formation of HAp, where the c axes of the OCP and HAp unit cells are along the same direction during the structural transition. While this model is consistent with the results of some TEM studies,[26,27] a recent computational study shows that the c axes of the OCP and HAp should be at opposite directions in order to minimize the free energy at the interface between OCP and HAp.[28] It is by no means trivial to verify this computational prediction experimentally because TEM results cannot distinguish the alignment of two crystallographic axes from parallel to anti-parallel fashion. Furthermore, OCP is meta-stable and it will appear only if the pH in the crystallization system is below 6. In our previous work, we developed an in-vitro system to realize a single-crystal-to-single-crystal transformation from OCP to HAp in the presence of gelatin and urea.[29] The transformation of OCP to HAp is initiated by raising the pH condition from acidic to alkaline. Since a uniform pH increase of the reaction mixture is achieved by slow decomposition of urea at 100°C, our in-vitro system is an ideal model system for the study of the molecular mechanism of OCP to HAp transition. While all the phosphorus atoms in a unit cell of HAp are equivalent, there are six crystallographically non-equivalent phosphorous sites in OCP. As such, solid-state ^{31}P NMR is well suited to characterize the OCP to HAp transformation at the molecular level.

The high-resolution ^{31}P NMR studies of OCP can be dated back to the 1980s[30,31] and the complete spectral assignment has been made very recently.[32,33] Throughout the years, a large variety of advanced NMR techniques such as ^{31}P{^{1}H} cross-polarization (CP) at variable contact delays,[30] dipolar dephasing technique,[31] heteronuclear correlation spectroscopy (HETCOR),[34-36] differential cross polarization,[37,38] and multi-nuclear double-resonance techniques[39,40] had been successfully used to characterize the structures of synthetic hydroxyapatite, calcified tissues and apatite formation. Therefore, in the present study we chose to use a series of solid-state ^{31}P NMR techniques including ^{31}P{^{1}H} Lee-Goldburg spectroscopy[41,42] and ^{31}P homonuclear double-quantum (DQ) NMR[43] to monitor the OCP to HAp transition. The in-vitro system we developed earlier, in the absence of gelatin, is used to prepare calcium phosphate precipitated at different pH conditions. From the DQ NMR measurements we are able to show that the c axes of the OCP and HAp unit cells are at opposite directions during the transformation. Furthermore, the data of the ^{31}P{^{1}H} cross-polarization NMR suggest that water molecules enter the hydration layers of OCP crystals via the hydrolysis reaction $HPO_4^{2-} + OH^- = PO_4^{3-} + H_2O$, which also accounts for the deprotonation of the HPO_4^{2-} ions during the transformation. Overall, our NMR data provide hitherto the most detailed description of the OCP to HAp transformation mechanism at the molecular level.

Experimental

Sample Preparation and Characterization. Urea (99.5%) , sodium phosphate monobasic dehydrate ($H_2NaPO_4 \cdot 2H_2O$) (99%) and calcium nitrate tetrahydrate ($Ca(NO_3)_2 \cdot 4H_2O$) (99%) were used as received (Acros). A mixture of 10 mmol $Ca(NO_3)_2 \cdot 4H_2O$, 10 mmol $H_2NaPO_4 \cdot 2H_2O$ and 20 mmol urea were dissolved in 400 mL doubly distilled water and then sealed in a polypropylene container. The aqueous solution was kept at 100°C for different periods. The precipitates thus obtained were filtered, washed and then dried at 60°C for one day. A series of samples were obtained at different reaction times, *viz.* 1.5 h, 3 h, 4 h, 5 h, 6 h, 7 h, 9 h, 12 h and 96 h. All the samples will henceforth be labeled based on their reaction times. X-Ray diffraction analysis was performed on a Philips X'Pert diffractometer, using Cu-Kα radiation ($\lambda = 1.5418$ Å). The Rietvald analyses were done by the software EXPGUI.[44,45] The field emission SEM were taken on a JEOL-JSM-6700F field emission scanning electron microscope operated at 10 kV. The TEM and electron diffraction (ED) patterns were taken on Hitachi S-7100 and Philips FEI Tecnai 20 G^2 instruments operating at 75 kV and 200 kV, respectively.

Solid-State NMR. All NMR experiments were carried out at ^{31}P and ^{1}H frequencies of 121.5 and 300.1 MHz, respectively, on a Bruker DSX300 NMR spectrometer equipped with a commercial 4-mm probe. All spectra were measured at room temperature. The sample was confined to the middle 1/3 of the rotor volume using Teflon spacers. The variation of magic-angle spinning (MAS) frequency was limited to ± 3 Hz using a commercial pneumatic control unit. Chemical shifts were externally referenced to 85% phosphoric acid and TMS for ^{31}P and ^{1}H, respectively. The ^{31}P MAS spectra were measured at a spinrate of 10 kHz and with 70 kHz proton decoupling. An exponential window function of 20 Hz line broadening was applied to each FID before the Fourier transformation.

The $^{31}P\{^{1}H\}$ CP heteronuclear correlation (HETCOR) spectra were measured at a spinrate of 10 kHz. During the contact time (2.5 ms) the ^{1}H nutation frequency was set equal to 50 kHz and that of ^{31}P was ramped through the Hartmann-Hahn matching sideband.[46] Quadrature detection in the F_1 dimension was achieved by the hypercomplex approach. Typically, for each t_1 increment 32 transients were accumulated, and a total of 50 increments were done at steps of 100 μs.

The $^{31}P\{^{1}H\}$ Lee-Goldburg CP (LG-CP) spectra were measured at a spinrate of 10 kHz. The flip angle of the pulse after the t_1 evolution is adjusted so that the spin-temperature inversion can be realized by phase alternating the first $\pi/2$ pulse. During the contact time the ^{1}H nutation frequency and the resonance offset were set equal to 50 and 35.35 kHz, respectively, to fulfill the Lee-Goldburg irradiation condition. The ^{31}P DQ experiments were carried out under MAS spinning frequency of 10 kHz based on the so-called HSMAS-DQ technique.[33,47] To prepare the initial spin system identically for each transient, a saturation comb was applied prior to the recovery delay (8 s). During the DQ excitation and reconversion periods, the ^{31}P $\pi/2$ and π pulses were set to 5 and 30 μs long, respectively. The π pulse trains were phase cycled according to the XY-8 scheme.[48] The DQ reconversion period was set equal to the excitation period. Proton decoupling was set to 85 kHz during the DQ excitation/reconversion periods. A more detailed description of the experiment was given elsewhere.[33]

Results and Analyses

A. SEM. The pH values of the reaction mixture at different times are summarized in Table 1. Referring to the SEM images of our sample series shown in Figure 1, the crystals of the 1.5-h sample are poorly faceted rectangular plates. The blade-like crystals of the 3-h sample is the characteristic morphology of OCP. As the pH value of the reaction mixture rose to 5.01 at which the 4-h sample was collected, notches become found on the rectangular OCP crystals. Formation of slits along the c axis is also observed in previous study.[14,29] The 12-h sample was collected at pH of 6.69 and the crystals are mainly hexagonal rod-shaped.

B. TEM and ED. The 3-h, 6-h and 12-h samples were characterized by TEM and ED. The long edge of the blade-like OCP crystal is found to be along the *c* axis. The selected-area electron diffraction (SAED) patterns of the 3-h and 12-h samples can be assigned to the reflections along the [110] zone axis of OCP and the [210] zone axis of HAp, respectively. Consequently, the SAED patterns of the two samples can be served as a reference for the analysis of the SAED pattern of the 6-hr sample. Figure 2(a) shows the TEM image of the 6-h sample. Consistent with what has been observed in the SEM image, the blade-like crystal splits along its long edge. Referring to Figure 2(b), the SAED pattern of the notch area can be indexed to the [210] zone axis of HAp as well as the [110] zone axis of OCP. Both the c axes of HAp and OCP in the 6-hr sample are parallel or anti-parallel with respect to the slits along the elongated side of the blade-like crystal. This alignment of the crystallographic c axes of OCP and HAp is an important structural constraint for the OCP to HAp transformation (*vide infra*).

C. XRD. As an independent approach to identify the crystalline phases of our samples, the XRD patterns were measured (Figure 3). Any reflections at 2θ = 4.9°, 10.8° and 13.1° can be considered as the characteristic peaks of OCP (JCPDS 44-0778), HAp (JCPDS 24-0033) and monetite (JCPDS 09-0080), respectively. For the 1.5-h sample, the absence of the reflections at 2θ = 10.8° and 13.1° indicates that the sample is pure OCP. For the 3-h sample, trace amount of monetite is present in addition to OCP. The crystalline phase of HAp becomes observable for the 4-h sample. For the samples with longer reaction time, the HAp crystalline phase becomes more prominent at the expense of OCP and monetite. Eventually, the 12-h sample is pure HAp. Note that the two characteristic reflections of brushite ($CaHPO_4{\cdot}2H_2O$) at 2θ = 11.6° and 23.4° are not found in our samples (JCPDS 11-0293). The variation in the lattice parameters was analyzed by Rietvald analysis. As summarized in Table 2, the lattice parameters of the 3-h and 5-h samples are approximately the same but both the *a* and *b* axes of the OCP lattice have significant increase in the 4-h sample.

D. Solid-State NMR. Figure 4 shows the ^{31}P MAS spectra measured for our sample series, together with the spectral assignment we made earlier.[32] It is quite clear that the samples of reaction times from 1.5 h to 5 h contain mainly the OCP species. The crystallinity is rather poor for the 1.5-h sample because the corresponding signals have larger line widths than the 3-h sample. This observation is consistent with our SEM data, in which the crystals of the 1.5-h sample are found to be poorly faceted. Presumably, there are a lot of *excess* water molecules in the 1.5-h sample which cannot be accommodated in the OCP lattice. Judging from the NMR spectrum, the molecular structure of the 3-h sample is closest to that of pure OCP, in spite of the fact that trace amount of monetite is present in it. The ^{31}P chemical shift data and the assignment of the 3-h sample are summarized in Table 3. As the reaction time proceeds to 6 h, a significant change in the signal pattern is observed, showing that the system has undergone a considerable change in the phosphorus environments. Note that the 6-h spectrum is not a superposition of the 3-h (OCP) and the 12-h (HAp) spectra. Therefore, re-precipitation is unlikely the predominant transformation mechanism. The structural transition is essentially completed after 12 h because the spectra of the 12-h and 96-h samples are identical. The spectrum of the 12-h sample shows a single peak positioned at 3.2 ppm and is readily assigned to the PO_4^{3-} group of HAp.[49] This series of spectra demonstrate that the transformation of OCP to HAp can be effectively monitored by taking ^{31}P as the probe nucleus.

$^{31}P\{^1H\}$ Heteronuclear Correlation (HETCOR). To obtain a better spectral resolution we measured the $^{31}P\{^1H\}$ HETCOR spectra for the sample series. Figure 5 shows the HETCOR spectra of the 1.5-h, 3-h and 5-h samples. Consider the spectrum of the 1.5-h sample, the ^{31}P peak at -0.2 ppm (P5 and P6) is correlated to the ^1H signals at 5.5 and 13.3 ppm, which have been assigned to the structural water and the acidic proton of the HPO_4^{2-} ions.[50] Note that a relatively weak correlation peak can also be identified for the ^1H signal at 0.2 ppm and the P2 signal (3.3 ppm). This correlation peak is a well-known marker for apatite-like structures.[34,35,40,50] For the spectrum of the 3-h sample, an additional set of cross peaks denoted by a rectangle is observed, which is due to the HPO_4^{2-} group of monetite.[30,32,50] As the reaction time proceeds further, the corresponding HETCOR spectra show that the intensity of the apatite component increases at the expense of the monetite and the OCP signals (see Figure S 1 of the Supporting Information). Overall, our HETCOR data is in complete agreement with the XRD results.

^{31}P{^{1}H} Lee-Goldburg Cross Polarization. Recently, it has been shown that the LG homonuclear decoupling technique can be combined with CP to achieve polarization transfer with efficient suppression of ^{1}H-^{1}H spin diffusion.[41,42] Therefore, it is possible to investigate the hydration state of the individual phosphorus species by measuring the LG-CPMAS spectra with variable contact times. The intensities of the four resolved ^{31}P signals (P1, P2/P4, P3, P5/P6) were fitted by the following equation as a function of contact time (τ_{CP}) and relaxation time ($T_{1\rho}^{H}$):

$$I(t) = I_0\{1-\exp(-t/\tau_{CP})\}\exp(-t/T_{1\rho}^{H})$$

Typical fitting of the raw data was shown in Figure S 2 of the Supporting Information. The parameters τ_{CP} and $T_{1\rho}^{H}$ obtained for our sample series were shown in Figure 6, which do not show any strong correlation in the non-linear least-squares fittings. Consider the data of the 1.5-h sample, the relative τ_{CP} and $T_{1\rho}^{H}$ values are consistent with the facts that (i) P5 and P6 are HPO_4^{2-} species; (ii) P3 is hydrogen bonded to one of the HPO_4^{2-} groups; (iii) the distance between P2 and its closest neighboring water molecule is 3.5 Å; (iv) P1 is rather isolated from all the water molecules (distance > 4.6 Å).[25] For the 3-h sample, the τ_{CP} and $T_{1\rho}^{H}$ values of the PO_4^{3-} species increase considerably. Together with the fact that the ^{31}P signal line widths are narrower for the 3-h sample, it can be surmised that the crystallinity of the 3-h sample improves when those *excess* water molecules are expelled from the structure. For the 4-h and 5-h samples, the τ_{CP} values of all the PO_4^{3-} species decrease significantly and then increase again. An opposite trend was observed for the $T_{1\rho}^{H}$ data. This interesting variation of the τ_{CP} and $T_{1\rho}^{H}$ values of the PO_4^{3-} species is possibly due to a change in the hydration level of the phosphate ions. As the pH of the reaction mixture increases continuously due to the decomposition of urea, the equilibrium of the following reaction shifts to the right:

$$HPO_4^{2-} + OH^{-} = PO_4^{3-} + H_2O.$$

When the pH value reaches 5.01 at which we collect the 4-h sample, more water molecules will enter the hydration layer of the OCP structure, resulting in the formation of straight notches along the c-axis for the 4-h sample (Figure 1). Indeed, the Rietvald analysis of the XRD patterns show that both the *a* and *b* axes of the OCP unit cells increase considerably for the 4-h sample. Our interpretation is also in line with the ^{31}P MAS spectrum of the 4-h sample, where the line widths of the P1 and P2/P4 signals are somewhat broadened due to an increase in structural disorder. Consequently, the water molecules in the 4-h sample will cause a decrease in the τ_{CP} value because we have more water molecules surrounding the PO_4^{3-} species. On the other hand, $T_{1\rho}^{H}$ is sensitive to molecular motions in the frequency range around the effective LG irradiation field (*c.a.* 61 kHz).[51] Therefore, as more water molecules enter the OCP hydration layer, the more frequent collision among the water molecules, which should be much faster than the inverse of 61 kHz, will cause an increase in $T_{1\rho}^{H}$. As the pH of the reaction mixture increases further, the excessive water molecules in the hydration layer start to diffuse out of the OCP structure, resulting in an increase in τ_{CP} and a decrease in $T_{1\rho}^{H}$ for the 5-h sample. Accordingly, the cell dimensions of the 5-h sample become comparable to those of the 3-h sample (Table 2). Note that the variation in the CP dynamics of P3 is not as dramatic as those of P1, P2 and P4 because P3 is hydrogen bonded to the acidic proton of P6.[25]

^{31}P-^{31}P Double Quantum NMR. When two or more nuclear spins are in close proximity, they become coupled through the homonuclear dipole-dipole interaction. The magnitude of such interaction is inversely proportional to the third power of the internuclear distance. The so-called DQ coherence is a concerted evolution of coupled spins. The two-dimensional ^{31}P DQ spectrum of the 1.5-h sample is shown in Figure 7(a), where there are eight sets of auto- and cross-correlation peaks assigned to the OCP signals. Surprisingly, in the DQ spectra measured for the 3-h, 4-h and 5-h samples we do not observe any correlation peaks due to monetite (see Figure S 3 of the Supporting Information). Referring to Figure 7(a), by varying the DQ excitation and reconversion periods systematically, one can fit the intensities of the correlation peaks as a function of the excitation time based on the following equation[40]

$$I(\tau_{exe}) = A\tau_{exe}^{2}\exp\{-\tau_{exe}^{2}/B\}$$

In the above equation the build up of the DQ signals is described by a parabolic function[52,53] and the decay of the DQ signals is approximated by a Gaussian function.[54] Figure 7(b) illustrates such a fit for the P3-P6 DQ signals of the 1.5-h sample, in which the signal intensities had been normalized with respect to the MAS signals measured under identical conditions (spinning frequency, saturation comb and relaxation delay).[33] In principle, the parameter *A* can be used to determine the van Vleck's second moment of the coupled spins, whose magnitude depends on both the number of interacting spins and the internuclear distances.[55] However, the quantification of the second moment in the present study is not warranted due to the different efficacy of proton decoupling for different phosphorus species. Nevertheless, the variation of the parameter *A* should reflect the same variation in the second moment for a particular DQ signal, provided that the efficacy of the proton decoupling remains approximately the same. On the other hand, since the values of the parameter *B* are affected by both the ^{31}P spin-spin relaxation times and the spatial arrangement of the interacting phosphorus species, it is difficult to interpret the data trend unequivocally.

Figure 8 summarizes the values of the parameter *A* extracted for the cross-correlation peaks of our sample series. As expected, the *A* values for the 1.5-h sample are attenuated significantly due to insufficient proton decoupling. For the 3-h sample, the following data trend is parallel to what we expected from the calculated van Vleck's second moment:

A_{P2-P3}	>	$A_{P3-P5/P6}$	>	$A_{P2-P5/P6}$	>	$A_{P1-P5/P6}$	>	A_{P1-P3}
(3.19)		(1.84)		(1.08)		(0.46)		(0.35)

where the bracketed data denote the corresponding second moments (× 10^6 rad^2/s^2) calculated based on the X-ray structural data. As revealed in Figure 6, the efficacy of proton decoupling should be very similar for the 3-h and the 5-h samples. Therefore it is legitimate to calculate the percentage change of their *A* values corresponding to the same DQ coherence and compare the results with what we expected from our model for the OCP transformation (*vide infra*).

E. Computer Assisted Lattice Matching. It has been well established that the apatitic layer of OCP is structurally very similar to HAp. Indeed, our TEM/ED results are consistent with the scenarios that the *c* axes of the OCP and HAp unit cells are parallel or anti-parallel to one another during the phase transformation. For the OCP to HAp transformation, we assume that the phosphorus sites of OCP will take the shortest pathways to migrate to the nearest phosphorus sites of HAp. We generate two unit-cell models, *viz.* the guest and the host. The guest model contains the Cartesian coordinates of 24 phosphorus atoms in four unit cells of HAp while the host model contains the coordinates of 96 phosphorus atoms in 2 × 2 × 2 unit cells of OCP. Initially, the crystallographic *c* axes of both models are aligned in the same direction. The coordinates of the guest lattice are then mapped onto the host lattice rotationally and translationally. The rotation is about the *c* axis at steps of one degree and the translations are along three orthogonal axes at steps of 0.5 Å. The mean-square deviations (χ^2) between the OCP phosphorus sites of the apatite layer and the corresponding nearest HAp sites are calculated for each matching step. For the best matching with minimum χ^2, the shortest distances between selected OCP sites are calculated after they have been mapped onto the corresponding HAp sites. In other words, we label all the phosphorous atoms in the HAp lattice by the name tags of the six non-equivalent phosphorus sites in OCP and then calculate the corresponding distances of, say, P2-P3. Based on the distance information the van Vleck's second moments arising from P2-P3 are calculated using the following formula:[55]

$$M_2 = \frac{3}{5}\gamma^4\hbar^2 I(I+1)\sum_j \frac{1}{r_j^6}$$

The ratio of the P2-P3 M_2 values calculated for the matched HAP lattice and the OCP lattice are thus obtained. Similarly we obtained the ratios corresponding to the M_2 values of P1-P3, P1-P5/P6 and so on. All the calculations were then repeated for opposite alignment of the crystallographic *c* axes of the guest and host models (see Table S1 of the Supporting Information). Provided that the phosphorus sites of OCP will take the shortest pathways to migrate to the nearest phosphorus sites of HAp, the ratios of the experimental *A* values of P2-P3 measured for the 3-h and 5-h samples should be very similar to that calculated in our lattice matching model. Figure 9 plots the calculated ratios versus the ratios of the experimental *A* values. Note that a perfect agreement between the calculated and experimental ratios is not expected because the OCP to HAp transformation is not yet completed for the 5-h sample. Overall, our DQ experimental data are more consistent with the scenario that the crystallographic *c* axes of OCP and HAp are in opposite direction during the transformation. In addition, the lattice matching results for the anti-parallel alignment of the c-axes show that during the structural transformation the *b* axis of OCP is parallel to the *a* or *b* axis of HAP, where the *a* and *b* axes of HAP are equivalent because of the hexagonal symmetry of the unit cells.

Discussion

Double-Quantum NMR in Multiple-Spin Systems. DQ NMR spectroscopy under magic angle spinning has been the major research area in the solid-state NMR community for many years. Since the pioneering work of Tycko,[56] numerous pulse sequences designed for DQ NMR have been reported in the literature.[57-60] Our previous work illustrates that the excitation of DQ coherence is inherently difficult in multiple-spin system due to the dephasing effect of other passive spins.[33] It has also been shown that distance measurement by DQ NMR spectroscopy in homonuclear spin system is practical only if the two-spin approximation holds.[61] Nevertheless, here we have demonstrated that it remains possible to employ DQ NMR spectroscopy to monitor the change of the spatial arrangement of interacting spins, provided that an adequate structural model is constructed to interpret the variation of the DQ signal intensities. In this work, our computer assisted lattice matching provides such a model in which the structural constraint obtained by SAED measurements is incorporated. We note in passing that Levitt and co-workers have successfully employed solid-state ^{29}Si DQ dipolar recoupling NMR to help elucidate the crystal structures of siliceous zeolite model compounds by measuring distance-dependent dipolar interactions between naturally abundant ^{29}Si nuclei in the zeolite frameworks, where the two-spin approximation clearly holds for two interacting ^{29}Si nuclei.[62,63]

OCP to HAp transition. In an early study by Eanes and Meyer, the nature of the phase changes occurring in spontaneously precipitated amorphous calcium phosphate (ACP) was studied under physiological condition.[9] Based on the measured ion concentrations and Ca/P ratio, it was concluded that the ACP precipitate would first transform into an OCP-like phase which subsequently hydrolyzed into apatite. This result is consistent with the Ostwald-Lussac law of stages, which states that under conditions of sequential precipitation the initial phase formed is the one with the highest solubility followed by other crystalline phases in order of decreasing solubility.[1] For our in-vitro system, we also observe the co-precipitation of monetite at 100ºC. In the thermodynamic aspect, the co-precipitation of monetite is not unexpected because the solubility product of brushite, the hydrated form of monetite, is very similar to that of OCP at pH around 4.71 to 5.12.[64] The detection of co-precipitation of monetite by the HETCOR NMR technique is of great interest in the study of biomineralization because diffraction techniques are unlikely to distinguish between HAp, OCP or monetite when the crystallites are thinner than 10 nm as reported for bone.[65] Based on the similarity of the calcium phosphate chains present in both the OCP and monetite structures, it has been speculated the formation of intracrystalline mixture of OCP and monetite by direct precipitation or by hydrolysis of OCP.[65] From our NMR data, however, we have no direct evidence for the existence of such intracrystalline mixture. The absence of the monetite ^{31}P signals in the DQ spectra of our 3-h, 4-h and 5-h samples could be explained by the argument that the amount of the monetite phase is too low to give any appreciable DQ signals.

Some years ago, Nelson and co-workers described the OCP to HAp transformation as a simple dehydration process.[12] Here, we could refine this description further for our in-vitro system as follows. The OCP crystals obtained at 1.5 h contain a lot of structural waters, rendering the crystallinity rather poor. The amorphous character of the crystals reveals that the formation of OCP crystals is preceded by the precipitation of ACP. When the pH of the reaction mixture is lower than 4.71, those water molecules in excess will be eventually driven out of the lattice, resulting in an improvement of the crystallinity. As the pH increases to around 5, water molecules will reenter the OCP lattice, presumably through the hydration layer of the OCP structure. This reversal in water flow direction is accompanied by a significant lengthening of the crystallographic *a* and *b* axes, causing an expansion of the OCP lattice. The "crowded" water molecules in the hydration layer then provide a collisional mechanism for the relocation of the HPO_4^{2-} groups (P5 and P6) as shown in Figure 10. In spite of the 2.1 % mismatch between the (100) crystal planes of OCP and HAp, the structural stress induced by the movement of P5 and P6 will cause the apatite layers in the blade-like OCP crystals splitted across the b axis. The HPO_4^{2-} ions are subsequently deprotonated and the water molecules of the hydration layers are released to stabilize the structure. Those apatite layers serve as nucleation centers for further crystal growth, leading to the formation of hexagonal HAp rods eventually, where the c axis of the newly formed HAp lattice is anti-parallel to that of the precursor OCP lattice.

Implication in Biomineralization. According to the crystallographic data and our assignment of the ^{31}P MAS spectrum of the 3-h sample, the peaks positioned at -0.2 (P5, P6), 2.0 (P3), 3.3 (P2, P4) and 3.7 (P1) ppm should have an intensity ratio of 2:1:2:1 but what has been measured for our OCP sample is 3:1:1:1 (Table 3). To rationalize the ^{31}P NMR peak intensity ratio we have previously suggested that some of the PO_4^{3-} groups at the P2 and P4 sites are involved in the following transformation to become HPO_4^{2-}ions:[32]

$$HPO_4^{2-} + OH^- = PO_4^{3-} + H_2O.$$

In our analysis of the $^{31}P\{^1H\}$ LG-CP data, the same mechanism can be applied to explain the intrusion of water molecules into the hydration layers and the deprotonation of the HPO_4^{2-} ions. We surmise that this hydrolysis reaction may also take an important role in the formation of biological apatites in bones or teeth.

Conclusion

In summary, we have established a very useful in-vitro system to obtain HAp nanorods with different morphologies by homogeneous precipitation of OCP crystals. Our data obtained by a series of physical techniques, with particular emphasis in solid-state NMR, provide a detailed description of the molecular mechanism of OCP to HAp transformation. For the first time it has been shown experimentally that OCP crystals transform to HAp topotaxially along their c axes with anti-parallel relationship, instead of the parallel relationship as presumed in the literature. Furthermore, we find that the hydrolysis reaction of the PO_4^{3-} and HPO_4^{2-} ions is the key chemical reaction for OCP to HAp transformation. While the scope of this work is limited to the molecular mechanism of OCP to HAp transition, the solid-state NMR approach established here can be readily applied to the studies of bones and teeth.

Table 1. Summary of the pH values of the reaction mixture at different periods

Reaction Time (h)	pH
0	4.35
1.5	4.50
3	4.71
4	5.01
5	5.12
6	5.87
12	6.69

Table 2. Summary of the lattice parameters obtained by Rietvald analysis.

Sample	*a* [Å]	*b* [Å]	*c* [Å]	cell volume [Å^3]
1.5-h	19.7316(8)[a]	9.5615(3)	6.8508(2)	1224.96(7)
3-h	19.7049(9)	9.5525(4)	6.8447(2)	1222.59(8)
4-h	19.8456(38)	9.5941(17)	6.8445(9)	1232.03(32)
5-h	19.7017(10)	9.5490(5)	6.8471(2)	1222.57(9)

[a] The bracketed values are error estimations.

Table 3. ^{31}P chemical shift data and the assignment of the 3-h sample

	^{31}P δ_{iso} [ppm]	Intensity ratio		
P1	3.7	1	PO_4^{3-}	Apatite layer
P2, P4	3.3	1	PO_4^{3-}	Apatite layer
P3	2.0	1	PO_4^{3-}	Interface
P5, P6	-0.2	3	HPO_4^{2-}	Hydration layer

REFERENCES

(1) Mann, S., *Biomineralization - Principles and Concepts in Bioinorganic Materials Chemistry*. Oxford University Press: New York, 2001.
(2) Dorozhkin, S. V.; Epple, M., *Angew. Chem. Int. Ed.* **2002,** *41*, 3130.
(3) Iijima, M.; Moradian-Oldak, J., *J. Mater. Chem.* **2004,** *14*, 2189.
(4) Brown, W. E., *Clin. Orthop.* **1966,** *44*, 205.
(5) Iijima, M.; Nelson, D. G. A.; Pan, Y.; Kreinbrink, A. T.; Adachi, M.; Goto, T.; Moriwaki, Y., *Calcif. Tissue Int.* **1996,** *59*, 377.
(6) Bodier-Houlle, P.; Steuer, P.; Voegel, J. C.; Cuisinier, F. J. G., *Acta Crystallogr. D* **1998,** *54*, 1377.
(7) Aoba, T.; Komatsu, H.; Shimazu, Y.; Yagishita, H.; Taya, Y., *Connect. Tissue Res.* **1998,** *39*, 129.
(8) Nancollas, G. H.; Tomazic, B., *J. Phys. Chem.* **1974,** *78*, 2218.
(9) Eanes, E. D.; Meyer, J. L., *Calcif. Tissue Res.* **1977,** *23*, 259.
(10) Boskey, A. L.; Posner, A. S., *J. Phys. Chem.* **1976,** *80*, 40.
(11) Chickerur, N. S.; Tung, M. S.; Brown, W. E., *Calcif. Tissue Int.* **1980,** *32*, 55.
(12) Nelson, D. G. A.; McLean, J. D., *Calcif. Tissue Int.* **1984,** *36*, 219.
(13) Eanes, E. D.; Posner, A. S., *Mater. Res. Bull.* **1970,** *5*, 377.
(14) Iijima, M.; Kamemizu, H.; Wakamatsu, N.; Goto, T.; Doi, Y.; Moriwaki, Y., *J. Cryst. Growth* **1997,** *181*, 70.
(15) Kniep, R.; Busch, S., *Angew. Chem.-Int. Edit. Engl.* **1996,** *35*, 2624.
(16) Iijima, M.; Moriwaki, Y.; Yamaguchi, R.; Kuboki, Y., *Connect. Tissue Res.* **1997,** *36*, 73.
(17) Schwarz, K.; Epple, M., *Chem.-Eur. J.* **1998,** *4*, 1898.

(18) Busch, S.; Dolhaine, H.; DuChesne, A.; Heinz, S.; Hochrein, O.; Laeri, F.; Podebrad, O.; Vietze, U.; Weiland, T.; Kniep, R., *Eur. J. Inorg. Chem.* **1999**, 1643.

(19) Falini, G.; Gazzano, M.; Ripamonti, A., *J. Mater. Chem.* **2000,** *10*, 535.

(20) Iijima, M.; Moriwaki, Y.; Takagi, T.; Moradian-Oldak, J., *J. Cryst. Growth* **2001,** *222*, 615.

(21) Peters, F.; Epple, M., *J. Chem. Soc.-Dalton Trans.* **2001**, 3585.

(22) Iijima, M.; Moriwaki, Y.; Wen, H. B.; Fincham, A. G.; Moradian-Oldak, J., *J. Dent. Res.* **2002,** *81*, 69.

(23) Brown, W. E., *Nature (London)* **1962,** *196*, 1048.

(24) Kay, M. I.; Young, R. A.; Posner, A. S., *Nature (London)* **1964,** *204*, 1050.

(25) Mathew, M.; Brown, W. E.; Schroeder, L. W.; Dickens, B., *J. Crystallogr. Spectrosc. Res.* **1988,** *18*, 235.

(26) Suvorova, E. I.; Madsen, H. E. L., *J. Cryst. Growth* **1999,** *199*, 677.

(27) Iijima, M.; Tohda, H.; Moriwaki, Y., *J. Cryst. Growth* **1992,** *116*, 319.

(28) Fernandez, M. E.; Zorrilla-Cangas, C.; Garcia-Garcia, R.; Ascencio, J. A.; Reyes-Gasga, J., *Acta Crystallogrc.* **2003,** *B59*, 175.

(29) Zhan, J.; Tseng, Y.-H.; Chan, J. C. C.; Mou, C.-Y., *Advan. Func. Mater.* **2005**.

(30) Rothwell, W. P.; Waugh, J. S.; Yesinowski, J. P., *J. Am. Chem. Soc.* **1980,** *102*, 2637.

(31) Aue, W. P.; Roufosse, A. H.; Glimcher, M. J.; Griffin, R. G., *Biochemistry* **1984,** *23*, 6110.

(32) Tseng, Y. H.; Zhan, J. H.; Lin, K. S. K.; Mou, C. Y.; Chan, J. C. C., *Solid State Nucl. Magn. Reson.* **2004,** *26*, 99.

(33) Tseng, Y. H.; Mou, Y.; Mou, C. Y.; Chan, J. C. C., *Solid State Nucl. Magn. Reson.* **2005,** *27*, 266.

(34) Santos, R. A.; Wind, R. A.; Bronnimann, C. E., *J. Magn. Reson. Ser. B* **1994,** *105*, 183.

(35) Kaflak-Hachulska, A.; Samoson, A.; Kolodziejski, W., *Calcif. Tissue Int.* **2003,** *73*, 476.

(36) Cho, G. Y.; Wu, Y. T.; Ackerman, J. L., *Science* **2003,** *300*, 1123.

(37) Wu, Y.; Ackerman, J. L.; Strawich, E. S.; Rey, C.; Kim, H. M.; Glimcher, M. J., *Calcif. Tissue Int.* **2003,** *72*, 610.

(38) Isobe, T.; Nakamura, S.; Nemoto, R.; Senna, M.; Sfihi, H., *J. Phys. Chem. B* **2002,** *106*, 5169.

(39) Chan, J. C. C.; Ohnsorge, R.; Meise-Gresch, K.; Eckert, H.; Holand, W.; Rheinberger, V., *Chem. Mater.* **2001,** *13*, 4198.

(40) Lin, K. S. K.; Tseng, Y. H.; Mou, Y.; Hsu, Y. C.; Yang, C. M.; Chan, J. C. C., *Chem. Mater.* **2005,** *17*, 4493.

(41) van Rossum, B. J.; de Groot, C. P.; Ladizhansky, V.; Vega, S.; de Groot, H. J. M., *J. Am. Chem. Soc.* **2000,** *122*, 3465.

(42) Ladizhansky, V.; Vega, S., *J. Chem. Phys.* **2000,** *112*, 7158.

(43) Ernst, R. R.; Bodenhausen, G.; Wokaun, A., *Principles of Nuclear Magnetic Resonance in One and Two Dimensions*. Clarendon Press: Oxford, 1987.

(44) Larson, A. C.; von Dreele, R. B., *Los Alamos National Laboratory Report LA-UR* **2000**, 86-748.

(45) Toby, B. H., *J. Appl. Cryst.* **2001,** *34*, 210.

(46) Metz, G.; Wu, X. L.; Smith, S. O., *J. Magn. Reson. A* **1994,** *110*, 219.

(47) Oyler, N. A.; Tycko, R., *J. Phys. Chem. B* **2002,** *106*, 8382.

(48) Gullion, T.; Baker, D. B.; Conradi, M. S., *J. Magn. Reson.* **1990,** *89*, 479.

(49) Tropp, J.; Blumenthal, N. C.; Waugh, J. S., *J. Am. Chem. Soc.* **1983,** *105*, 22.

(50) Yesinowski, J. P.; Eckert, H., *J. Am. Chem. Soc.* **1987,** *109*, 6274.

(51) Freeman, R., *Spin Choreography: Basic Steps in High Resolution NMR*. Oxford University Press: New York, 1998.

(52) Bertmer, M.; Eckert, H., *Solid State Nucl. Magn. Reson.* **1999,** *15*, 139.

(53) Gunne, J.; Eckert, H., *Chem.-Eur. J.* **1998,** *4*, 1762.

(54) Engelsberg, M.; Norberg, R. E., *Phys. Rev. B* **1972,** *5*, 3395.

(55) Abragam, A., *Principles of Nuclear Magnetism*. Clarendon Press: Oxford, 1961.

(56) Tycko, R.; Dabbagh, G., *Chem. Phys. Lett.* **1990,** *173*, 461.

(57) Tycko, R., *Annu. Rev. Phys. Chem.* **2001,** *52*, 575.
(58) Baldus, M., *Prog. Nucl. Magn. Reson. Spectrosc.* **2002,** *41*, 1.
(59) Luca, S.; Heise, H.; Baldus, M., *Accounts Chem. Res.* **2003,** *36*, 858.
(60) Schnell, I., *Prog. Nucl. Magn. Reson. Spectrosc.* **2004,** *45*, 145.
(61) Gunne, J., *J. Magn. Reson.* **2003,** *165*, 18.
(62) Brouwer, D. H.; Darton, R. J.; E., M. R.; Levitt, M. H., *J. Am. Chem. Soc.* **2005,** *127*, 10365.
(63) Brouwer, D. H.; Kristiansen, P. E.; Fyfe, C. A.; Levitt, M. H., *J. Am. Chem. Soc.* **2005,** *127*, 542.
(64) Heughebaert, J. C.; Nancollas, G. H., *J. Phys. Chem.* **1984,** *88*, 2478.
(65) Brown, W. E.; Smith, J. P.; Lehr, J. R.; Frazier, A. W., *Nature (London)* **1962,** *196*, 1050.

Supporting Information.

Table S1. Calculated second moments based on the computer assisted lattice matching.

	Calculated Second Moment [10^6 rad^2/s^2]		
	OCP	HAp↑↑ (ratio in %)[a]	HAp↑↓ (ratio in %)[b]
P3-P5/P6	1.84	1.07 (58 %)	1.84 (100 %)
P2-P5/P6	1.08	1.84 (170 %)	1.07 (99 %)
P1-P5/P6	0.46	0.17 (37 %)	0.16 (35 %)
P2-P3	3.19	1.45 (45 %)	1.45 (45 %)
P1-P3	0.35	0.76 (217 %)	0.37 (105 %)

[a] HAp↑↑ denotes the HAp lattice matched to the OCP lattice with both c axes aligned in parallel fashion. The ratio is obtained with respect to the second moments calculated for the OCP lattice.

[b] HAp↑↓ denotes the HAp lattice matched to the OCP lattice with both c axes aligned in anti-parallel fashion.

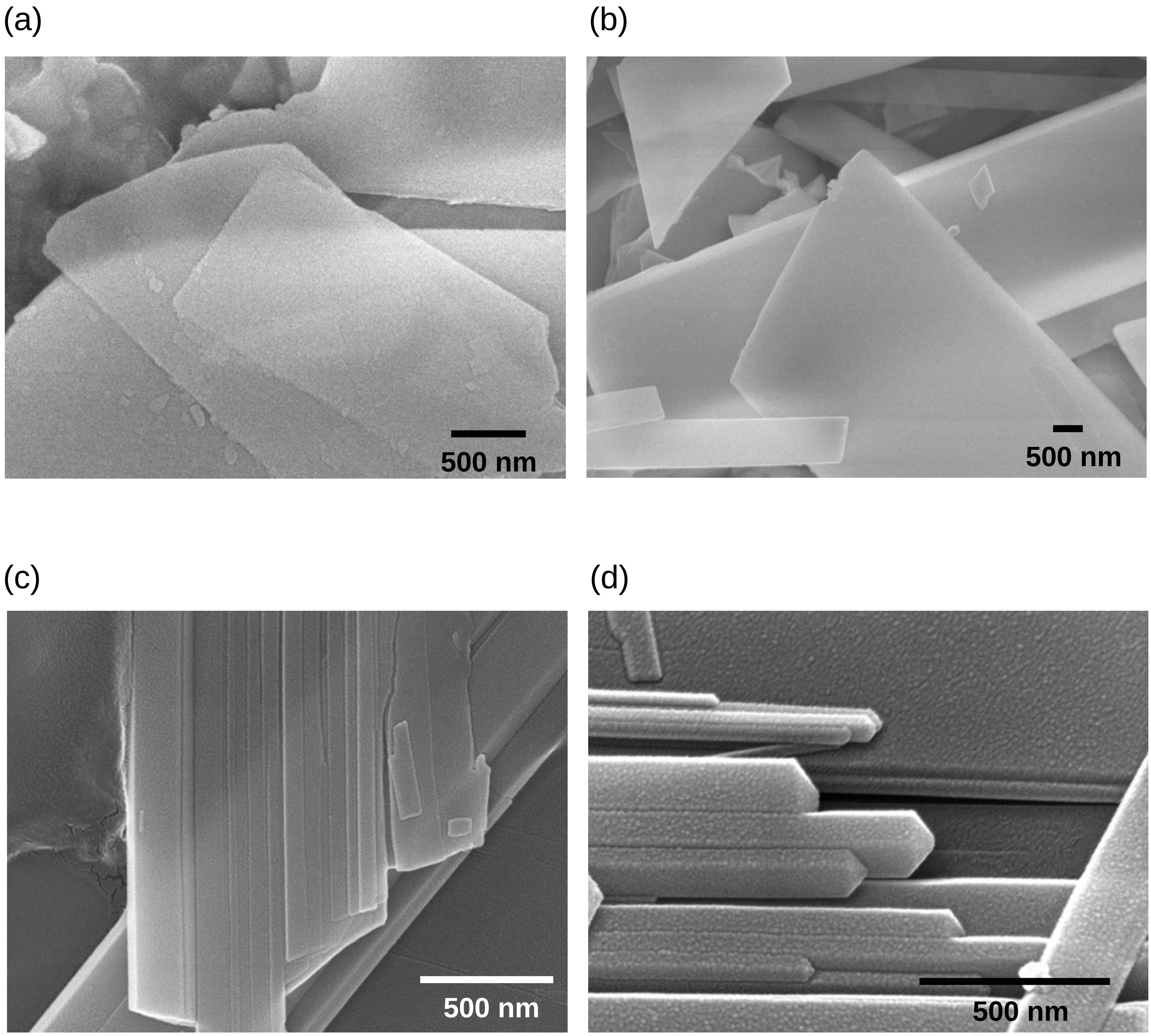

Figure 1. SEM images of the calcium phosphate precipitate collected at different reaction times. (a) 1.5 h; (b) 3 h; (c) 4 h; (d) 12 h.

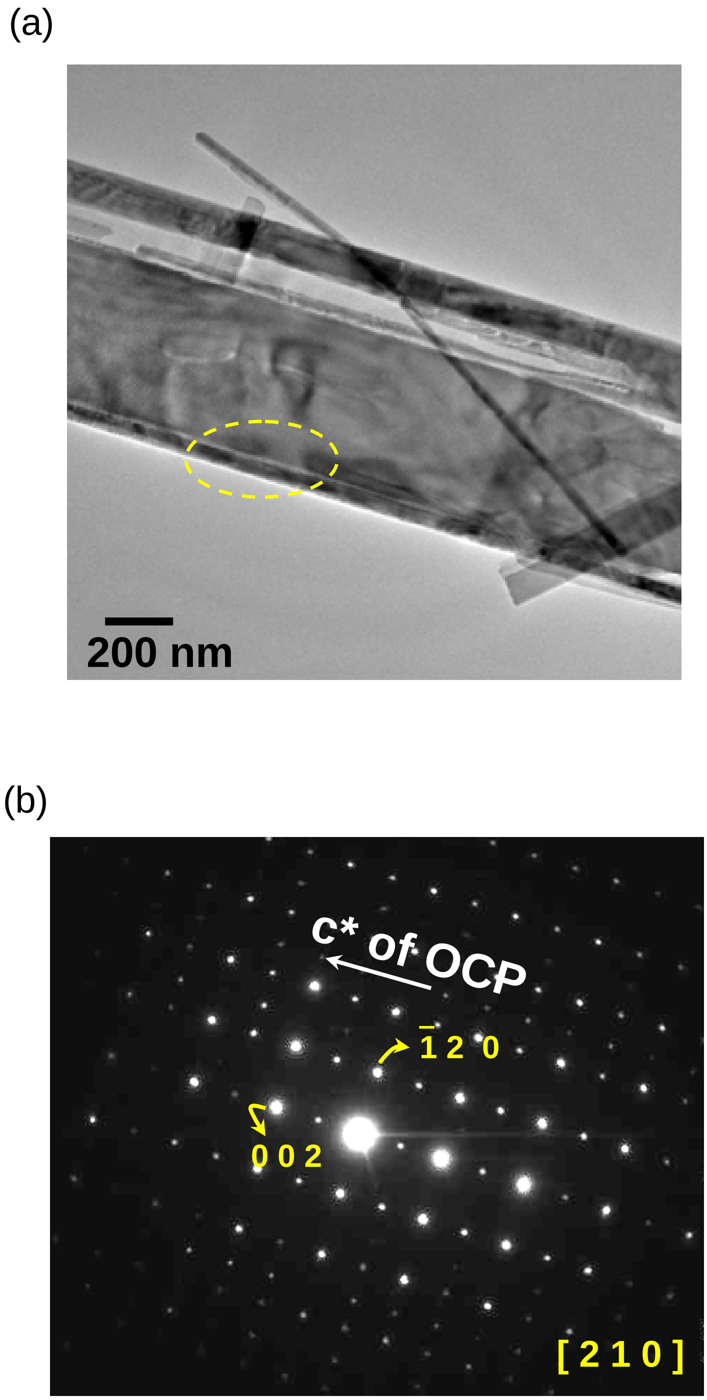

Figure 2. (a) TEM images and (b) SAED pattern measured for the 6-h sample. The SAED pattern was taken from the ellipsoidal region highlighted in (a).

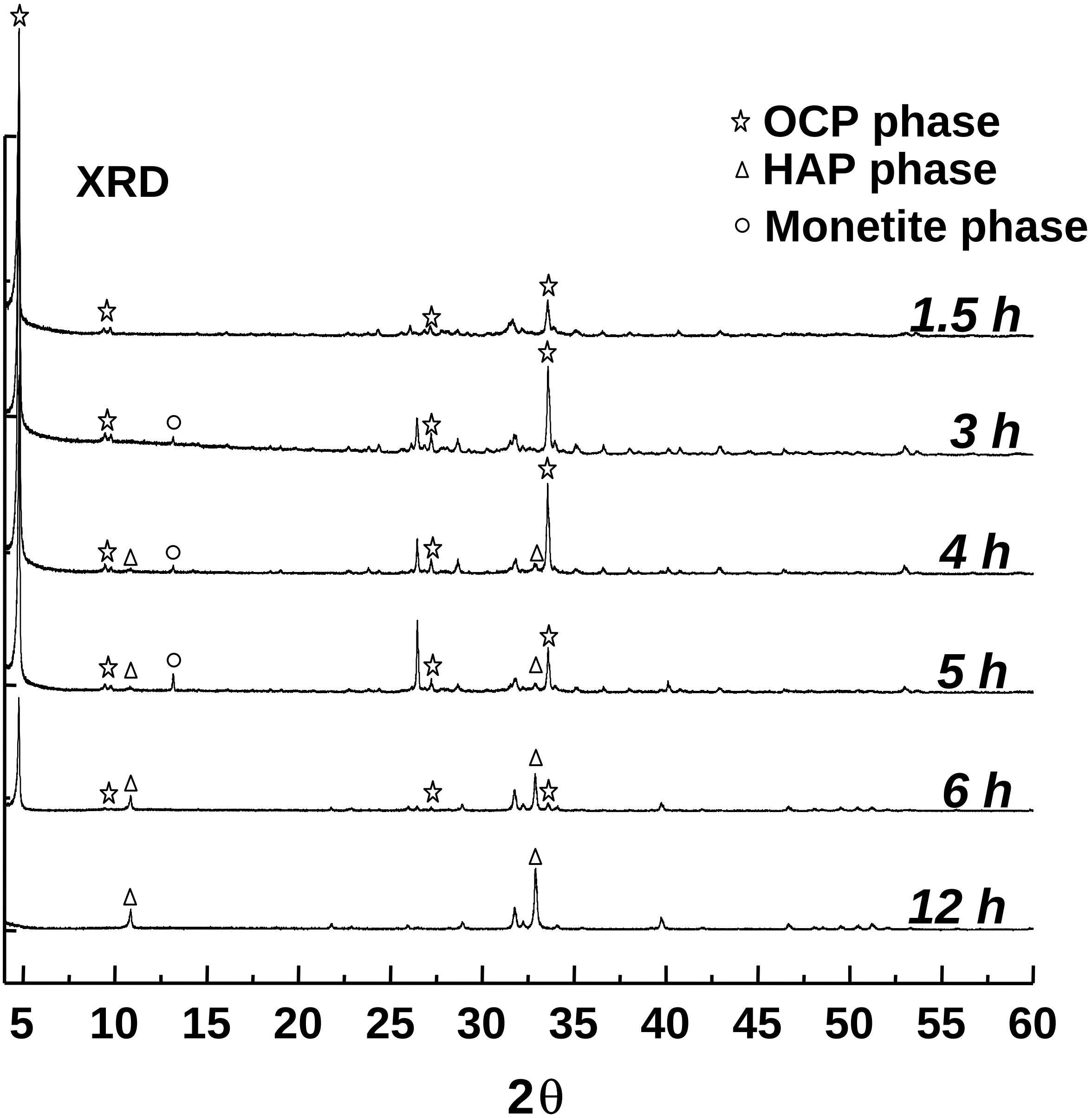

Figure 3. XRD patterns measured for samples obtained at different reaction times.

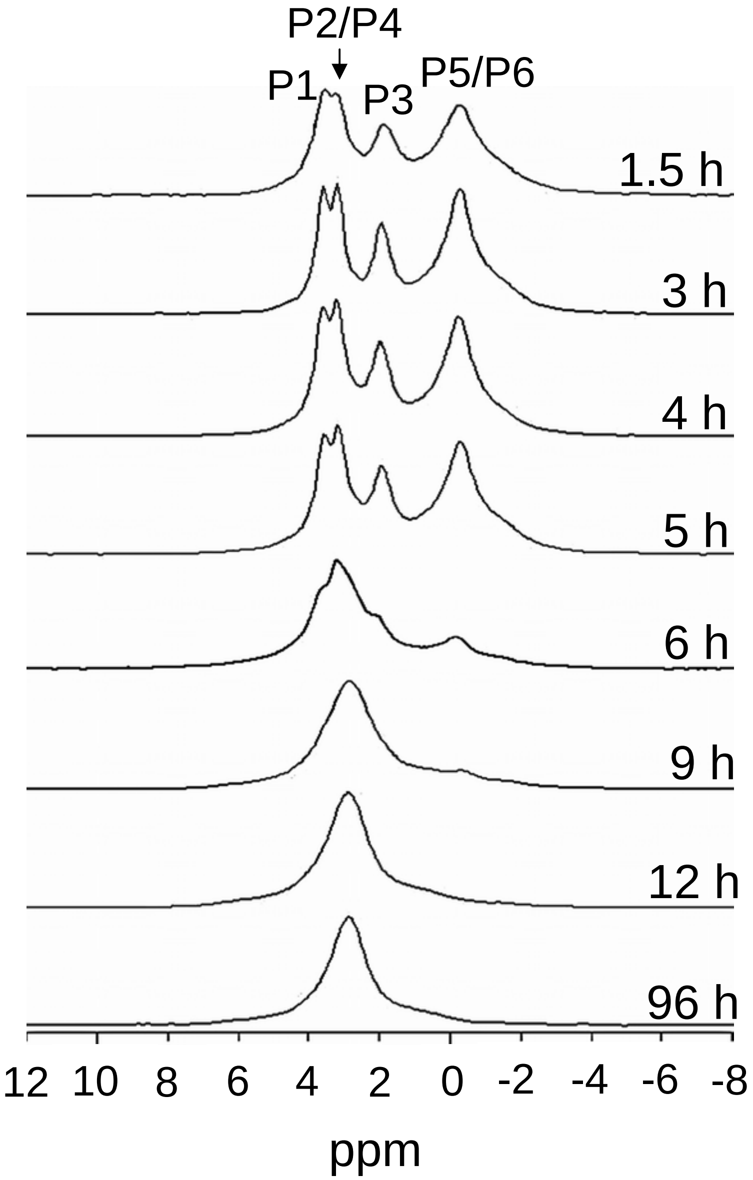

Figure 4. ^{31}P MAS spectra measured for our sample series at 10 kHz spinning frequency and 7.05 Tesla.

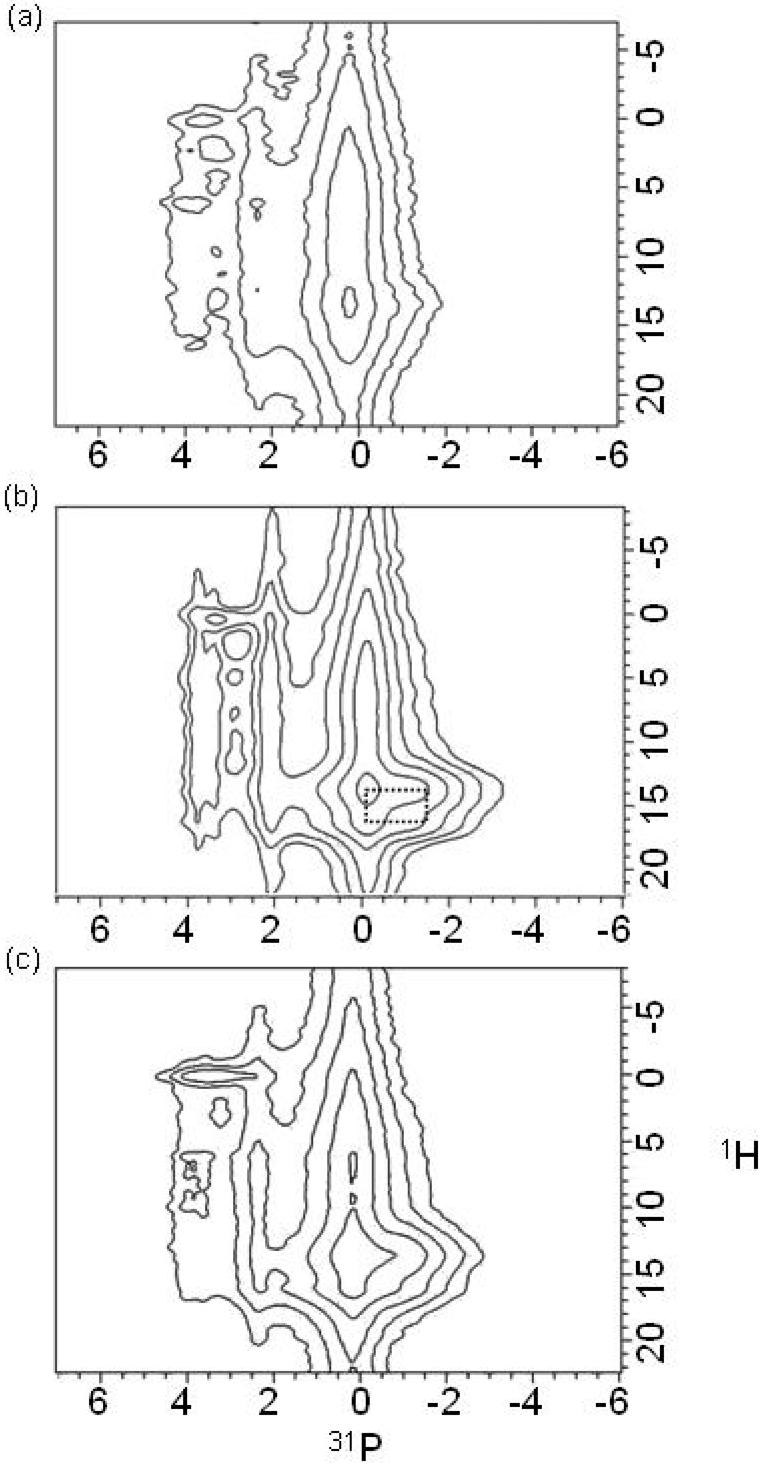

Figure 5. ^{31}P{^{1}H} HETCOR spectra measured for samples (a) 1.5-h; (b) 3-h; (c) 5-h.

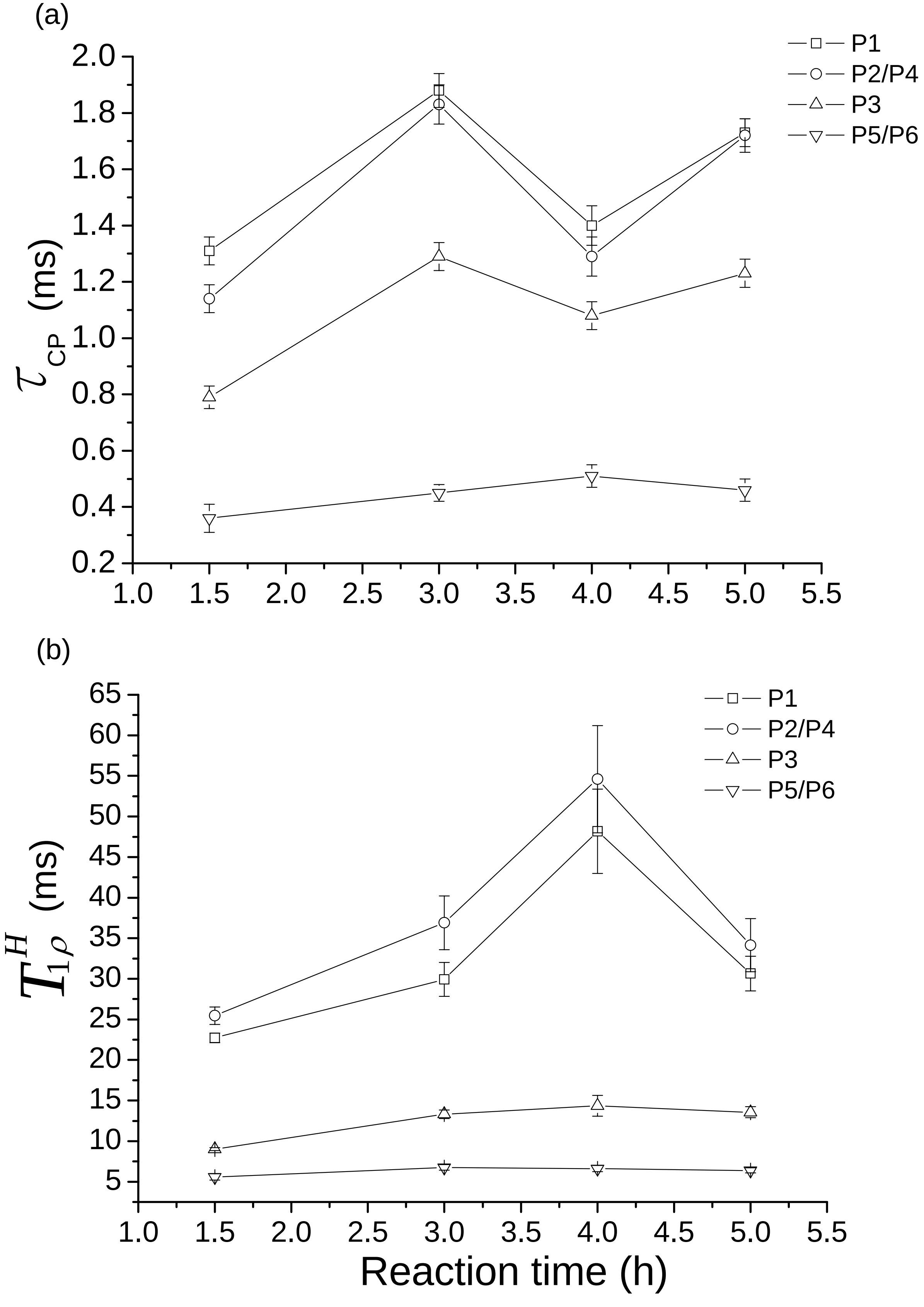

Figure 6. LG-CP parameters obtained for our sample series: (a) τ_{CP} ; (b) $T_{1\rho}^{H}$

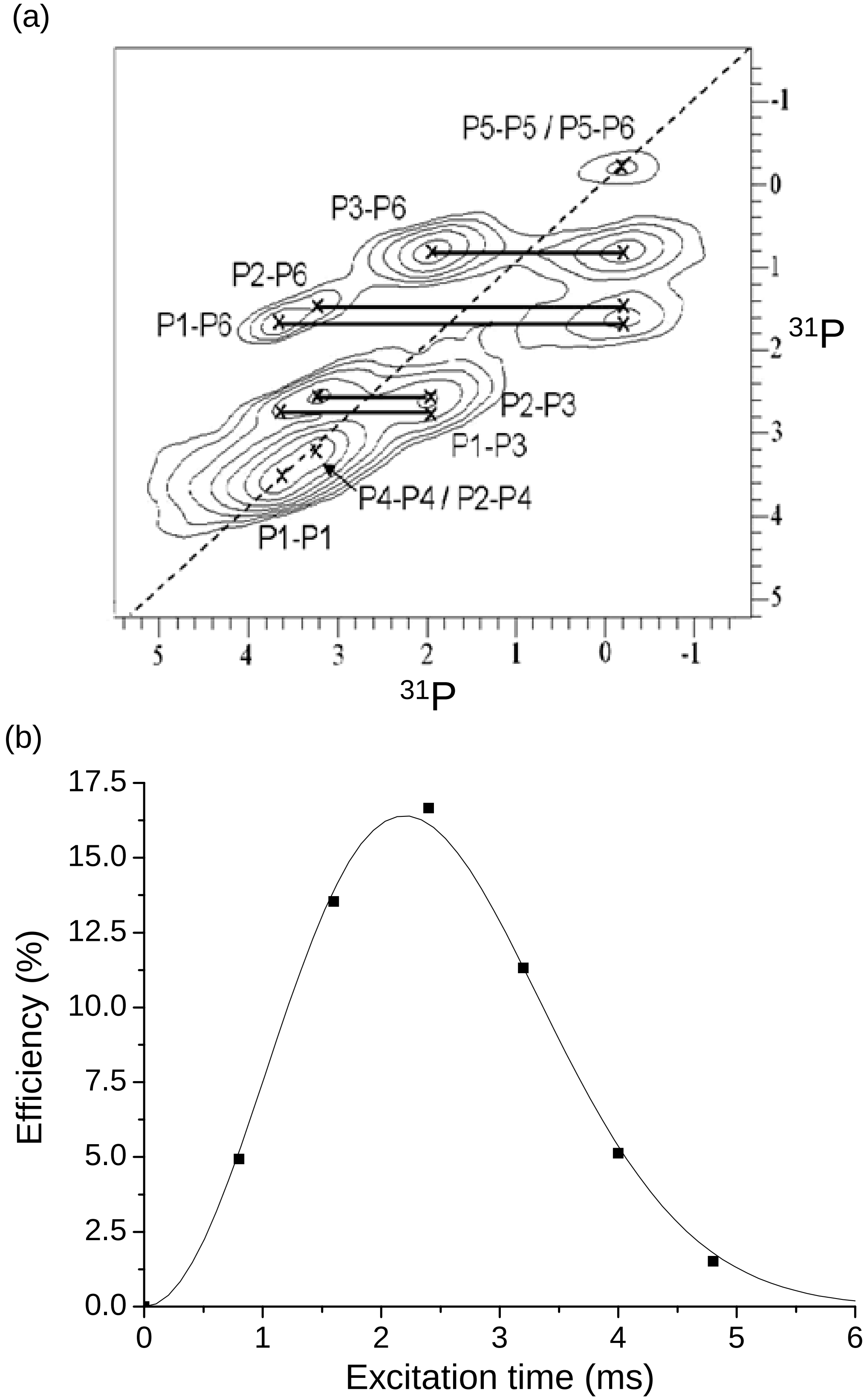

Figure 7. (a) ^{31}P DQ correlation spectrum of the 1.5-h sample. The DQ excitation time was set to 3.2 ms. (b) Fitting of the modulation of the normalized P3-P6 DQ signals (excitation efficiency) as a function of excitation time.

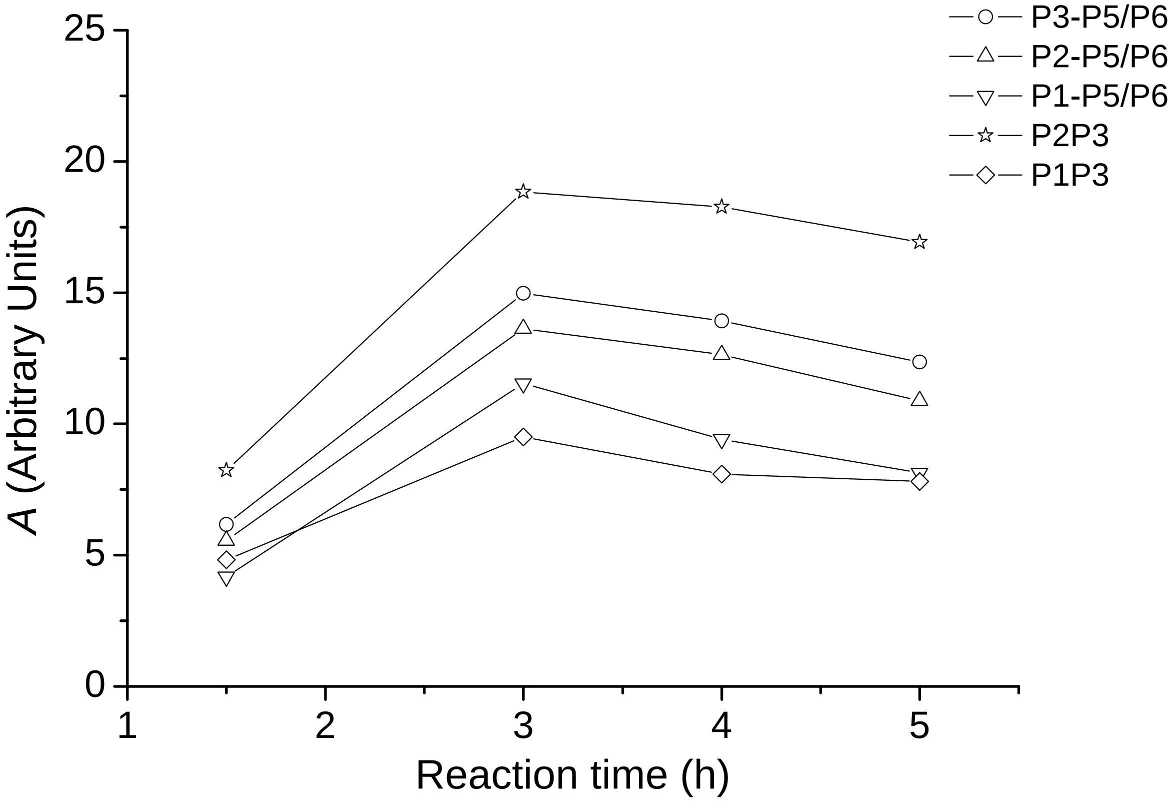

Figure 8. Plot of the parameter *A* extracted for the cross-correlation peaks. The sizes of the symbols are larger than the error bars.

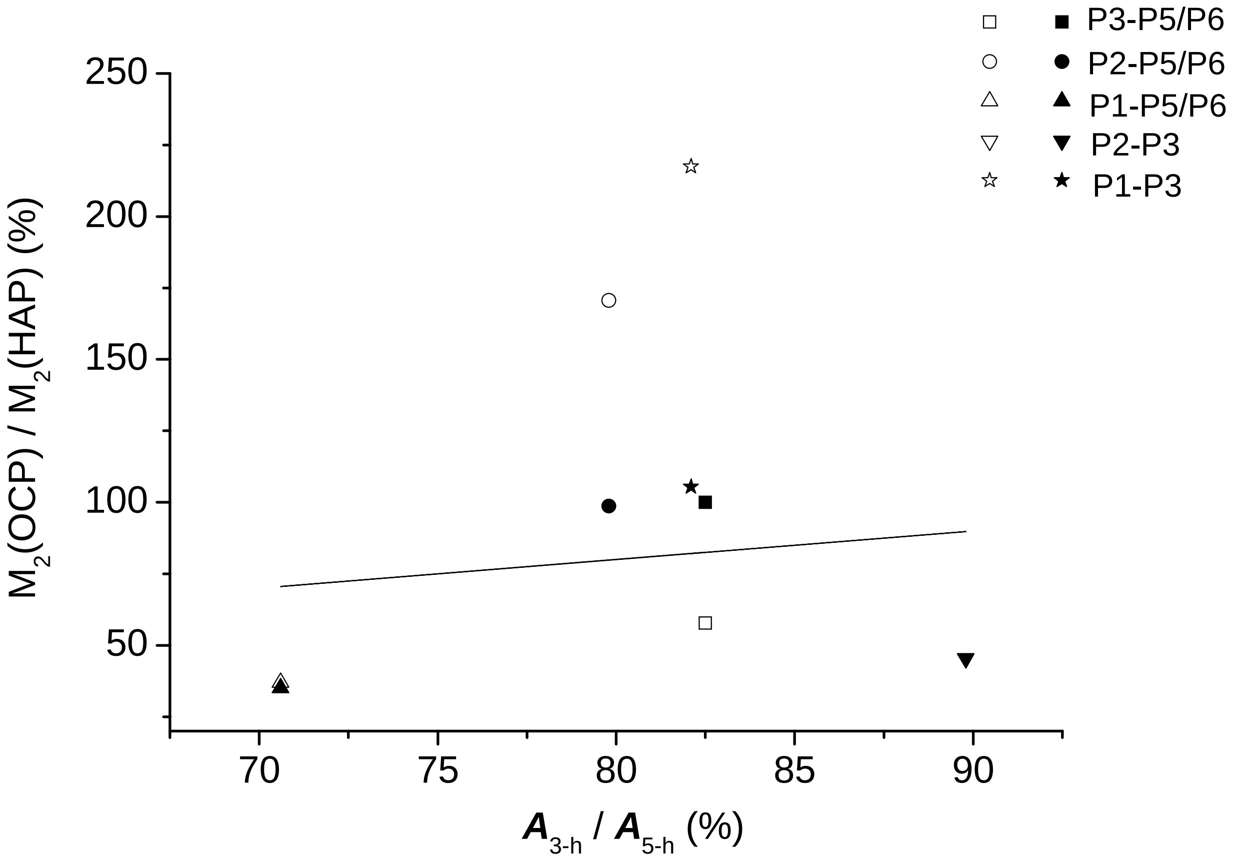

Figure 9. Plot of the calculated ratios of the second moments of the OCP and the matched HAp lattice versus the ratios of the experimental *A* values measured for the 3-h and 5-h samples. The filled and open symbols denote the calculated data for anti-parallel and parallel alignment of the crystallographic c axes of OCP and HAp, respectively. The solid line denotes perfect agreement.

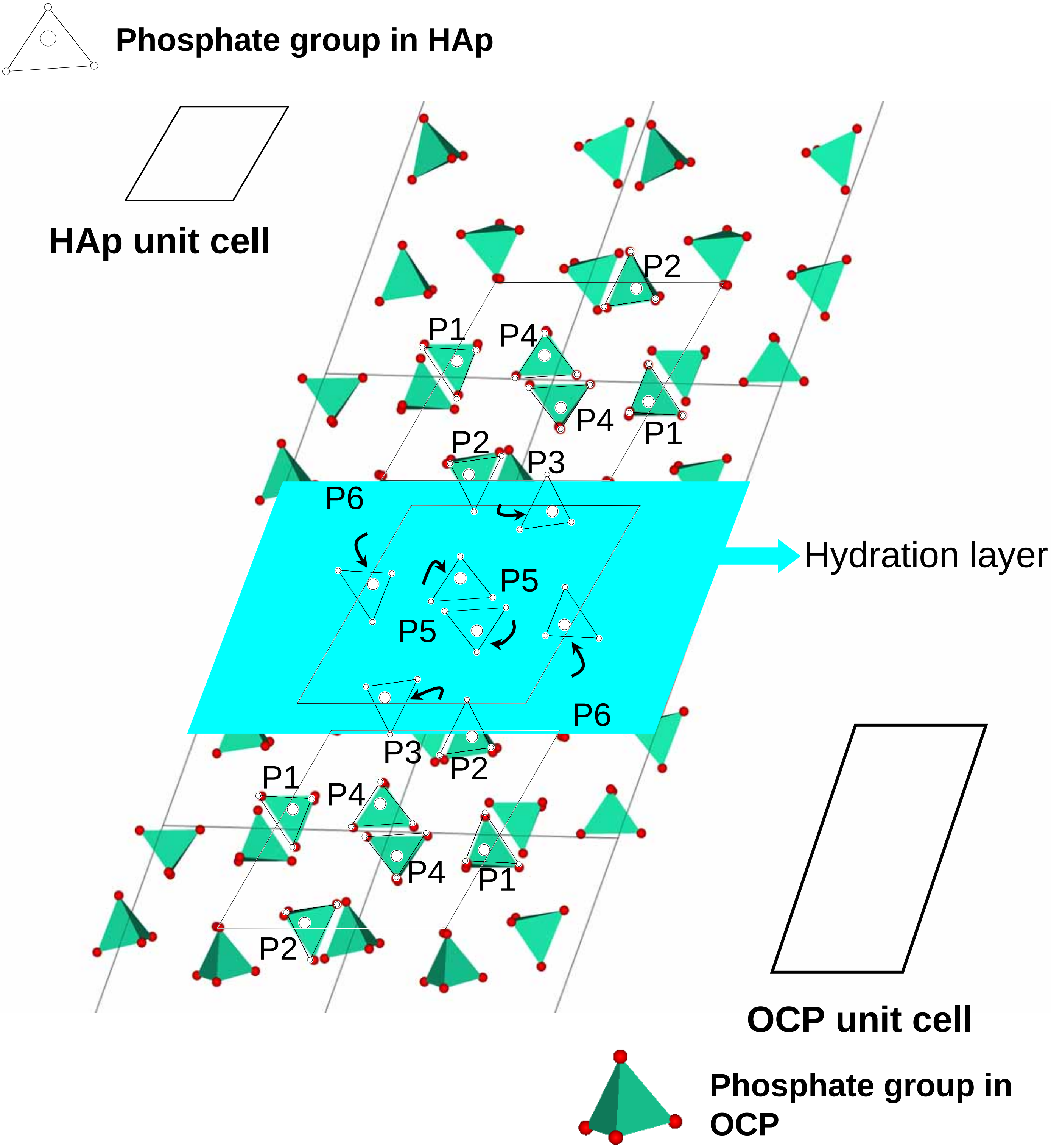

Figure 10. Possible movement of P5 and P6 in an OCP crystal to generate HAp structure is indicated by arrows. The structures are projected down the c axis.

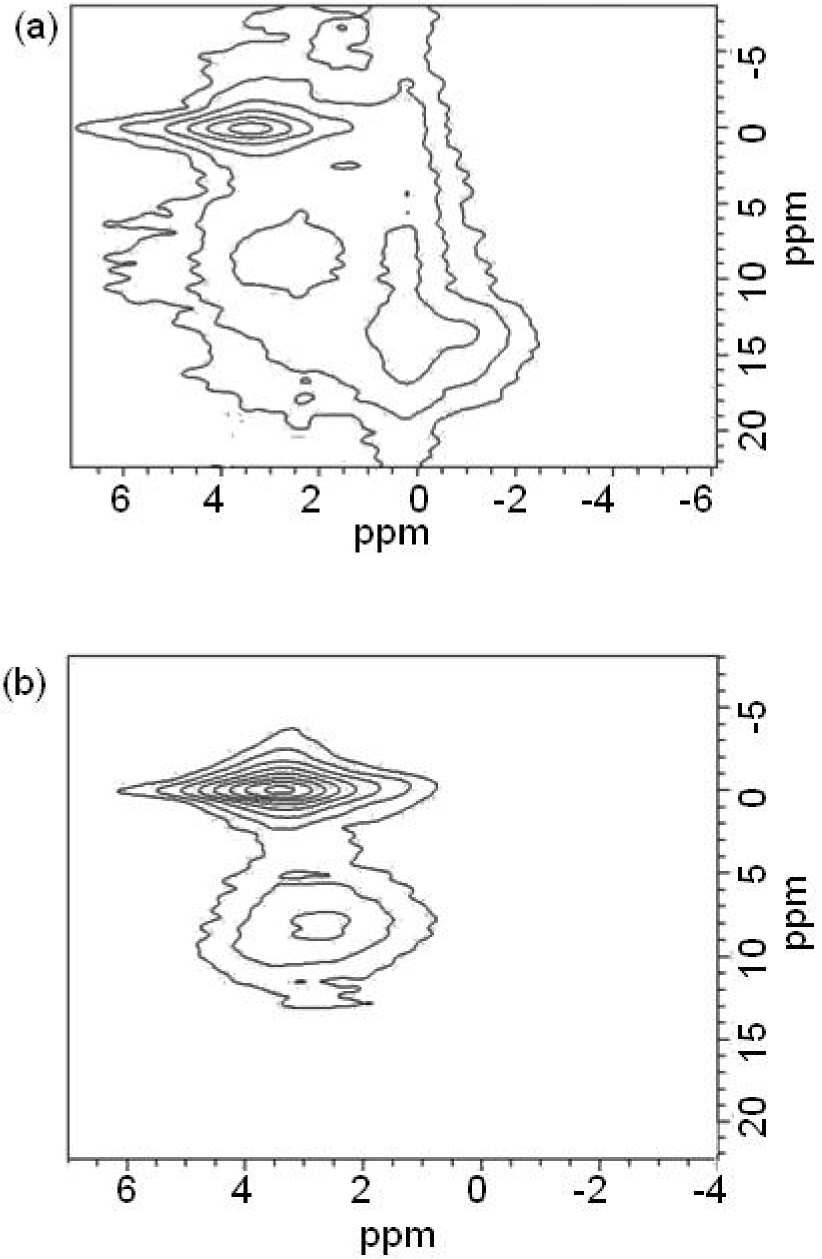

Figure S1. $^{31}P\{^{1}H\}$ HETCOR spectra measured for samples (a) 6-h; (b) 12-h.

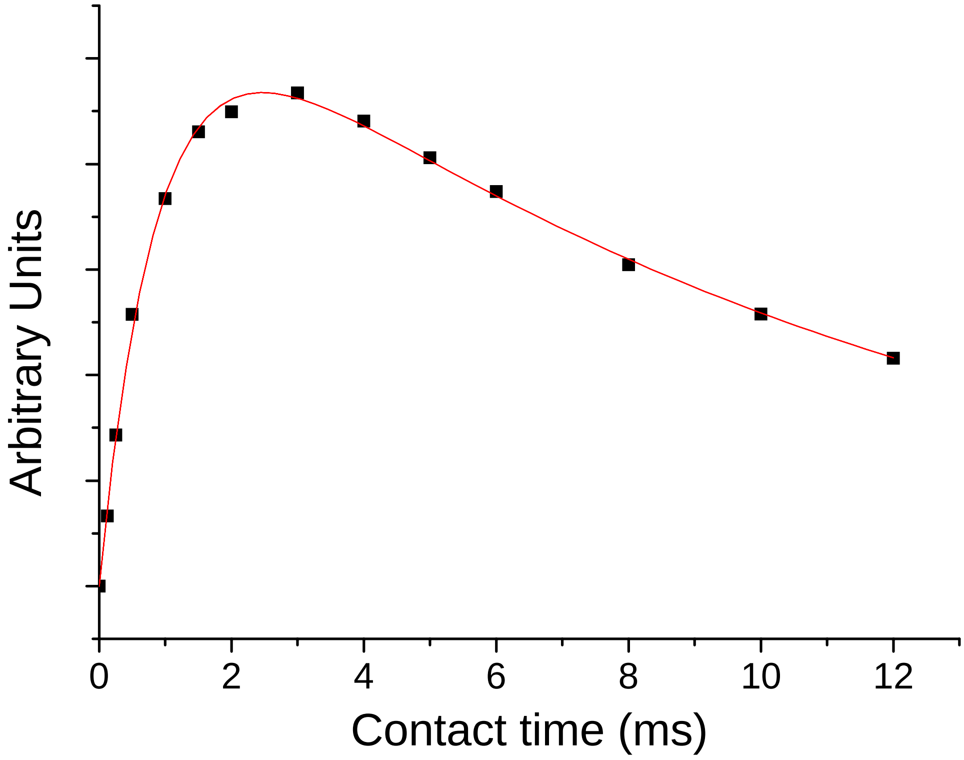

Figure S2. Typical fitting of the raw data of $^{31}P\{^{1}H\}$ LG-CP variable contact time experiment.

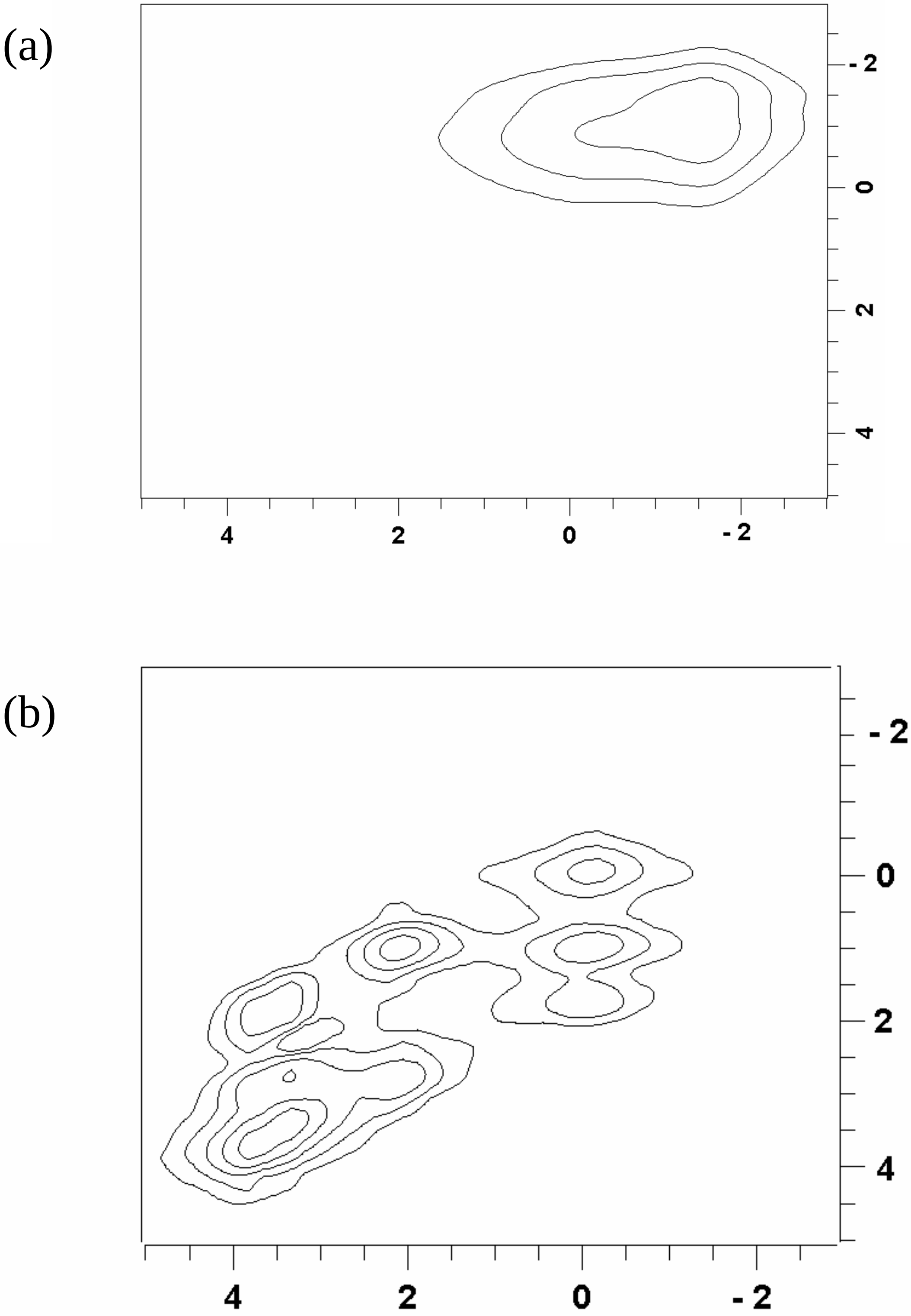

Figure S3. ^{31}P DQ spectra of (a) monetite; (b) 4-h sample.

II-E. C-13 Homonuclear Polarization Transfer in Biological Solids without Proton Decoupling

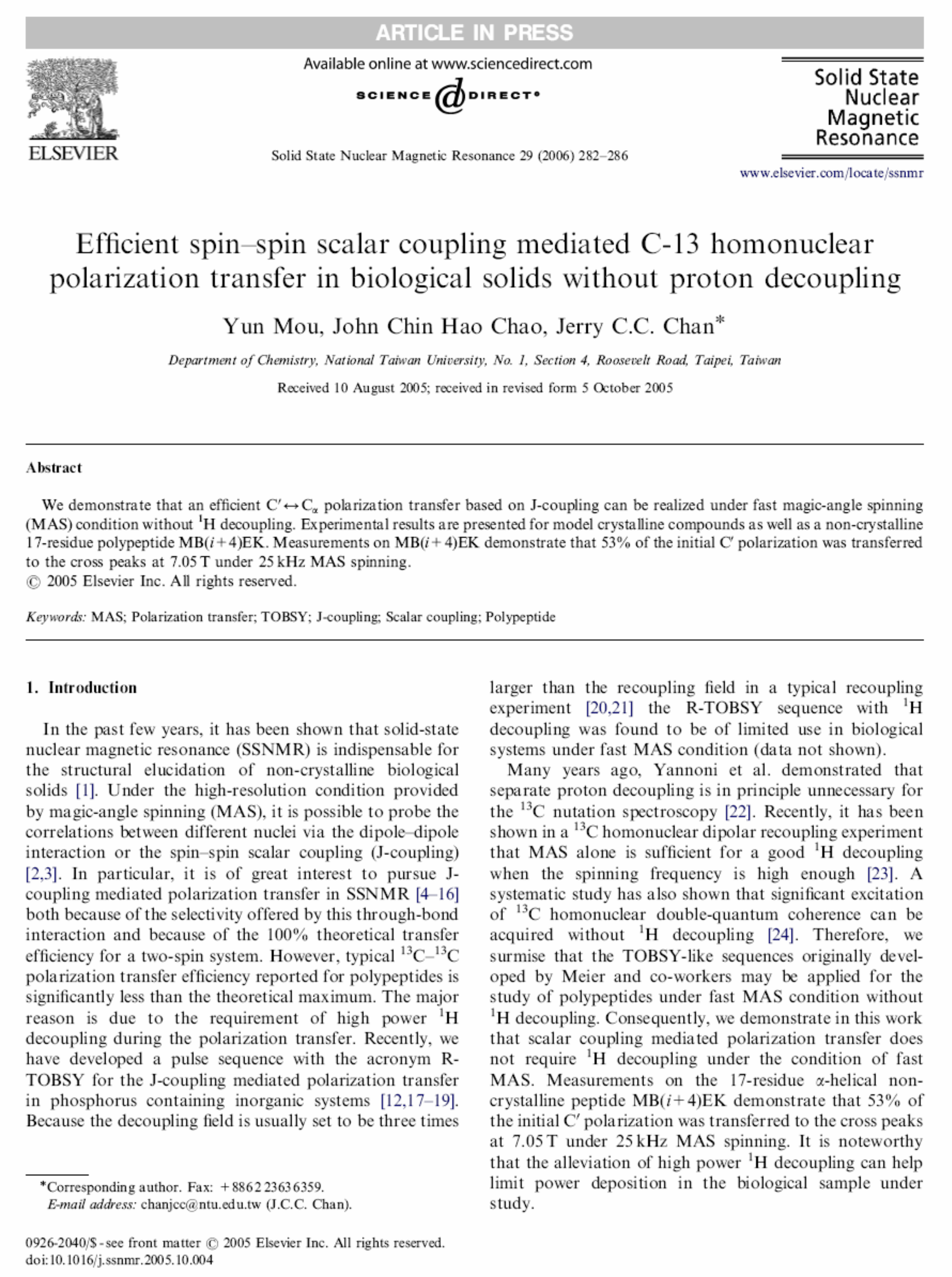

ARTICLE IN PRESS

Available online at www.sciencedirect.com

SCIENCE DIRECT•

ELSEVIER

Solid State Nuclear Magnetic Resonance 29 (2006) 282–286

Solid State Nuclear Magnetic Resonance

www.elsevier.com/locate/ssnmr

Efficient spin–spin scalar coupling mediated C-13 homonuclear polarization transfer in biological solids without proton decoupling

Yun Mou, John Chin Hao Chao, Jerry C.C. Chan*

Department of Chemistry, National Taiwan University, No. 1, Section 4, Roosevelt Road, Taipei, Taiwan

Received 10 August 2005; received in revised form 5 October 2005

Abstract

We demonstrate that an efficient $C' \leftrightarrow C_\alpha$ polarization transfer based on J-coupling can be realized under fast magic-angle spinning (MAS) condition without ^{1}H decoupling. Experimental results are presented for model crystalline compounds as well as a non-crystalline 17-residue polypeptide MB($i+4$)EK. Measurements on MB($i+4$)EK demonstrate that 53% of the initial C′ polarization was transferred to the cross peaks at 7.05 T under 25 kHz MAS spinning.

Keywords: MAS; Polarization transfer; TOBSY; J-coupling; Scalar coupling; Polypeptide

1. Introduction

In the past few years, it has been shown that solid-state nuclear magnetic resonance (SSNMR) is indispensable for the structural elucidation of non-crystalline biological solids [1]. Under the high-resolution condition provided by magic-angle spinning (MAS), it is possible to probe the correlations between different nuclei via the dipole–dipole interaction or the spin–spin scalar coupling (J-coupling) [2,3]. In particular, it is of great interest to pursue J-coupling mediated polarization transfer in SSNMR [4–16] both because of the selectivity offered by this through-bond interaction and because of the 100% theoretical transfer efficiency for a two-spin system. However, typical ^{13}C–^{13}C polarization transfer efficiency reported for polypeptides is significantly less than the theoretical maximum. The major reason is due to the requirement of high power ^{1}H decoupling during the polarization transfer. Recently, we have developed a pulse sequence with the acronym R-TOBSY for the J-coupling mediated polarization transfer in phosphorus containing inorganic systems [12,17–19]. Because the decoupling field is usually set to be three times larger than the recoupling field in a typical recoupling experiment [20,21] the R-TOBSY sequence with ^{1}H decoupling was found to be of limited use in biological systems under fast MAS condition (data not shown).

Many years ago, Yannoni et al. demonstrated that separate proton decoupling is in principle unnecessary for the ^{13}C nutation spectroscopy [22]. Recently, it has been shown in a ^{13}C homonuclear dipolar recoupling experiment that MAS alone is sufficient for a good ^{1}H decoupling when the spinning frequency is high enough [23]. A systematic study has also shown that significant excitation of ^{13}C homonuclear double-quantum coherence can be acquired without ^{1}H decoupling [24]. Therefore, we surmise that the TOBSY-like sequences originally developed by Meier and co-workers may be applied for the study of polypeptides under fast MAS condition without ^{1}H decoupling. Consequently, we demonstrate in this work that scalar coupling mediated polarization transfer does not require ^{1}H decoupling under the condition of fast MAS. Measurements on the 17-residue α-helical non-crystalline peptide MB($i+4$)EK demonstrate that 53% of the initial C′ polarization was transferred to the cross peaks at 7.05 T under 25 kHz MAS spinning. It is noteworthy that the alleviation of high power ^{1}H decoupling can help limit power deposition in the biological sample under study.

---

*Corresponding author. Fax: +886 2 2363 6359.
E-mail address: chanjcc@ntu.edu.tw (J.C.C. Chan).

0926-2040/$ - see front matter © 2005 Elsevier Inc. All rights reserved.
doi:10.1016/j.ssnmr.2005.10.004

2. Experimental

2.1. Sample preparation

[U-^{13}C,^{15}N]-alanine and [U-^{13}C,^{15}N]-valine were purchased from Cambridge Isotopes Laboratories. The peptide MB($i+4$)EK (sequence Ac-AEAAAKEAAAKEA-AAKA-NH$_2$) was synthesized using standard FMOC solid-phase methods on a Perkin-Elmer/Applied Biosystems model 433A peptide synthesizer, with uniform ^{13}C and ^{15}N labeling of lysine at position 6 (Lys6) and alanine at position 9 (Ala9). Purification was accomplished with preparative scale HPLC, using a reverse-phase C18 column. The purity of the product was checked by ESI-MS and the sample was subsequently lyophilized for NMR measurements.

2.2. Solid-state NMR

All NMR experiments were carried out at 7.05 T on a Bruker DSX300 NMR spectrometer equipped with a 2.5 mm double-resonance probe. The spectra were measured at a spinning frequency of 25 kHz.^{13}C chemical shifts were referenced to TMS using adamantane as the secondary standard. During the CP contact time (1.5 ms) the ^{1}H nutation frequency was set to 50 kHz and that of ^{13}C was ramped linearly through the Hartmann Hahn matching sideband. Recycle delay was set to 4 s. The $\pi/2$ Gaussian selective pulse was set to 475 and 280 µs long for [U-^{13}C,^{15}N]-alanine and [U-^{13}C,^{15}N]-valine, respectively. The pulse sequence used for the measurements of the MB($i+4$)EK sample is shown in Fig. 1. For the R-TOBSY pulse block, the ^{13}C nutation frequency was set to 125 kHz. The R-TOBSY mixing time was set to 9.6 ms. No supercycle was used. Proton TPPM decoupling during the acquisition period was set to 100 kHz.

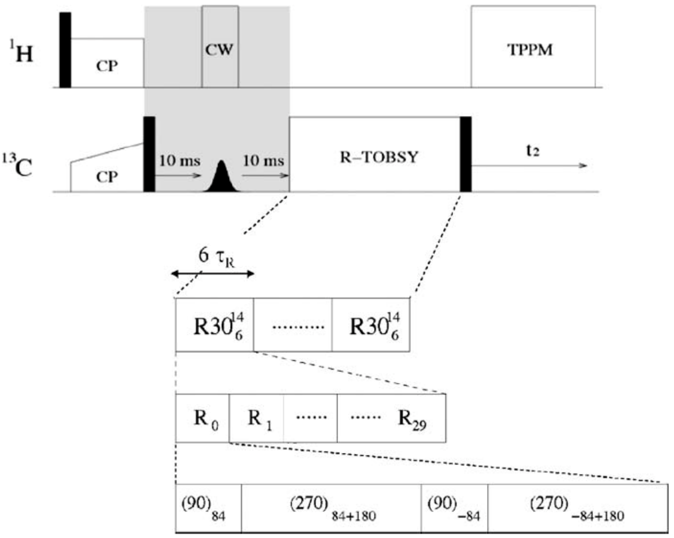

Fig. 1. Pulse sequence for the measurements on model compounds. Black rectangular blocks represent $\pi/2$ pulses. The Gaussian-shaped pulse is a selective $\pi/2$ pulse positioned in the aliphatic region. The shaded part is to be replaced by t_1 evolution and then a $\pi/2$ flip-back pulse in the 2-D analogue.

Quadrature detection for 2D spectra in the F1 dimension was achieved by the hypercomplex approach. Spectral artifacts are suppressed by inverting the phase of the flip-back ^{13}C $\pi/2$ pulse and alternating addition and subtraction of FID signals. Together with CYCLOPS our phase cycling has a total of eight steps. For each t_1 increment 88 transients were accumulated, and a total of 256 increments were done at steps of one rotor period. To reduce the sample heating due to fast MAS spinning, a stream of dry cooling air at −11 °C (800 L/h) was used to keep the sample temperature at around 30 °C, calibrated by measurements on lead (II) nitrate. Consequently, the stability of the spinning frequency is slightly deteriorated (±10 Hz).

2.3. Numerical simulation

All numerical studies in this work were carried out using SIMPSON (version 1.1.0.) [25]. For our simulations, the maximum time step over which the Hamiltonian is approximated to be time-independent was set to 1.0 µs. Typically, a powder averaging scheme containing 320 REPULSION angles (α and β) and 36 γ angles was chosen [26]. Relaxation effects were ignored. The spin cluster used for simulations was constructed based on the structural parameters of alanine. There are three carbons (C', C_α, C_β) and one proton (H_α) in the spin cluster. The J-coupling constants between C'/C_α and C_α/C_β were set to 50 and 35 Hz, respectively. For simplicity, the orientations of CSA tensors with respect to the dipolar framework were set arbitrarily. The simulation was done based on the R-TOBSY sequence. Initially the polarizations of C_α and C_β were nullified. Other simulation parameters were matched to the experimental conditions.

3. Results and discussion

Referring to the data measured for [U-^{13}C, ^{15}N]-alanine shown in Fig. 2a, the maximum $^{13}C_\alpha$ and $^{13}C_\beta$ peak intensities (normalized by the initial C' intensity) are found at the mixing times of 8.64 and 14 ms, respectively. Because typical J-coupling constants for C' C_α and C_α C_β spin pairs are about 50 and 35 Hz, respectively, our data show that J-coupling is indeed the predominant mechanism for the polarization transfer. This interpretation is also corroborated by numerical simulations shown in Fig. 2a. The agreement between the experimental (symbols) and simulation data (lines) is excellent. Experimentally, 74% of the initial C' polarization has been transferred to C_α and C_β at the mixing time of 8.64 ms, for which the raw spectra are shown in Fig. 2c. The decay of the total polarization remains less than 10% through out the experiment. Fig. 2b shows the results obtained for [U-^{13}C, ^{15}N]-valine. Although at mixing time equal to 0 ms there are some residual C_α and C_γ signals due to pulse imperfection, the overall results are consistent with what we obtained for

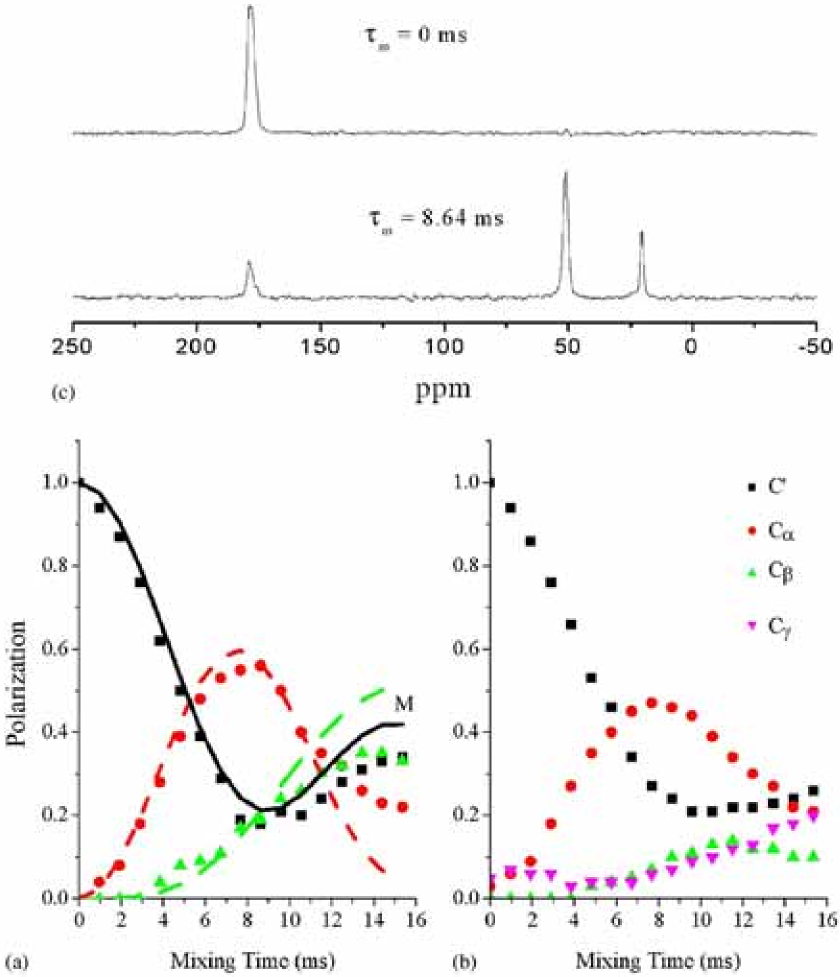

Fig. 2. Plot of peak intensities of different carbon species as a function of mixing time for (a) [U-^{13}C, ^{15}N]-alanine and (b) [U-^{13}C, ^{15}N]-valine. The ^{13}C spectra in (c) were obtained for [U-^{13}C, ^{15}N]-alanine with mixing times (τ_m) equal to 0 and 8.64 ms. The lines in (a) denote the results of numerical simulations.

[U-^{13}C, ^{15}N]-alanine. Additional measurements show that the transfer efficiency will be significantly attenuated if proton decoupling is applied during the mixing time even when the Hartmann Hahn matching condition has been avoided (data not shown). To verify that such high transfer efficiency is not due to relaxation effects, we also measured the two-dimensional ^{13}C ^{13}C correlation spectrum for [U-^{13}C, ^{15}N]-alanine (Fig. 3a). The pulse sequence in Fig. 1 was hence modified by replacing the shaded part by a t_1 evolution with ^{1}H TPPM decoupling [27] followed by a $\pi/2$ flip-back pulse. The mixing time was set to 9.6 ms. For comparison, we also measured a control spectrum where the ^{13}C rf power was nullified during the polarization transfer period (Fig. 3b). After normalizing the cross-peak intensities by the C′ signal of the control spectrum, we obtain an overall $C' \rightarrow \{C_\alpha, C_\beta\}$ and $C_\alpha \rightarrow \{C', C_\beta\}$ transfer efficiency of 69% and 66%, respectively. As expected, the total magnetization decayed to 89% of the control signal.

As a stringent test case, we measured the ^{13}C ^{13}C correlation spectrum for a 17-residue non-crystalline polypeptide with uniform ^{13}C and ^{15}N labeling of lysine at position 6 (Lys6) and alanine at position 9 (Ala9). The 17-residue peptide MB($i+4$)EK has been shown to be highly α-helical [28 30]. To check the tolerance of our pulse sequence with respect to rf inhomogeneity, we purposely confined the sample in the bottom 1/2 of the rotor volume using Teflon spacers. Fig. 4 shows the correlation spectrum obtained with a mixing time of 9.6 ms. The total experimental time was 25 h. By comparison with the control spectrum, we obtain a $C' \rightarrow \{C_{\text{aliphatic}}\}$ transfer efficiency of 53% and the total magnetization decayed to 80% of the control signal. The superb transfer efficiency can also be appreciated by visual inspection of the projection shown in Fig. 4, in which the C′ C_α cross-peak intensity is larger than that of the diagonal C′ signal.

4. Conclusion

In this work we have resolved two important issues. Firstly, we have achieved a good ^{13}C ^{13}C polarization transfer efficiency in a uniformly labeled non-crystalline polypeptide, demonstrating the applicability of our

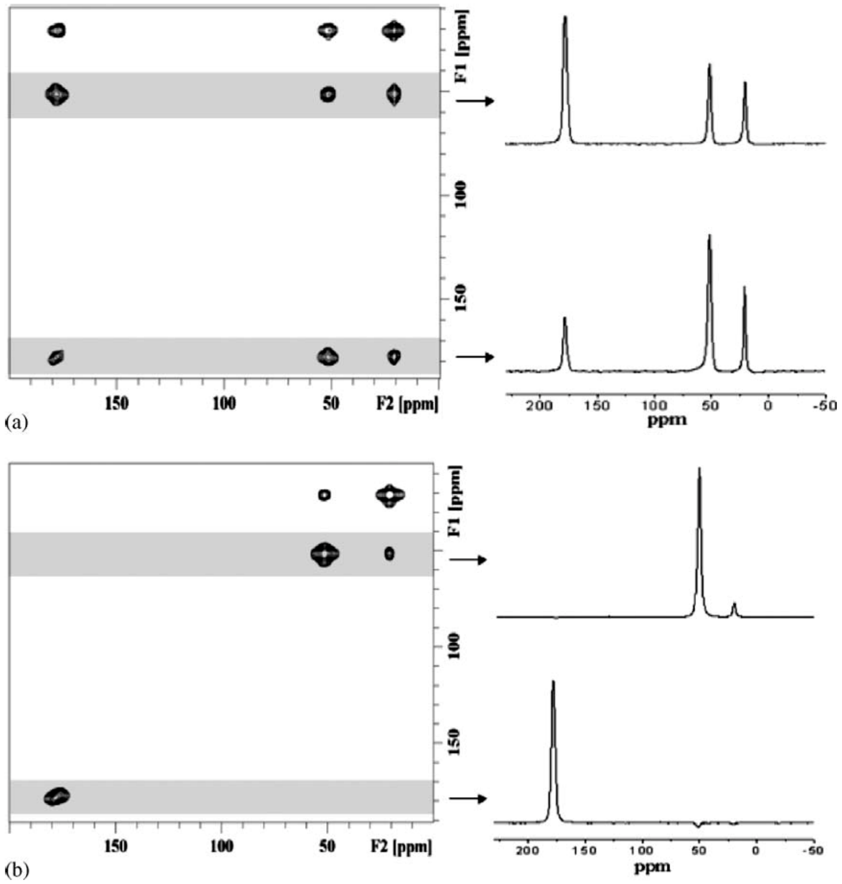

Fig. 3. (a) ^{13}C–^{13}C two-dimensional correlation spectra measured for [U-^{13}C,^{15}N]-alanine. Mixing time was set equal to 9.6 ms. (b) Control spectrum measured for [U-^{13}C,^{15}N]-alanine, where the rf power of the ^{13}C channel was nullified during the R-TOBSY mixing period.

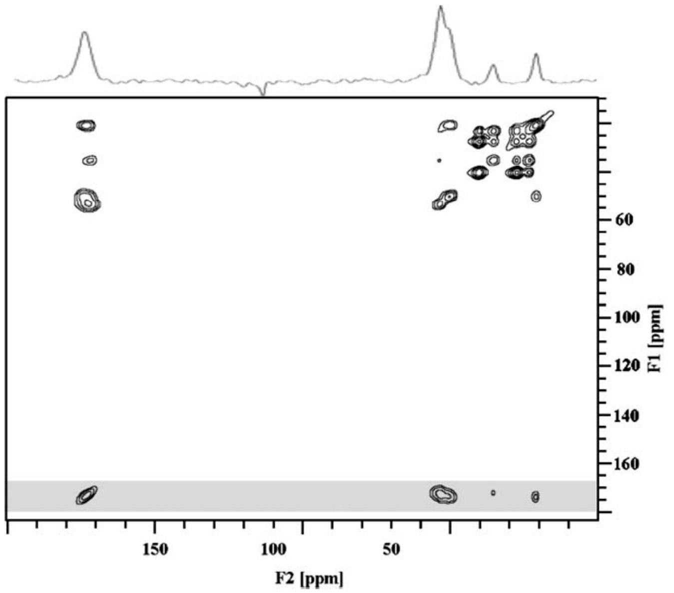

Fig. 4. ^{13}C–^{13}C correlation spectrum measured for the MB($i+4$)EK polypeptides at 7.05 T under 25 kHz MAS spinning. The projection of the shaded region is shown to highlight the excellent $C' \rightarrow C_\alpha$ transfer efficiency.

approach to the studies of real biological systems. Secondly, we show that a simultaneous high power ^1H decoupling is NOT necessary for J-coupling mediated ^{13}C ^{13}C polarization transfer. Although we do not have access to a high-field magnet to further evaluate the performance of our approach, numerical simulation does show that the same transfer efficiency can be achieved in 18.8 T. This no-decoupling approach, coined as NO-DEC by Baldus and co-workers [24], was first tested for dipolar recoupling experiments and it was shown that removing proton decoupling will somewhat attenuate the transfer efficiency to a lower value. Our work, on the other hand, shows that it is necessary to switch off the proton decoupling to achieve a good transfer efficiency for J-coupling-based transfer. We believe that this NO-DEC approach is quite general and can be immediately incorporated into most existing TOBSY-like sequences [5,6,10,11,13]. Altogether, we anticipate that J-coupling mediated polarization transfer can find fruitful applications in many structural problems involving non-crystalline solids and systems with significant dynamics.

Acknowledgments

This work was supported by grants from the National Science Council and the Ministry of Education.

References

[1] R. Tycko, Prog. Nucl. Magn. Reson. Spectrosc. 42 (2003) 53–68.
[2] M. Baldus, Prog. Nucl. Magn. Reson. Spectrosc. 41 (2002) 1–47.
[3] I. Schnell, Prog. Nucl. Magn. Reson. Spectrosc. 45 (2004) 145–207.
[4] A. Ramamoorthy, T. Fujiwara, K. Nagayama, J. Magn. Reson. A 104 (1993) 366–368.
[5] M. Baldus, B.H. Meier, J. Magn. Reson. A 121 (1996) 65–69.
[6] M. Baldus, R.J. Iuliucci, B.H. Meier, J. Am. Chem. Soc. 119 (1997) 1121–1124.
[7] A. Lesage, C. Auger, S. Caldarelli, L. Emsley, J. Am. Chem. Soc. 119 (1997) 7867–7868.
[8] R. Verel, J. van Beek, B.H. Meier, J. Magn. Reson. 140 (1999) 300–303.
[9] A. Lesage, M. Bardet, L. Emsley, J. Am. Chem. Soc. 121 (1999) 10987–10993.
[10] A.S.D. Heindrichs, H. Geen, C. Giordani, J.J. Titman, Chem. Phys. Lett. 335 (2001) 89–96.
[11] E.H. Hardy, R. Verel, B.H. Meier, J. Magn. Reson. 148 (2001) 459–464.
[12] J.C.C. Chan, G. Brunklaus, Chem. Phys. Lett. 349 (2001) 104–112.
[13] E.H. Hardy, A. Detken, B.H. Meier, J. Magn. Reson. 165 (2003) 208–218.
[14] M. Ernst, A. Detken, A. Bockmann, B.H. Meier, J. Am. Chem. Soc. 125 (2003) 15807–15810.
[15] L.J. Mueller, D.W. Elliott, G.M. Leskowitz, J. Struppe, R.A. Olsen, K.-C. Kim, C.A. Reed, J. Magn. Reson. 168 (2004) 327–335.
[16] L. Duma, W.C. Lai, M. Carravetta, L. Emsley, S.P. Brown, M.H. Levitt, ChemPhysChem 5 (2004) 815–833.
[17] S. Reiser, G. Brunklaus, J.H. Hong, J.C.C. Chan, H. Eckert, A. Pfitzner, Chem. Eur. J. 8 (2002) 4228–4233.
[18] G. Brunklaus, J.C.C. Chan, H. Eckert, Z. Phys. Chem. 217 (2003) 1627–1639.
[19] G. Brunklaus, J.C.C. Chan, H. Eckert, S. Reiser, T. Nilges, A. Pfitzner, Phys. Chem. Chem. Phys. 5 (2003) 3768–3776.
[20] Y. Ishii, J. Ashida, T. Terao, Chem. Phys. Lett. 246 (1995) 439–445.
[21] A.E. Bennett, C.M. Rienstra, J.M. Griffiths, W.G. Zhen, P.T. Lansbury, R.G. Griffin, J. Chem. Phys. 108 (1998) 9463–9479.
[22] C.S. Yannoni, R.D. Kendrick, J. Chem. Phys. 74 (1981) 747–749.
[23] Y. Ishii, J. Chem. Phys. 114 (2001) 8473–8483.
[24] C.E. Hughes, S. Luca, M. Baldus, Chem. Phys. Lett. 385 (2004) 435–440.
[25] M. Bak, J.T. Rasmussen, N.C. Nielsen, J. Magn. Reson. 147 (2000) 296–330.
[26] M. Bak, N.C. Nielsen, J. Magn. Reson. 125 (1997) 132–139.
[27] A.E. Bennett, C.M. Rienstra, M. Auger, K.V. Lakshmi, R.G. Griffin, J. Chem. Phys. 103 (1995) 6951–6958.
[28] F.J. Blanco, R. Tycko, J. Magn. Reson. 149 (2001) 131–138.
[29] H.W. Long, R. Tycko, J. Am. Chem. Soc. 120 (1998) 7039–7048.
[30] J.C.C. Chan, R. Tycko, J. Am. Chem. Soc. 125 (2003) 11828–11829.

II-F. Frequency Selective Polarization Transfer Based on Multiple Chemical Shift Precession

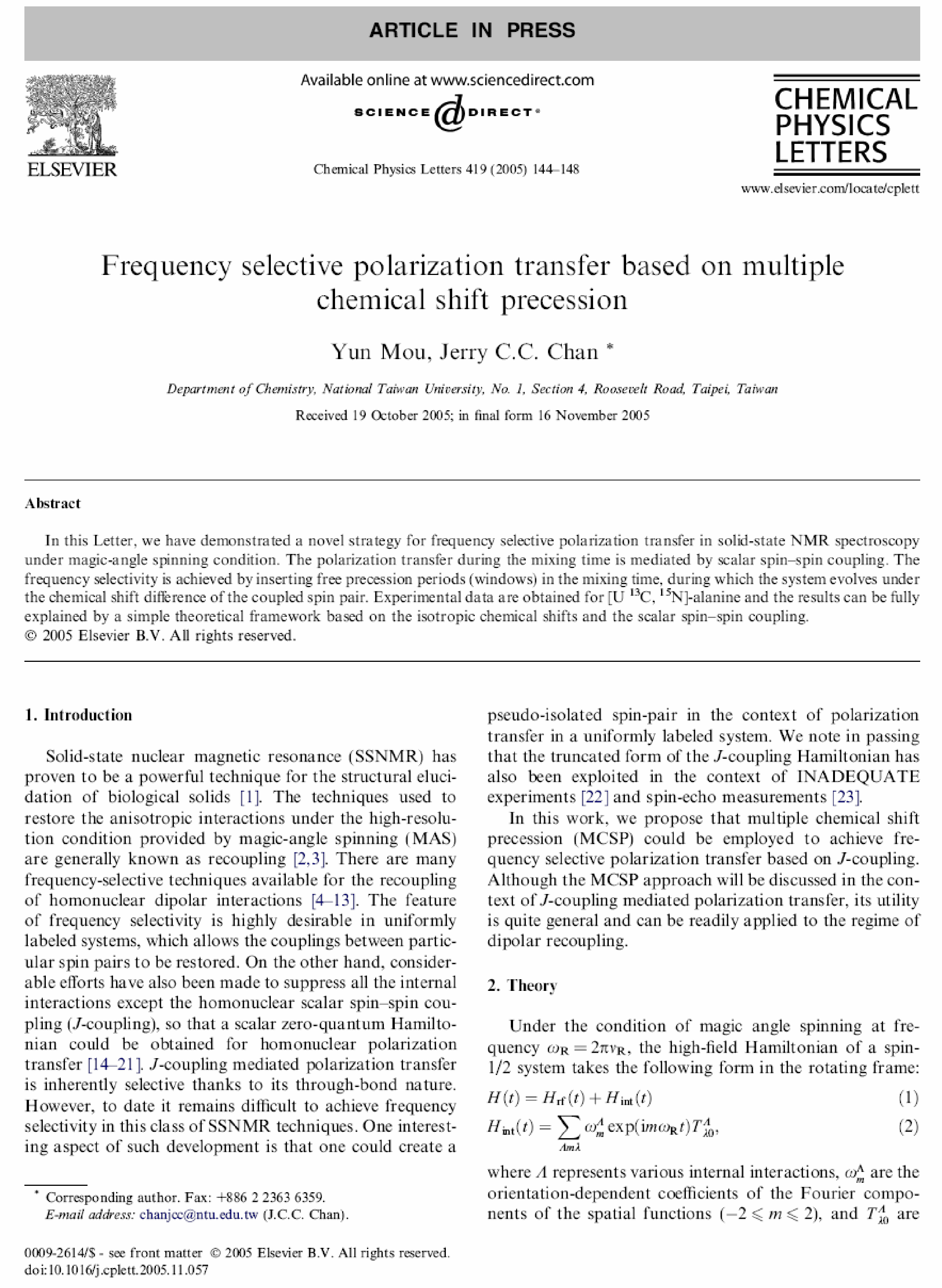

ARTICLE IN PRESS

ELSEVIER

Available online at www.sciencedirect.com
SCIENCE DIRECT®

Chemical Physics Letters 419 (2005) 144–148

CHEMICAL PHYSICS LETTERS

www.elsevier.com/locate/cplett

Frequency selective polarization transfer based on multiple chemical shift precession

Yun Mou, Jerry C.C. Chan *

Department of Chemistry, National Taiwan University, No. 1, Section 4, Roosevelt Road, Taipei, Taiwan

Received 19 October 2005; in final form 16 November 2005

Abstract

In this Letter, we have demonstrated a novel strategy for frequency selective polarization transfer in solid-state NMR spectroscopy under magic-angle spinning condition. The polarization transfer during the mixing time is mediated by scalar spin–spin coupling. The frequency selectivity is achieved by inserting free precession periods (windows) in the mixing time, during which the system evolves under the chemical shift difference of the coupled spin pair. Experimental data are obtained for [U ^{13}C, ^{15}N]-alanine and the results can be fully explained by a simple theoretical framework based on the isotropic chemical shifts and the scalar spin–spin coupling.

1. Introduction

Solid-state nuclear magnetic resonance (SSNMR) has proven to be a powerful technique for the structural elucidation of biological solids [1]. The techniques used to restore the anisotropic interactions under the high-resolution condition provided by magic-angle spinning (MAS) are generally known as recoupling [2,3]. There are many frequency-selective techniques available for the recoupling of homonuclear dipolar interactions [4–13]. The feature of frequency selectivity is highly desirable in uniformly labeled systems, which allows the couplings between particular spin pairs to be restored. On the other hand, considerable efforts have also been made to suppress all the internal interactions except the homonuclear scalar spin–spin coupling (*J*-coupling), so that a scalar zero-quantum Hamiltonian could be obtained for homonuclear polarization transfer [14–21]. *J*-coupling mediated polarization transfer is inherently selective thanks to its through-bond nature. However, to date it remains difficult to achieve frequency selectivity in this class of SSNMR techniques. One interesting aspect of such development is that one could create a pseudo-isolated spin-pair in the context of polarization transfer in a uniformly labeled system. We note in passing that the truncated form of the *J*-coupling Hamiltonian has also been exploited in the context of INADEQUATE experiments [22] and spin-echo measurements [23].

In this work, we propose that multiple chemical shift precession (MCSP) could be employed to achieve frequency selective polarization transfer based on *J*-coupling. Although the MCSP approach will be discussed in the context of *J*-coupling mediated polarization transfer, its utility is quite general and can be readily applied to the regime of dipolar recoupling.

2. Theory

Under the condition of magic angle spinning at frequency $\omega_R = 2\pi\nu_R$, the high-field Hamiltonian of a spin-1/2 system takes the following form in the rotating frame:

$$H(t) = H_{\rm rf}(t) + H_{\rm int}(t) \tag{1}$$

$$H_{\rm int}(t) = \sum_{\Lambda m \lambda} \omega_m^\Lambda \exp(im\omega_R t) T_{\lambda 0}^\Lambda, \tag{2}$$

where Λ represents various internal interactions, ω_m^Λ are the orientation-dependent coefficients of the Fourier components of the spatial functions $(-2 \leqslant m \leqslant 2)$, and $T_{\lambda 0}^\Lambda$ are

---

[*] Corresponding author. Fax: +886 2 2363 6359.
E-mail address: chanjcc@ntu.edu.tw (J.C.C. Chan).

0009-2614/$ - see front matter © 2005 Elsevier B.V. All rights reserved.
doi:10.1016/j.cplett.2005.11.057

irreducible tensor operators of rank λ. Previously, we have demonstrated that the pulse sequence R-TOBSY [18], which falls within the symmetry class RN_n^ν described by Levitt [24,25], can be used to realize homonuclear polarization transfer via spin–spin scalar coupling (J-coupling) in biological solids without proton decoupling [21].

2.1. Two-spin system

For simplicity we first consider a two-spin system. The spin dynamics during the polarization transfer and the free evolution periods can be described elegantly based on the single transition operator formalism [26–28]. Accordingly, in the interaction frame defined by rf field of the R-TOBSY sequence, the average Hamiltonian calculated to the lowest order is [18]

$$\bar{H}^* = 2\pi J(\mathbf{I}^{(1,4)} - \mathbf{I}^{(2,3)} + S_x^{(2,3)}), \tag{3}$$

where $\mathbf{I}^{(i,j)}$ is the identity operator of the subspace (i,j). On the other hand, in the absence of rf irradiation the averaged Hamiltonian in the rotating frame over one rotor period is

$$\bar{H}^{\mathrm{R}} = \omega_\Sigma S_z^{(1,4)} + \omega_\Delta S_z^{(2,3)} + 2\pi J(\mathbf{I}^{(1,4)} - \mathbf{I}^{(2,3)}), \tag{4}$$

where ω_Σ and ω_Δ denote the sum and difference, respectively, of the isotropic chemical shifts of the two interacting spins in angular frequency unit. For brevity, all the identity operators will be discarded in the subsequent discussion. Referring to the pulse sequence shown in Fig. 1, the shaded part after cross-polarization serves to select the S_1 polarization, which is subsequently identified with the ^{13}C polarization of the carbonyl carbon in our experiment. Hence, the initial density matrix operator is written as

$$\sigma^*(0) = S_{1z} = S_z^{(1,4)} + S_z^{(2,3)}, \tag{5}$$

where σ^* denotes the density operator in the interaction frame. Based on the commutation relations of the single transition operators [26,27], Eq. (5) can be calculated as

$$\sigma^*(\tau_1) = S_z^{(1,4)} + S_z^{(2,3)}\cos(2\pi J\tau_1) - S_y^{(2,3)}\sin(2\pi J\tau_1). \tag{6}$$

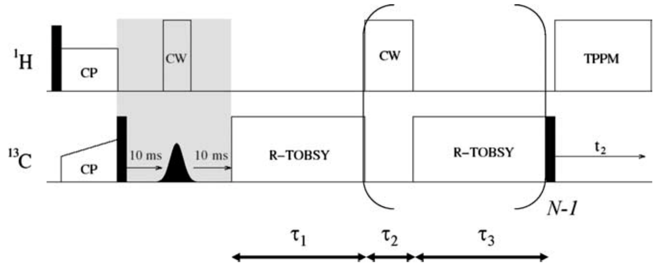

Fig. 1. Pulse sequence for the measurements on [U ^{13}C, ^{15}N]-alanine. Black rectangular black blocks represent $\pi/2$ pulses. The Gaussian-shaped pulse is a selective $\pi/2$ pulse positioned in the aliphatic region. The shaded part is meant for the preparation of the C′ polarization. N denotes the number of R-TOBSY mixing periods. Experimentally, we have $\tau_1 = \tau_3 = \tau$ and the total mixing time $N \times \tau$ is set to the optimum value for the polarization transfer from C′ to C$_\alpha$.

Because the R-TOBSY sequence is cyclic and periodic, the rotating frame and the interaction frame overlap whenever τ_1 equals to an integral multiple, say m, of the R-TOBSY cycle time ($6\tau_{\mathrm{R}}$). Consequently, for $\tau_1 = m(6\tau_{\mathrm{R}})$ the density matrix operator during the free precession period (τ_2) becomes:

$$\begin{aligned}\sigma^{\mathrm{R}}(\tau_2) = {} & S_z^{(1,4)} + S_z^{(2,3)}\cos(2\pi J\tau_1) - S_y^{(2,3)}\sin(2\pi J\tau_1) \\ & \times \cos(\omega_\Delta\tau_2) + S_x^{(2,3)}\sin(2\pi J\tau_1)\sin(\omega_\Delta\tau_2).\end{aligned} \tag{7}$$

Eventually, the evolution of the density matrix operator during the second R-TOBSY mixing period (τ_3) can be calculated as

$$\begin{aligned}\sigma^*(\tau_3) = {} & S_z^{(1,4)} + S_z^{(2,3)}\cos(2\pi J\tau_1)\cos(2\pi J\tau_3) \\ & - S_y^{(2,3)}\cos(2\pi J\tau_1)\sin(2\pi J\tau_3) \\ & - S_y^{(2,3)}\sin(2\pi J\tau_1)\cos(\omega_\Delta\tau_2)\cos(2\pi J\tau_3) \\ & - S_z^{(2,3)}\sin(2\pi J\tau_1)\cos(\omega_\Delta\tau_2)\sin(2\pi J\tau_3) \\ & + S_x^{(2,3)}\sin(2\pi J\tau_1)\sin(\omega_\Delta\tau_2).\end{aligned} \tag{8}$$

When the duration of the free precession period is chosen as $\tau_2 = 2\pi/\omega_\Delta$, we have

$$\begin{aligned}\sigma^*(\tau_3) = {} & S_z^{(1,4)} + S_z^{(2,3)}\cos[2\pi J(\tau_1 + \tau_3)] \\ & - S_y^{(2,3)}\sin[2\pi J(\tau_1 + \tau_3)].\end{aligned} \tag{9}$$

The above result is equivalent to Eq. (6), showing that the free precession period practically has no effect on the spin dynamics. That is, for the total mixing time ($\tau_1 + \tau_3$) equal to $1/2J$, the initial polarization on the spin 1 will be completely transferred to the spin 2. On the other hand, when $\tau_2 = \pi/\omega_\Delta$, Eq. (8) becomes

$$\begin{aligned}\sigma^*(\tau_3) = {} & S_z^{(1,4)} + S_z^{(2,3)}\cos[2\pi J(\tau_1 - \tau_3)] \\ & - S_y^{(2,3)}\sin[2\pi J(\tau_1 - \tau_3)]\end{aligned} \tag{10}$$

When τ_1 is set equal to τ_3 the polarization transfer between the two spins will be quenched. Consequently, our approach has the selection rules $\tau_2 = 2\pi/\omega_\Delta$ (transfer) and $\tau_2 = \pi/\omega_\Delta$ (no transfer) for frequency selective polarization transfer.

2.2. Three-spin system

For a three-spin system S_1–S_2–S_3, the corresponding average Hamiltonians in different periods are:

$$\bar{H}^* = (2\pi J_{12})S_1S_2 + (2\pi J_{23})S_2S_3 + (2\pi J_{13})S_1S_3, \tag{11}$$

$$\begin{aligned}\bar{H}^{\mathrm{R}} = {} & \delta_1 S_{1z} + \delta_2 S_{2z} + \delta_3 S_{3z} + (2\pi J_{12})S_{1z}S_{2z} + (2\pi J_{23})S_{2z}S_{3z} \\ & + (2\pi J_{13})S_{1z}S_{3z}.\end{aligned} \tag{12}$$

The evolution of the spin system can be calculated as

$$\begin{aligned}\sigma^*(\tau_3) = {} & \exp\{-\mathrm{i}\bar{H}^*\tau_3\}\exp\left\{-\mathrm{i}\bar{H}^{\mathrm{R}}\tau_2\right\}\exp\{-\mathrm{i}\bar{H}^*\tau_1\}S_{1z} \\ & \times \exp\{\mathrm{i}\bar{H}^*\tau_1\}\exp\left\{\mathrm{i}\bar{H}^{\mathrm{R}}\tau_2\right\}\exp\{\mathrm{i}\bar{H}^*\tau_3\}.\end{aligned} \tag{13}$$

Since it is not trivial to evaluate Eq. (13) analytically, we have to resort to numerical simulations.

3. Experimental

All NMR experiments were carried out at ^{13}C and ^{1}H frequencies of 75.5 and 300.1 MHz, respectively, on a Bruker DSX300 NMR spectrometer equipped with a commercial 2.5 mm probe. The spectra were measured at room temperature at a spinning frequency of 25 kHz. MAS frequency variation was limited to ±10 Hz using a commercial pneumatic control unit. The samples were confined in the middle 1/2 of the rotor volume using Teflon spacers. During the cross-polarization contact time (1.5 ms) the ^{1}H nutation frequency was set to 50 kHz and that of ^{13}C was ramped through the Hartmann–Hahn matching. The $\pi/2$ Gaussian selective pulse was set to 475 µs long and positioned at the mid-point between the C_α and C_β resonances. Recycle delay was set to 4 s. Proton decoupling was set to 100 kHz. For the R-TOBSY pulse block, the ^{13}C nutation frequency was set to 125 kHz as required by the pulse symmetry [18]. The overall R-TOBSY mixing time was set to 9.6 ms. A total of eight transients were accumulated for each spectrum based on the CYCLOPS phase cycling scheme. The corresponding pulse sequence is shown in Fig. 1.

We have employed two packages for our numerical simulations, viz. MathNMR [29] and SIMPSON [30]. For our SIMPSON simulation (version 1.1.0.), the maximum time step over which the Hamiltonian is approximated to be time-independent was set to 1.0 µs. Typically, a powder averaging scheme containing 100 REPULSION angles (α and β) [31] and 18 γ angles was chosen. Relaxation effects were ignored. There are altogether four spins (C', C_α, C_β and H_α) in the spin cluster. The geometrical and the NMR parameters of the spin system were based on the structural [32] and NMR [33] parameters of alanine. The C'–C_α and C_α–C_β J-coupling constants were set to 50 and 35 Hz, respectively. For simplicity, the orientation of CSA tensors with respect to the dipolar framework was set arbitrarily. Initially the polarizations of C_α and C_β were nullified. Other simulation parameters were matched to the experimental conditions.

4. Results and discussion

The NMR parameters of the ^{13}C species of alanine including the chemical shifts (C', 145 ppm; C_α, 31 ppm; C_β, 0 ppm) as well as the J couplings (C'–C_α, 50 Hz; C_α–C_β, 35 Hz) are taken to define a three-spin system. To understand the dynamics of the three-spin system described by Eq. (13), we employ the package MathNMR, which is developed for symbolic calculations in NMR [29], to calculate the projection of the density matrix operator onto the operators S_{1z} (C'), S_{2z} (C_α) and S_{3z} (C_β) at different τ_2 values. Fig. 2 shows the calculated polarizations of the three carbon species as a function of the precession period τ_2, where we have $\tau_1 = \tau_3 = 5$ ms. For $\tau_2 = 0$, the initial polarization of the C' carbon is largely transferred to C_α and C_β, just as what we expected for a regular TOBSY-like experiment [14]. As the τ_2 value increases to the time point t_a or t_c, which are close to the no transfer condition between C' and C_α, both the C_α and C_β polarizations become diminished. Indeed, the oscillations of the C' and C_α polarizations could be well understood based on the aforementioned selections rules, where we have optimum polarization transfer from C' to C_α when τ_2 is equal to 125 µs (t_b) and 234 µs (t_d) at 7.05 T. Note that the C_β polarization does not follow a simple modulation pattern because its magnitude is affected both by the C_α polarization and the small J-coupling between C_α and C_β. It is interesting to find that the C_α polarization shows a maximum at the time point t_d. Because the total polarization is a constant of motion, it is obvious that the gain in C_α polarization can be obtained at the expense of the C' and C_β polarizations. Although it is impossible to find a particular τ_2 that both C' and C_β polarizations are at minimum simultaneously, it remains possible to apply multiple τ_2 free precession periods to achieve the goal. The idea has a close resemblance to the DANTE concept for selective excitation [34].

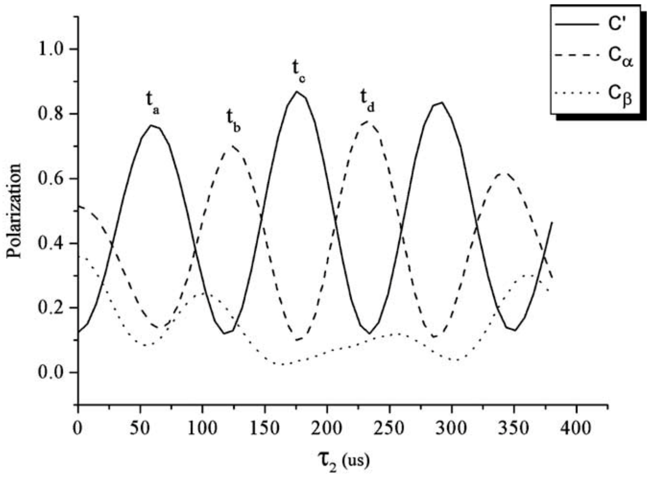

Fig. 2. Plot of the calculated polarizations of C', C_α and C_β as a function of the τ_2 precession time. The polarizations are normalized by the initial C' polarization. The calculations were based on Eq. (13), for which we set $\tau_1 = \tau_3 = 5$ ms.

Fig. 3 shows the calculated polarizations of C_α and C_β as the number of R-TOBSY mixing periods (N) increases, where the τ_2 period and the total mixing time are fixed at 117 µs and 10 ms, respectively. When N is equal to unity, the initial polarization of the C' carbon is largely transferred to C_α and C_β. As expected, the C_β polarization diminished monotonically as N increases because the τ_2 period differs considerably from the inverse of the chemical shift difference between C_α and C_β. Since the J-coupling between C' and C_β is negligible, the loss in the C_β polarization will results in an increase of the C_α polarization. Our treatment thus far has completely ignored the effects of anisotropic interactions during the τ_2 precession period.

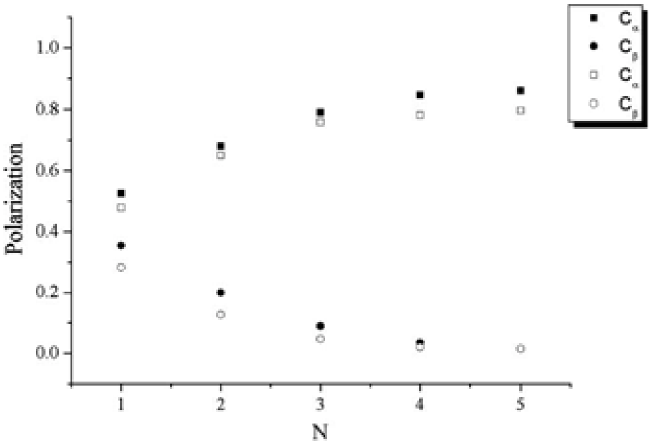

Fig. 3. Plot of the polarizations of C_α and C_β as the number of R-TOBSY mixing periods increase from 1 to 5. The polarization of C′ remains essentially unchanged. The open and filled symbols denote the SIMPSON simulation results and those calculated based on Eq. (13), respectively.

To evaluate the effects of chemical shift anisotropy and the homonuclear dipolar interaction we perform a SIMPSON simulation to verify the results shown in Fig. 3. The open symbols denote the SIMPSON simulation results, which are in good agreement to those calculated based on Eq. (13) (filled symbols).

Experimentally we test our MCSP approach on [U ^{13}C, ^{15}N]-alanine based on the pulse sequence shown in Fig. 1. Referring to Fig. 4, the upper trace represents the regular R-TOBSY experiment, i.e. $\tau_2 = 0$, in which a significant portion of the C′ polarization has been transferred to C_α and C_β [21]. As we set τ_2 equal to $1/\Delta$ and increase the N from 1 to 4, a significant increase in the C_α polarization is produced at the expense of the C_β polarization. This experimental observation is completely in line with our analysis based on Eq. (13). Clearly, the selectivity of the MCSP approach depends on the number of precession periods. An optimum value for N has to be determined experimentally. To stabilize the performance of our pulse sequence with respect to pulse imperfections the phase inversion supercycles are incorporated as shown in Fig. 4 [35]. A more elaborate theoretical consideration is required to understand whether these supercycles would further enhance the polarization transfer efficiency to C_α.

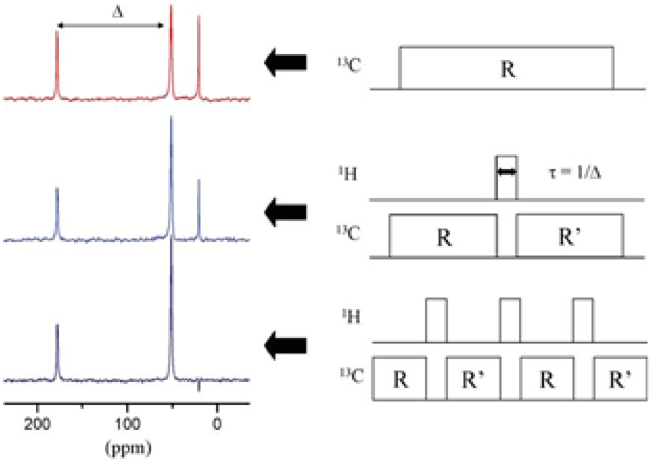

Fig. 4. Experimental results measured for [U ^{13}C, ^{15}N]-alanine based on the pulse sequence shown in Fig. 1. The polarization of C_α after the mixing period increases as the number of R-TOBSY mixing periods increases to 4. Accordingly, the C_β is nullified eventually.

Acknowledgements

This work was supported by grants from the National Science Council and the Ministry of Education. Part of the results described in this Letter was first presented at the 4th Alpine Conference on Solid-State NMR. The stimulating comments from the audience are gratefully acknowledged. We thank Prof. G. Bodenhausen for pointing out that the MCSP technique resembles the DANTE concept in the zero-quantum subspace. At the Alpine conference, we noticed that Tycko and coworkers had independently developed a very similar strategy for the frequency selective excitation of dipolar double-quantum coherence.

References

[1] R. Tycko, Prog. Nucl. Magn. Reson. Spectrosc. 42 (2003) 53.
[2] M. Baldus, Prog. Nucl. Magn. Reson. Spectrosc. 41 (2002) 1.
[3] S. Luca, H. Heise, M. Baldus, Accounts Chem. Res. 36 (2003) 858.
[4] E.R. Andrew, A. Bradbury, R.G. Eades, V.T. Wynn, Phys. Lett. 4 (1963) 99.
[5] B.H. Meier, W.L. Earl, J. Am. Chem. Soc. 109 (1987) 7937.
[6] D.P. Raleigh, M.H. Levitt, R.G. Griffin, Chem. Phys. Lett. 146 (1988) 71.
[7] M.G. Colombo, B.H. Meier, R.R. Ernst, Chem. Phys. Lett. 146 (1988) 189.
[8] D.P. Raleigh, F. Creuzet, S.K.D. Gupta, M.H. Levitt, R.G. Griffin, J. Am. Chem. Soc. 111 (1989) 4502.
[9] M.H. Levitt, D.P. Raleigh, F. Creuzet, R.G. Griffin, J. Chem. Phys. 92 (1990) 6347.
[10] K. Takegoshi, K. Nomura, T. Terao, Chem. Phys. Lett. 232 (1995) 424.
[11] K. Takegoshi, K. Nomura, T. Terao, J. Magn. Reson. 127 (1997) 206.
[12] P.R. Costa, B.Q. Sun, R.G. Griffin, J. Am. Chem. Soc. 119 (1997) 10821.
[13] K. Nomura, K. Takegoshi, T. Terao, K. Uchida, M. Kainosho, J. Am. Chem. Soc. 121 (1999) 4064.
[14] M. Baldus, B.H. Meier, J. Magn. Reson. A 121 (1996) 65.
[15] M. Baldus, R.J. Iuliucci, B.H. Meier, J. Am. Chem. Soc. 119 (1997) 1121.
[16] A.S.D. Heindrichs, H. Geen, C. Giordani, J.J. Titman, Chem. Phys. Lett. 335 (2001) 89.
[17] E.H. Hardy, R. Verel, B.H. Meier, J. Magn. Reson. 148 (2001) 459.
[18] J.C.C. Chan, G. Brunklaus, Chem. Phys. Lett. 349 (2001) 104.
[19] E.H. Hardy, A. Detken, B.H. Meier, J. Magn. Reson. 165 (2003) 208.
[20] M. Ernst, A. Detken, A. Bockmann, B.H. Meier, J. Am. Chem. Soc. 125 (2003) 15807.
[21] Y. Mou, J.C.H. Chao, J.C.C. Chan, Solid-State Nucl. Magn. Reson., in press.
[22] A. Lesage, C. Auger, S. Caldarelli, L. Emsley, J. Am. Chem. Soc. 119 (1997) 7867.
[23] L. Duma, W.C. Lai, M. Carravetta, L. Emsley, S.P. Brown, M.H. Levitt, Chem. Phys. Chem. 5 (2004) 815.
[24] M. Carravetta, M. Eden, X. Zhao, A. Brinkmann, M.H. Levitt, Chem. Phys. Lett. 321 (2000) 205.

[25] A. Brinkmann, M. Eden, M.H. Levitt, J. Chem. Phys. 112 (2000) 8539.
[26] A. Wokaun, R.R. Ernst, J. Chem. Phys. 67 (1977) 1752.
[27] S. Vega, J. Chem. Phys. 68 (1978) 5518.
[28] B.H. Meier, Polarization transfer and spin diffusion in solid state NMR, in: W.S. Warren (Ed.), Advances in Magnetic and Optical Resonance, vol. 18, Academic Press, New York, 1994, pp. 1 116.
[29] A. Jerschow, J. Magn. Reson. 176 (2005) 7.
[30] M. Bak, J.T. Rasmussen, N.C. Nielsen, J. Magn. Reson. 147 (2000) 296.
[31] M. Bak, N.C. Nielsen, J. Magn. Reson. 125 (1997) 132.
[32] M.S. Lehmann, T.F. Koetzle, W.C. Hamilton, J. Am. Chem. Soc. 94 (1972) 2657.
[33] A. Naito, S. Ganapathy, K. Akasaka, C.A. McDowell, J. Chem. Phys. 74 (1981) 3190.
[34] R. Freeman, Spin Choreography: Basic Steps in High Resolution NMR, Oxford University Press, New York, 1998.
[35] M.H. Levitt, Symmetry-based pulse sequence in magic-angle spinning solid-state NMR, in: D.M. Grant, R.K. Harris (Eds.), Encyclopedia NMR, vol. 9, Wiley, Chichester, 2002, pp. 165 196.

II-G. Attachment of Peptide onto HAp Surface

The peptide fragment of salivary statherin chosen in our study has 15 residues. According to earlier study this fragment is responsible for the interaction of statherin and inorganic phosphate clusters to prevent the precipitation of calcium phosphate in saliva. Experimentally we employed solid-state peptide synthesizer (Rainin Instrument Company) to prepare our target peptide. Standard Fmoc chemistry was used to attach residues sequentially to preloaded resin. The deprotection procedure was done by 20% (v/v) piperidine in DMF and the activation reagent was PyBop. The solution 95% TFA, 2.5% TIS and 2.5% H_2O was prepared for peptide cleavage. After precipitating the cleavage product in cold MTBE, the crude material was obtained by centrifuge. Peptide purification was done by HPLC (Beckman Coulter System Gold) using a Vydac C18 reverse-phase column (218TP1022) at 50°C. As shown in the following figure, the solvent gradient (Solution A: 5% ACN in water; Solution B: 95% ACN in water) was shown as line segments:

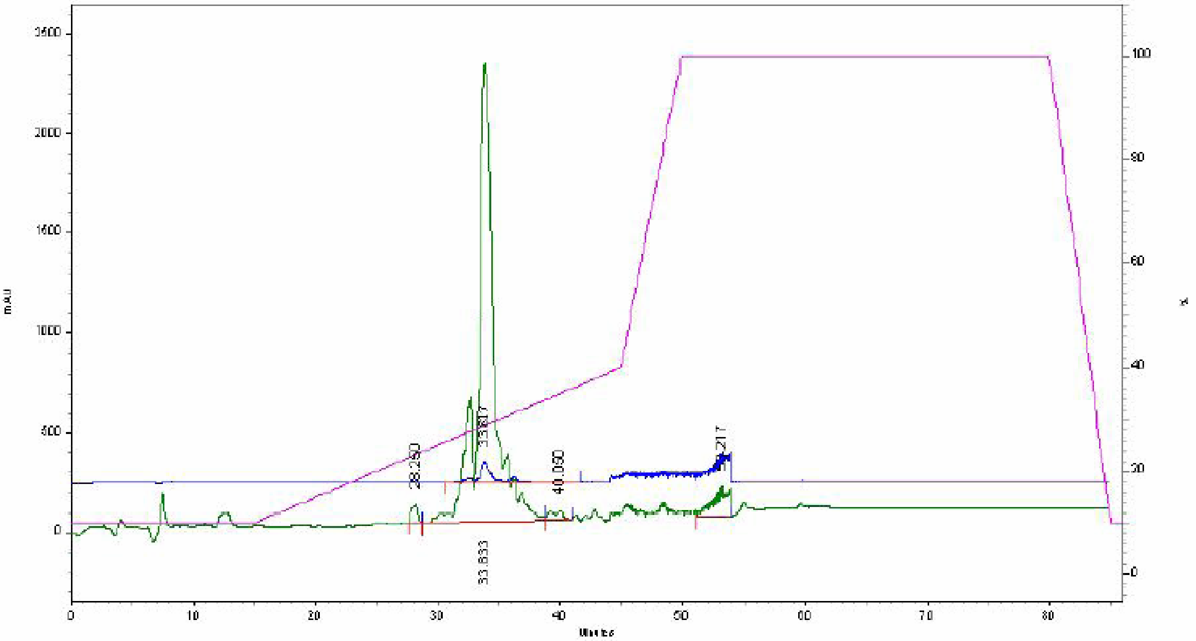

The sample collected at 32 to 34 mins was lyophilized and characterized by ESI-MS. According to the deconvolution of the MS spectrum done by BIOMASS, the purity of the target peptide is higher than 90%.

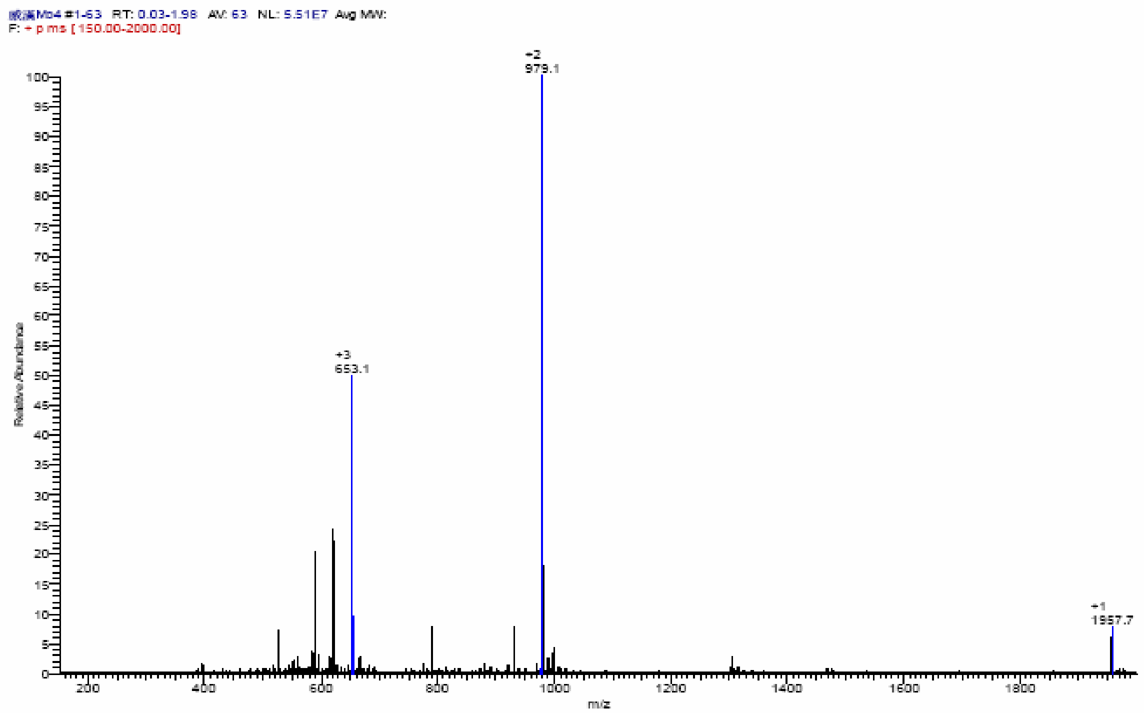

m/z	charge
653.13	3
979.07	2
1958.71	1

Deconvolution (BIOMASS deconvolution)

A mixture of 20 mg purified peptide and 50 mg hydroxyapatite in 5 ml phosphate buffer was prepared and shaken vigorously for 5 minutes. The mixture was then incubated in an orbital

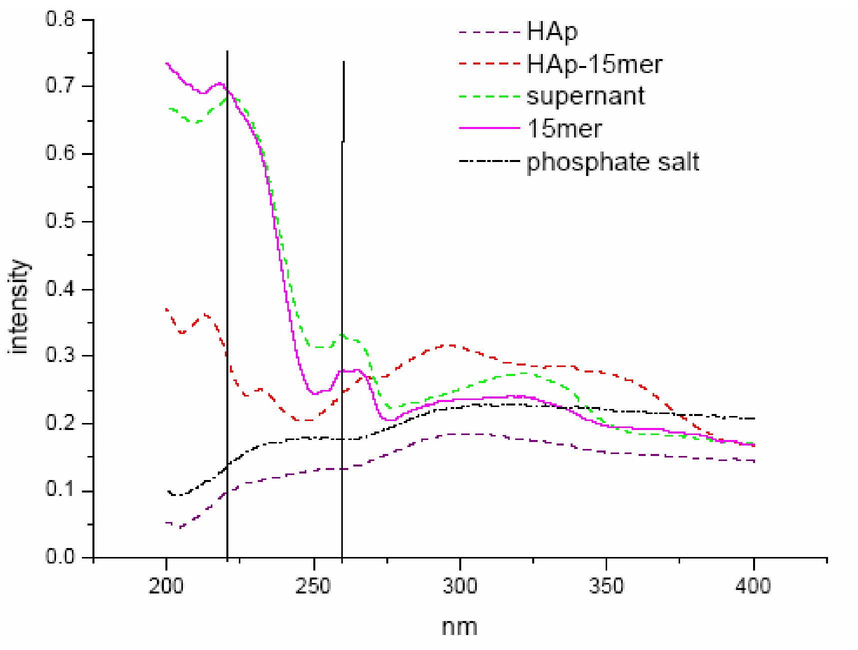

shaker (150 rpm) at 37°C. The sample and the supernatant were collected by centrifuge. After lyophilization and further washing, the solid UV spectra were measured. The peaks at 220 nm and 260 nm were adsorption bands due to peptide bonds and phenyl rings, respectively. Although the results are not conclusive, the weak adsorptions at 220 nm and 260 nm of the sample shows that it is a mixture of hydroxyapatite (HAp) and our target peptide (15mer). In addition, the FT-IR spectrum was measured for our sample:

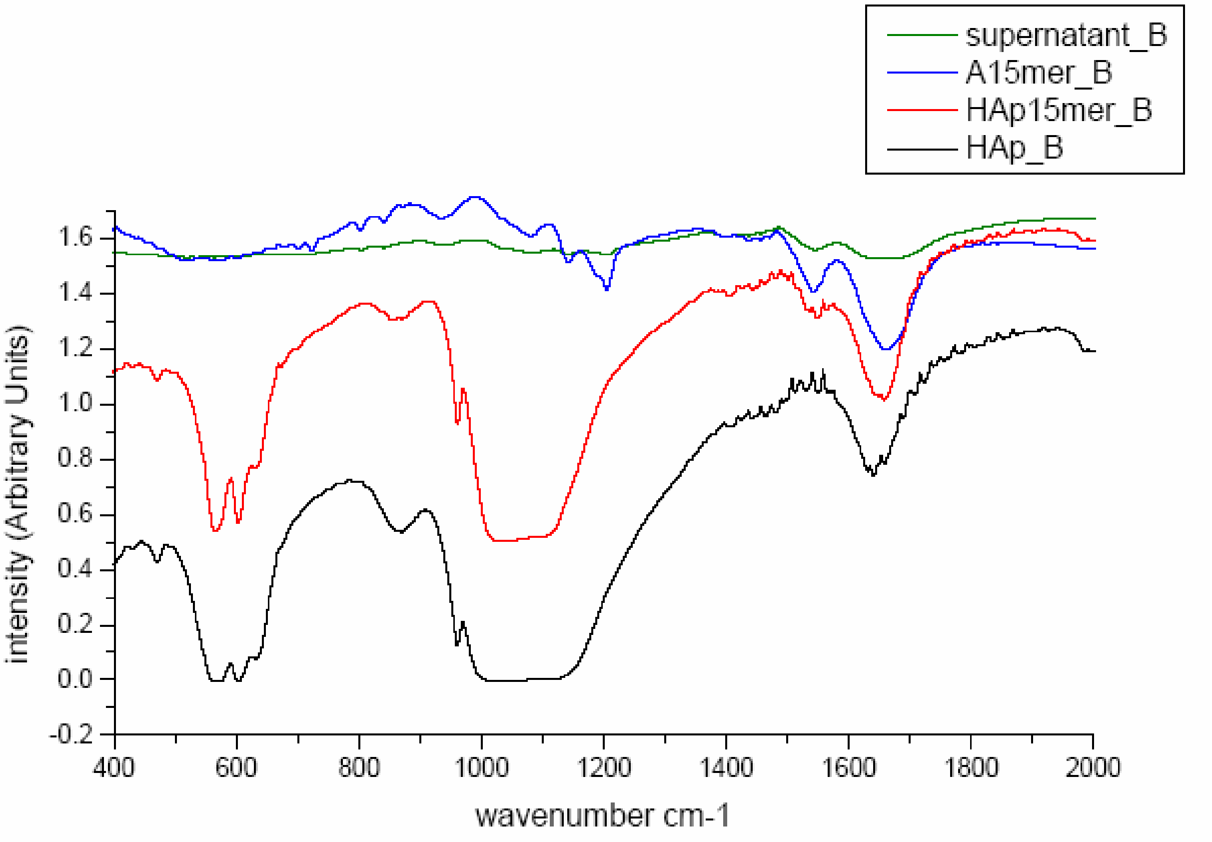

From the FT-IR spectrum one can identify the adsorptions of 1028, 605 and 565 cm^{-1} to PO_4^{3-} vibrational modes. Those around 1400-1430 cm^{-1} and 1560-1600 cm^{-1} can be assigned to the symmetric and asymmetric stretchings of carboxylate group, respectively. The adsorptions around 1485-1550 and 1590-1660 cm^{-1} are due to the symmetric and asymmetric stretchings of amino group, respectively. Therefore, the FT-IR data indicate that small amount of our target peptide has been attached to our HAp crystals. Ninhydrin test also proved that there are peptides attached to our sample surface. Similar results were obtained when we replace the synthetic HAp crystals by bioactive glasses soaked in simulated body fluid. While we have experimentally illustrated the concept of peptide attachment to bioactive glasses, the peptide amount at the current stage is still too limited to allow a thorough solid-state NMR characterization. Additional works are ongoing to increase the amount of the attached peptides.

III. Self Evaluation

In the past two years (Nov 2003 to Sept 2005), we had managed to prepare and characterize the target sol-gel glass systems, which were then soaked in simulated body fluid to induce the formation of HAP. The molecular mechanism of apatite formation on bioactive glass surface is studied using the techniques of XRD, EDX, SEM, FT-IR, and solid-state ^{31}P NMR. Using the sol-gel method a bioactive glass system containing glass beads of 2 to 3 microns in size is prepared with the composition containing 30% CaO – 70% SiO_2. Our experimental data support the apatite formation mechanism proposed by Hench concerning the precipitation and crystallization of calcium phosphate. The phosphate ions initially deposited on the glass surface are largely in amorphous phase and have substantial amount of water molecules in the surrounding. As the soaking time in simulated body fluid increases, some of the water molecules diffuse out of the phosphate lattice, leading to the formation of a crystalline phase. Our data show that the structure of the crystalline phase is different from type B carbonate apatite but similar to hydroxyapatite.

In addition, considerable efforts were made to develop solid-state NMR strategy to study our model compounds, *viz.* octacalcium phosphate (OCP) and HAp. This part of the works, which is in collaboration with Professor C. Y. Mou, has proven to be very fruitful. The molecular mechanism of OCP to HAp transformation in vitro has been studied by several physical techniques, with particular emphasis on solid-state ^{31}P homonuclear double-quantum (DQ) NMR spectroscopy. Together with computer assisted lattice matching, our NMR data reveal that OCP crystals transform to HAp topotaxially along their c axes with anti-parallel relationship, instead of the parallel relationship as presumed in the literature. Furthermore, the data of the $^{31}P\{^1H\}$ cross-polarization NMR suggest that water molecules enter the hydration layers of OCP crystals via the hydrolysis reaction $HPO_4^{2-} + OH^- = PO_4^{3-} + H_2O$, which also accounts for the deprotonation of the HPO_4^{2-} ions during the transformation.

We have also made a considerable progress in the development of new solid-state nuclear magnetic resonance (SSNMR) technique for the determination of backbone torsion angle ψ of polypeptides. In particular, we have resolved two important issues. Firstly, we have achieved a good ^{13}C-^{13}C polarization transfer efficiency in a uniformly labeled non-crystalline polypeptide, demonstrating the applicability of our approach to the studies of real biological systems. Secondly, we show that a simultaneous high power ^1H decoupling is NOT necessary for J-coupling mediated ^{13}C-^{13}C polarization transfer. We believe that this no-decoupling approach is quite general and can be immediately incorporated into most existing sequences. Altogether, we anticipate that J-coupling mediated polarization transfer can find fruitful applications in many structural problems involving non-crystalline solids and systems with significant dynamics.

Concerning the synthesis of our target peptide, we have initiated a collaboration with Dr. Steve S. F. Yu at the Chemistry Institute of Academia Sinica. The laboratory of Dr. Yu is well-equipped for peptide synthesis. As expected, it is relatively straightforward to prepare and purify our target peptide DpSpSEEKFLRRIGRFG. However, it proves to be very difficult to attach enough amount of the target peptide to HAp crystal surface for solid-state NMR study. The main difficulty is that the zeta-potential of HAp crystal surface is of negatively charged and therefore the conventional protocol of mixing the peptide solution and HAp crystal in buffer solution is not effective. Nevertheless, we have developed a new strategy to enhance the peptide attachment. This work will provide a roadmap for the future development of the idea described in this project.

Overall, this pilot project has proven the applicability of solid-state NMR spectroscopy to the investigation of the molecular mechanism of biomineralization. Although the major objective, characterization of the conformation of peptides attached on bioactive glass surface, has not yet accomplished, we have completed most of our specific aims. Upon the completion of this project, which is the very first NSC funded project of the principal investigator, the results have been resulted in six full papers (five published and one submitted). Additional experiments are still underway to study the glass-peptide interaction. Furthermore, this project has seeded many collaboration works and the NMR methodology developed in this project has provided a very solid foundation to further our study on teeth and bones

Appendix

Thanks to the traveling allowance provided in this project, I have attended the following international conference in solid-state NMR spectroscopy:
The 4th Alpine conference on Solid-State NMR, Charmonix, France.
September 11-14, 2005

The aim of the conference is to provide an international forum for high-level discussions to physicists, chemists, biologists and the other scientists with both an academic or industrial background, interested in the latest developments in solid-state NMR. The meeting focuses on the state of the art and theoretical and methodological developments, as well as on recent applications of solid-state NMR in fields as diverse as: organic and inorganic chemistry, catalysis, structural biology, materials science and polymer science.

Although I was not an invited speaker of the conference but I was encouraged by the organizer to give an oral presentation of my work. The "invitation" email is reproduced below:

Dear Jerry,
I am sending you this on behalf of the scientific committee for the 2005 Alpine solid-state NMR conference (http://www.alpine-conference.org/).
We hope very much that you can attend the conference and will shortly register and submit an abstract before the deadline (May 31). On the basis of the work we know about we expect to offer you a contributed talk at the conference.
The organizing committee will send out invitations after all the abstracts have come in.
Please be aware, however, that the conference does not usually pay expenses for contributing speakers. If you are eligible, you may be able to apply for a student stipend (details on the web site).
best wishes,
and I hope to see you in Chamonix,
malcolm
--
****
Malcolm Levitt
School of Chemistry
University of Southampton
Southampton SO17 1BJ
England.
tel. +44 23 8059 6753
fax: +44 23 8059 3781
mobile: +44 77 6652 2964
email: Malcolm.Levitt@soton.ac.uk
website: http://www.mhl.soton.ac.uk
****

The title of my talk is

"Efficient Spin-Spin Scalar Coupling Mediated 13C-13C Polarization Transfer in Solid-State NMR Spectroscopy."

Although the conference does not publish any proceedings, the materials of the presentation I gave there have been published:

1. Y Mou, JCH Chao, JCC Chan, 2006, "Efficient Spin-Spin Scalar Coupling Mediated C-13 Homonuclear Polarization Transfer in Solid-State NMR Spectroscopy," *Solid State Nucl. Magn. Reson.*, in press.
2. Y Mou and JCC Chan, 2006, "Frequency Selective Polarization Transfer Based on Multiple Chemical Shift Precession," *Chem. Phys. Lett.*, in press.

My presentation is a great success and I believe the NMR pulse sequence we have developed during the execution of this project has obtained adequate exposure. Indeed, we notice that the MCSP approach described in our project has a considerably impact on the community. In the same conference, another group led by Dr. Robert Tycko (Laboratory of Chemical Physics, NIH, Bethesda) also presented a technique based on a very similar principle. In the preprint of his submitted manuscript, it has been stated that:

"Independently, Chan and coworkers have shown that the introduction of chemical shift precession periods into the R-TOBSY recoupling sequence leads to frequency-selective polarization transfers. R-TOBSY produces a scalar, zero-quantum effective coupling Hamiltonian. Chemical shift precession periods produce a phase modulation that truncates the effective Hamiltonian to the form in Eq. (17) unless $n(\omega_I - \omega_S)$ is an integer multiple of 2π."